International Journal of Advances in Telecommunications Electrotechnics, Signals and Systems

a publication of the International Science and Engineering Society

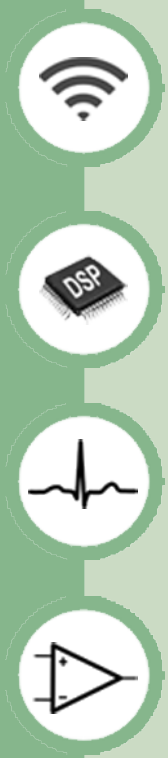

Vol. 3, No. 1
2014

ISSN: 1805-5443

www.ijates.org

I J A T E S²

International Journal of Advances in Telecommunications Electrotechnics, Signals and Systems

a publication of the International Science and Engineering Society

Vol. 3, No. 1, 2014 ISSN: 1805-5443

Aims and Scope

The International Journal of Advances in Telecommunications, Electronics, Signals and Systems (IJATES²) is an all-electronic international scientific journal with the aim to bring the most recent and unpublished research and development results in the area of electronics to the scientific and technical societies, and is supported by the ISES (International Science and Engineering Society, o.s.). The journal's scope covers all the aspects of telecommunication, signal processing, theory and design of circuits and systems for electronics.

The IJATES² is ready to publish experimental and theoretical full papers and letters submitted by prospective authors. Paper submitted for publication must be written in English and must follow a prescribed format. All papers are subjected to a critical peer-review prior to publication.

The IJATES² is an open access journal which means that all content is freely available without charge to the user or his/her institution. Users are allowed to read, download, copy, distribute, print, search, or link to the full texts of the articles in this journal without asking prior permission from the publisher or the author. This journal provides immediate open access to its content on the principle that making research freely available to the public supports a greater global exchange of knowledge.

www.ijates.org

CONTENTS

Vol. 3, No. 1, 2014 ISSN: 1805-5443

Fully Differential Universal Current-Mode Frequency Filters Based on Signal-Flow Graphs Method

L. Langhammer and J. Jerabek

***Abstract*— Two new circuits of 2nd order universal frequency filter designed using signal-flow graphs method are presented. Both filters were proposed in single-ended and fully-differential forms. Multiple-output current follower (MO-CF) and digitally adjustable current amplifier (DACA) used in proposal are described in the paper. The pole frequency and the quality factor of filters can be controlled by the current gain of digitally adjustable current amplifiers suitably placed in the circuit structure. The actual function of the proposed filters is verified using PSpice simulation. Simulation results of proposed filters are also included in this paper.**

***Keywords*— Current amplifier, Current follower, Current mode, Frequency filter, Fully differential, Single ended**

I. Introduction

There are multiple methods how to approach to design of frequency filters. One of the general filter-design method frequently used for the proposal of new filters is autonomous circuit design method described in [1-4]. An autonomous circuit is presented as a circuit of passive and active elements which possesses no excitation source and has no selected input or output terminal. Such a circuit is solely described by the characteristic equation. These autonomous circuits then serve as a default circuit to design various types of frequency filters [4]. We can also mention a method of synthetic immittance system which can be found for instance in [4-6]. Higher-order immittance synthetic elements consist of serial or parallel combinations of elementary D or E type dipoles. There are four synthetic elementary dipoles connections with immittance of higher order namely DP, DS, EP, ES [6]. Other known way how to propose frequency filters is using signal-flow graphs (SFGs) method described in papers such as [4], [7], [8]. For synthesis and analysis of electrical circuits Mason-Coates' (M-C) flow graphs are used. These graphs can be understood as diagrams representing mutual relations between nods and branches of the analyzed circuit. Using this method we can directly propose circuits of frequency filters in two steps. Firstly, a type of the transfer function is determined. Subsequently, the rules of M-C graphs are used to create a graph of the proposed circuit described by its transfer function. From this graph the circuit network can be easily made [7].

Manuscript received November 18, 2013 revised March 27, 2014.

L. Langhammer Faculty of Electrical Engineering and Communication, Brno University of Technology, Technicka 12, 616 00 Brno, Czech Republic (e-mail: xlangh01@stud.feec.vutbr.cz)

J. Jerabek Faculty of Electrical Engineering and Telecommunication, Brno University of Technology, Technicka 12, 616 00 Brno, Czech Republic (e-mail: jerabekj@feec.vutbr.cz)

Lately we can experience a trend of decreasing of supply voltage caused by reducing of the integrated circuit size. Growning requirements on circuit with low supply voltage force desingers to propose circuits working in the current mode to achieve sufficient signal to noise ratio. Furthermore, the frequency-limitation of the common operation amplifier leads to employing of other types of active elements. Active elements operating in the current mode can provide a high frequency bandwith and dynamic range [4]. Research in analog functional blocks is also focuded on the realization of the current-mode filters using different types of a current conveyor (CC) [9-11] and differential voltage current conveyor (DVCC) [12], [13]. We can mention filters with operational transconductance amplifiers (OTA) [14-15], current differencing transconductance amplifiers (CDTA) [16], [17]. Filters emploing fully differential current conveyors (FDCC) can be found in [18-20]. Papers [21], [22] describe various types of filters using current followers (CF). Furthermore, it is possible to come across filters operating with current differencing buffered amplifiers (CDBA) for instance in [23] and [24].

This article contains also fully-differential structures of proposed filters because of their advantages when compared to single-ended circuits such as lower harmonic distortion, greater dynamic range of the signal, greater attenuation of common-mode signal and better power supply rejection ratio. Fully-differential structures have also a few drawbacks namely the larger area taken on the chip which leads to higher power consumption and more complex design than single-ended structures [25], [26].

II. Active elements definition

Description of two active elements used for proposal are presented in this section. Their schematic symbols and signal-flow graphs are included. Description also contains 2nd level macro-models of these elements used in simulations of behavior of proposed circuits.

To obtain low number of transfer function terms it is required employing multi-output active elements to create feedbacks, which allow us to cancel out unwanted terms of the transfer function [7]. Therefore, first used element is a multiple-output current follower (MO-CF) formerly presented in [27]. The MO-CF has on input and 4 output terminals. This component has been implemented using a universal current conveyor (UCC) [28], [29] as it is shown in Fig. 1.

doi: 10.11601/ijates.v3i1.62

The relations between the input and outputs of the MO-CF are described by following equations:

$$i_{OUT1} = i_{OUT3} = +i_{IN}, \quad (1)$$

$$i_{OUT2} = i_{OUT4} = -i_{IN}. \quad (2)$$

Its schematic symbol, simplified signal-flow graph and 2nd level model is shown in Fig. 1.

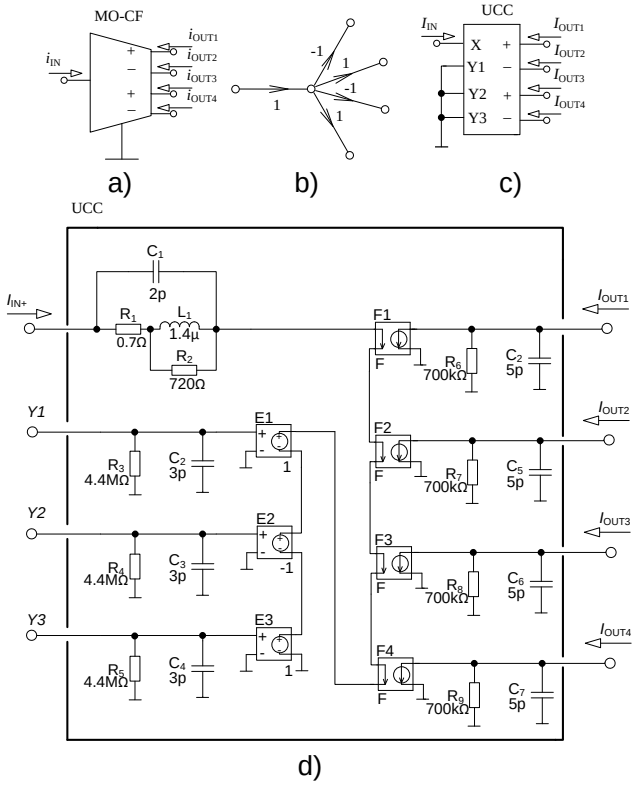

Fig. 1. A current follower a) schematic symbol, b) signal-flow graph, c) realization using the UCC, d) 2nd level macro-model

The second element is a digitally adjustable current amplifier (DACA) originally presented in [30]. This part has a differential current input and output and its current gain is adjustable [31]. The DACA circuit has been developed and implemented in cooperation of Brno University of Technology and ON Semiconductor Brno Design Center in the CMOS 0.35 mm technology. Its current gain can be set via 3-bit word in range from 1 to 8 with step of 1 [30].

The behavior of the DACA is given by the equations:

$$I_{OUT+} = A(I_{IN+} - I_{IN-}), \quad (3)$$

$$I_{OUT-} = -A(I_{IN+} - I_{IN-}), \quad (4)$$

$$I_{DIF} = 2A(I_{OUT+} - I_{OUT-}), \quad (5)$$

where A is a current gain of DACA.

Its schematic symbol, simplified signal-flow graph and 2nd level model is shown in Fig. 2.

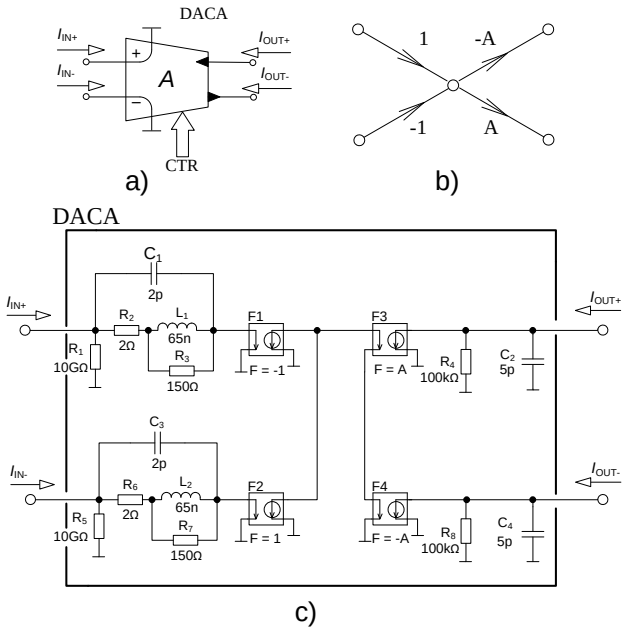

Fig. 2. A digitally adjustable current amplifier a) schematic symbol, b) signal-flow graph, c) 2nd level macro-model

III. PROPOSAL OF UNIVERSAL CURRENT-MODE FREQUENCY FILTERS

A. Description of the universal current-mode frequency filter

Circuits of filters proposed in this paper are based on analysis of previously presented filter published in [32]. It is 2nd order universal current-mode frequency filter. Scheme of this filter and its signal-flow graph can be seen in Fig. 3. It contains 3 multiple-output current followers and it is based on the fact that frequency filters of the second order can be made by appropriate setting of integrators [32].

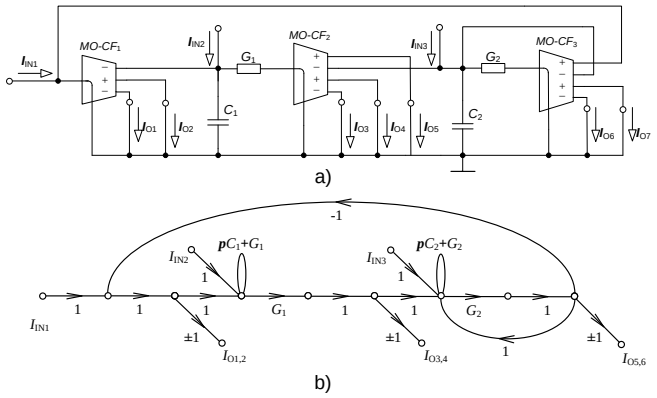

Fig. 3. 2nd order universal current-mode frequency filter presented in [32]

The denominator of all transfer functions of this filter is equal to:

$$D = s^2 C_1 C_2 + sC_2 G_1 + G_1 G_2. \quad (6)$$

Relation for the angular frequency and quality factor are:

$$\omega_0 = \sqrt{\frac{G_1 G_2}{C_1 C_2}}, \quad (7)$$

$$Q = \sqrt{\frac{G_2 C_1}{G_1 C_2}}, \quad (8)$$

where ω is angular frequency and Q is the filter quality factor.

From Fig. 3 can be seen that all current responses are taken directly from high impedance outputs of the active elements. The original circuit was presented with only one input, but further analysis paid to this circuit showed that there can be 3 basic inputs. Specific transfer function can be obtained from the particular output, or summing of some outputs:

$$I_{LP} = \frac{I_{O7}}{I_{IN1}} = \frac{I_{O1}}{I_{IN2}} = \frac{I_{O7}}{I_{IN2}} = \frac{I_{O3}}{I_{IN3}} = -\frac{I_{O6}}{I_{IN1}} = \\ = -\frac{I_{O2}}{I_{IN2}} = -\frac{I_{O6}}{I_{IN2}} = -\frac{I_{O4}}{I_{IN3}} = \frac{G_1G_2}{D}, \quad (9)$$

$$I_{BP} = \frac{I_{O4}}{I_{IN1}} = \frac{I_{O4}}{I_{IN2}} = \frac{I_{O1}+I_{O4}}{I_{IN3}} = \frac{I_{O7}+I_{O4}}{I_{IN3}} = \\ = --\frac{I_{O3}}{I_{IN1}} = -\frac{I_{O3}}{I_{IN2}} = -\frac{I_{O2}+I_{O3}}{I_{IN3}} = -\frac{I_{O6}+I_{O3}}{I_{IN3}} = \\ = \frac{sC_2G_1}{D}, \quad (10)$$

$$I_{HP} = \frac{I_{O2}+I_{O3}}{I_{IN1}} = -\frac{I_{O1}+I_{O4}}{I_{IN1}} = \frac{s^2C_1G_2}{D}, \quad (11)$$

$$I_{BS} = \frac{I_{O1}+I_{O4}+I_{O6}}{I_{IN1}} = -= \frac{I_{O2}+I_{O3}+I_{O7}}{I_{IN1}} = \\ = -\frac{s^2C_1G_2+G_1G_2}{D}, \quad (12)$$

$$I_{AP} = \frac{I_{O1}+I_{O4}+I_{O5}+I_{O6}}{I_{IN1}} = \\ = -\frac{s^2C_1G_2-sC_2G_1+G_1G_2}{D}. \quad (13)$$

The aim of designers of integrated circuits is that proposed filters should be universal. In other words, a filter should be able of realizing all types of filtering functions (low pass, band pass, high pass, band stop and all pass filter). From equations (9-13) is evident that this filter provides all types of the transfer functions, moreover, all types of these functions except an all pass filter are presented even in inverted form.

B. Proposal of new 2nd order universal current-mode frequency filters

Based on the rules of M-C graphs, new filters have been proposed using the filter presented in [32] as a pattern. First of them can been seen in Fig. 4. In this case, 2 digitally adjustable current amplifiers have been added. By changing the current gain of these amplifiers, the pole frequency of the filter can be adjusted independently of the quality factor. Fig. 5. shows the fully-differential version of the first proposed filter. Both F-D versions of proposed filters are designed with non-differential current followers instead of fully differential current followers (FDCFs) in order of easier implementation in form of PCB.

The denominator for the transfer functions of this filter is given by:

$$D = s^2C_1C_2 + sC_2G_1A_1 + G_1G_2A_1A_2. \quad (14)$$

In order to obtain particular transfer functions for the F-D filters factor A has to be replaced by $2A$ because of the differential gain of the DACA, which is twice higher than in case of S-E structures as is demonstrated by equation (5). The same applies for G_1, G_2 when their values must be twice higher than in case of S-E conductances. From equation (14) is obvious that in case $A_1 = A_2 = A$ it is possible to control the pole frequency of the filter independently of the quality factor of the filter by adjusting this parameter. That is proven by following relations expressing the relationship between the pole frequency and quality factor.

$$f_0 = \frac{A}{2\pi}\sqrt{\frac{G_1G_2}{C_1C_2}}, \quad (15)$$

$$Q = \sqrt{\frac{G_2C_1}{G_1C_2}}. \quad (16)$$

We can see that, Q is not depended on A parameter and that is why this parameter will not change when A is changing. Following equations represent the transfer functions of this filter:

$$I_{LP1} = -\frac{I_{O6}}{I_{IN1}} = -\frac{I_{O6}}{I_{IN2}} = \frac{I_{O5}}{I_{IN1}} = \frac{I_{O5}}{I_{IN2}} = \frac{G_1G_2A_1}{D}, \quad (17)$$

$$I_{LP2} = -\frac{I_{O3}}{I_{IN4}} = \frac{I_{O4}}{I_{IN4}} = \frac{G_1G_2A_2}{D}, \quad (18)$$

$$I_{LP3} = -\frac{I_{O6}}{I_{IN5}} = \frac{I_{O5}}{I_{IN5}} = \frac{G_1G_2A_1A_2}{D}, \quad (19)$$

$$I_{BP1} = -\frac{I_{O4}}{I_{IN1}} = -\frac{I_{O4}}{I_{IN2}} = \frac{I_{O3}}{I_{IN1}} = \frac{I_{O3}}{I_{IN2}} = \frac{sC_2G_1}{D}, \quad (20)$$

$$I_{BP2} = \frac{I_{O6}}{I_{IN3}} = -\frac{I_{O5}}{I_{IN3}} = \frac{sC_1G_2A_1}{D}, \quad (21)$$

$$I_{BP3} = -\frac{I_{O2}}{I_{IN4}} = \frac{I_{O1}}{I_{IN4}} = \frac{sC_1G_2A_2}{D}, \quad (22)$$

$$I_{BP4} = -\frac{I_{O4}}{I_{IN5}} = \frac{I_{O3}}{I_{IN5}} = \frac{sC_2G_1A_1A_2}{D}, \quad (23)$$

$$I_{HP1} = -\frac{I_{O2}}{I_{IN1}} = \frac{I_{O1}}{I_{IN1}} = \frac{s^2C_1C_2}{D}, \quad (24)$$

$$I_{HP2} = -\frac{I_{O2}}{I_{IN5}} = \frac{I_{O1}}{I_{IN5}} = \frac{s^2C_1C_2A_2}{D}, \quad (25)$$

$$I_{BS1} = -\frac{I_{O2}+I_{O6}}{I_{IN1}} = \frac{I_{O1}+I_{O5}}{I_{IN1}} = \frac{s^2C_1C_2+G_1G_2A_1}{D}, \quad (26)$$

$$I_{BS2} = -\frac{I_{O2}+I_{O6}}{I_{IN5}} = \frac{I_{O1}+I_{O5}}{I_{IN5}} = \\ = \frac{s^2C_1C_2A_2+G_1G_2A_1A_2}{D}, \quad (27)$$

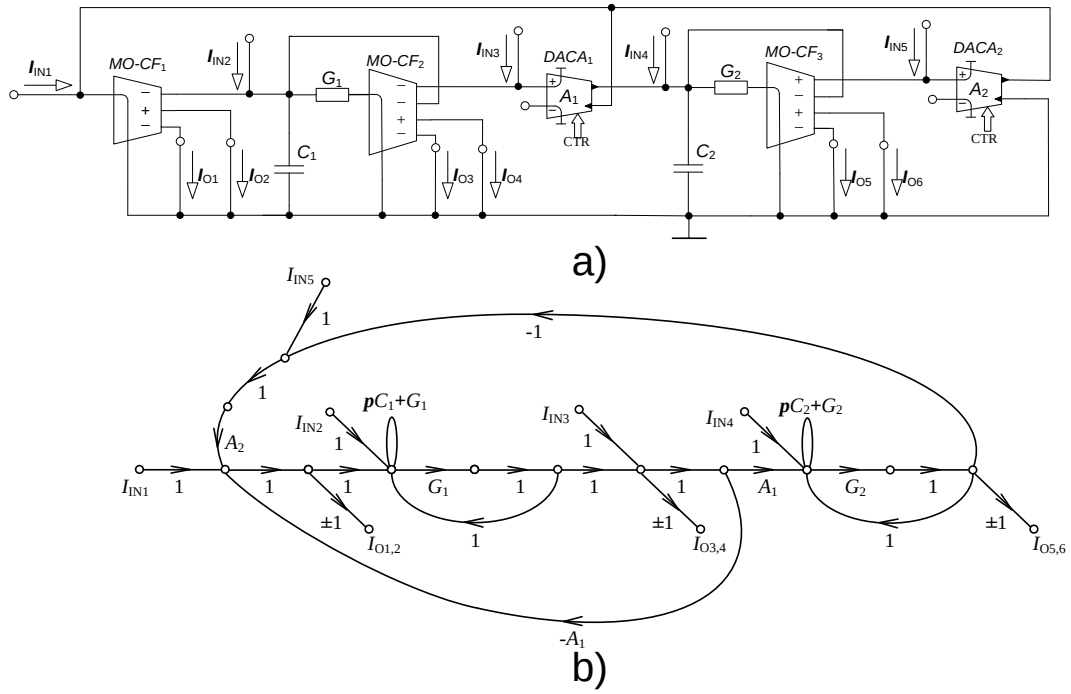

Fig. 4. First proposed 2nd order universal current-mode frequency using 2 DACAs S-E version a) scheme, b) signal-flow graph

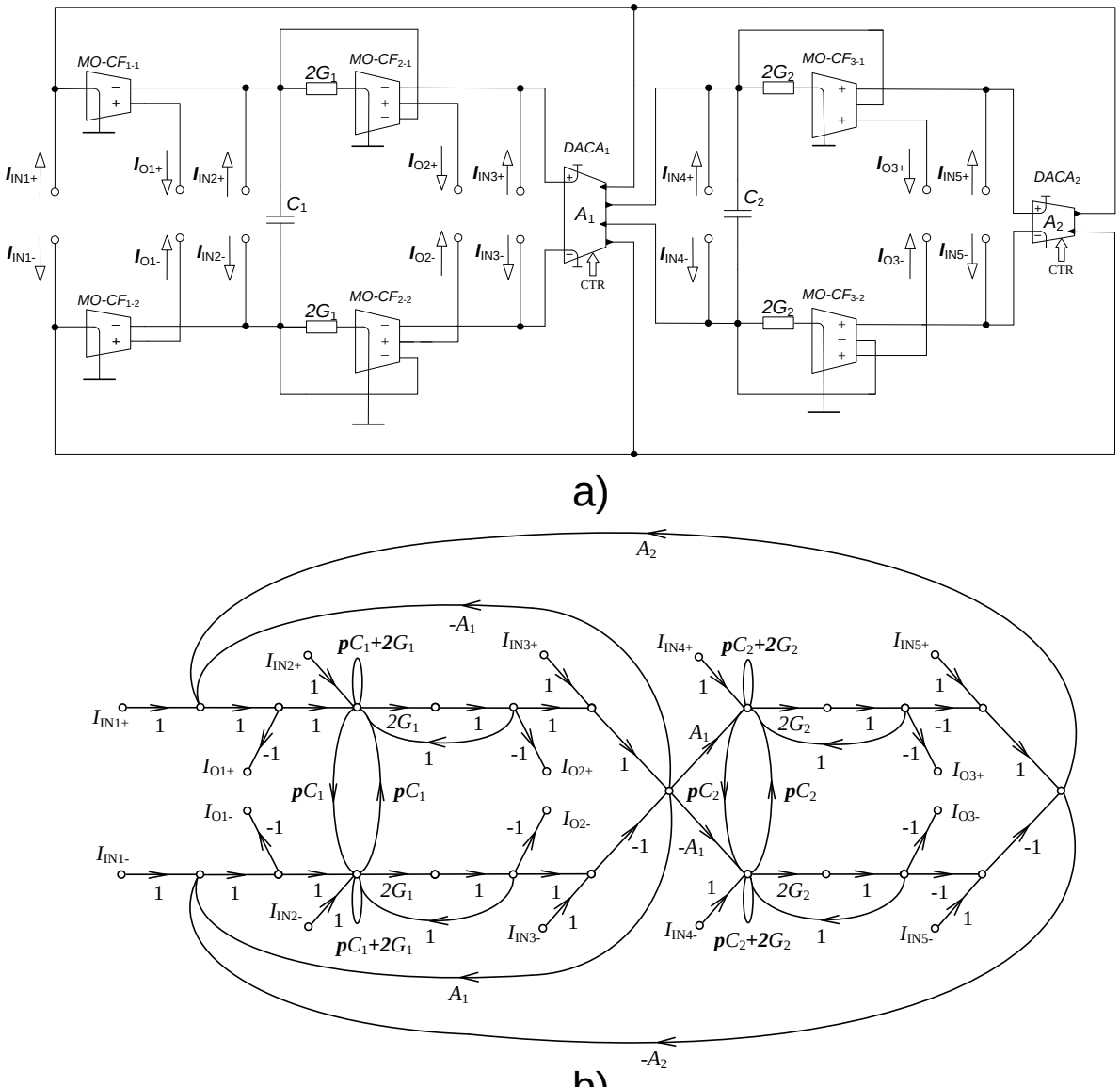

Fig. 5. First proposed 2nd order universal current-mode frequency using 2 DACAs F-D version a) scheme, b) signal-flow graph

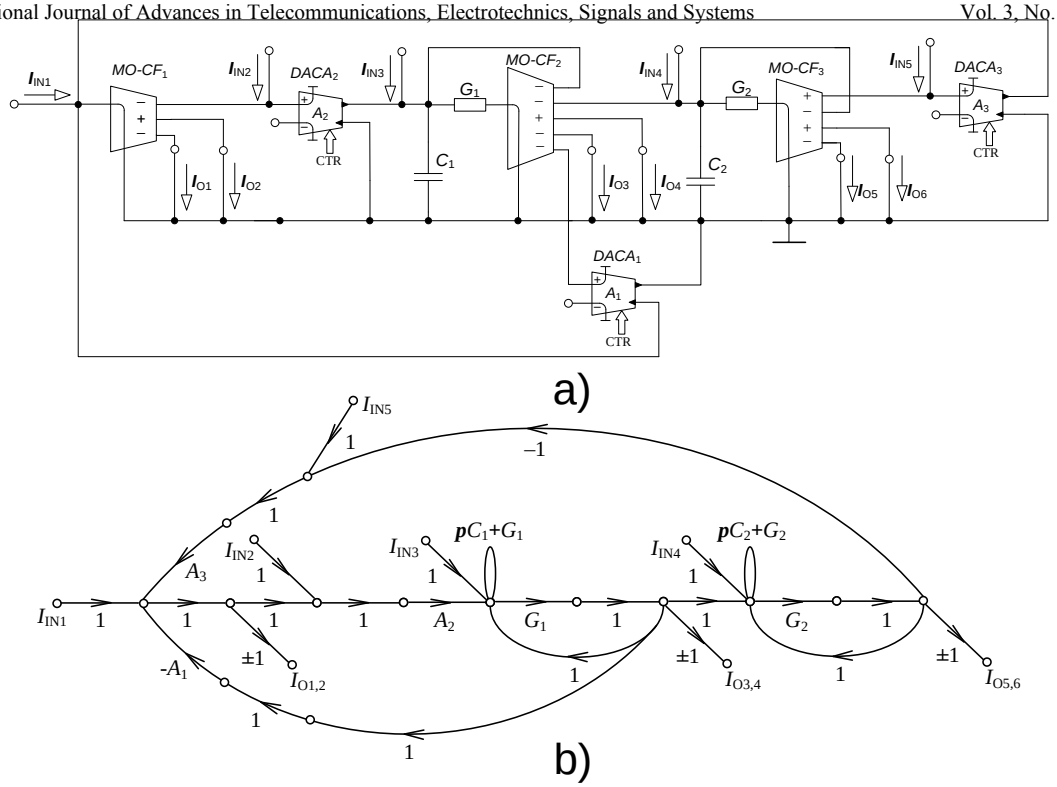

Fig. 6. Second proposed 2nd order universal current-mode frequency using 3 DACAs S-E version a) scheme, b) signal-flow graph

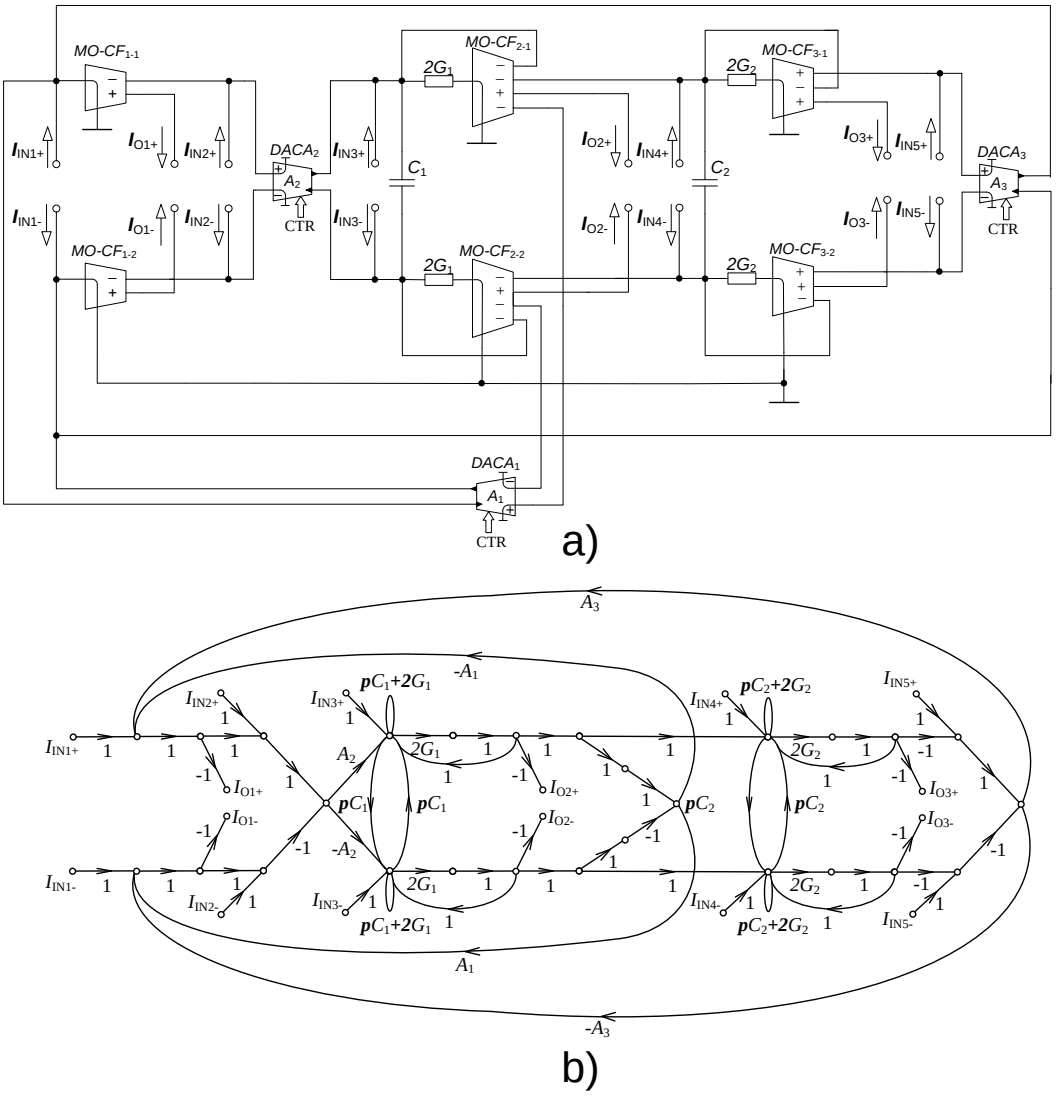

Fig. 7. Second proposed 2nd order universal current-mode frequency using 3 DACAs F-D version a) scheme, b) signal-flow graph

$$I_{AP1} = -\frac{I_{O2} + I_{O3} + I_{O6}}{I_{IN1}} = \frac{I_{O1} + I_{O4} + I_{O5}}{I_{IN1}} = \\ = \frac{s^2 C_1 C_2 - sC_2 G_1 + G_1 G_2 A_1}{D}, \quad (28)$$

$$I_{AP2} = -\frac{I_{O2} + I_{O3} + I_{O6}}{I_{IN5}} = \frac{I_{O1} + I_{O4} + I_{O5}}{I_{IN5}} = \\ = \frac{s^2 C_1 C_2 A_2 - sC_2 G_1 A_2 + G_1 G_2 A_1 A_2}{D}, \quad (29)$$

where A_1, A_2 is a current gain of $DACA_1$, $DACA_2$ respectively.

These equations show the fact that we can obtain high pass transfer function directly from the outputs of MO-CF1 to compare to previous circuit when it was necessary to sum two appropriate outputs in order to get high pass transfer function. This applies for the filter with 3 DACAs, too, that will be presented later.

Figure 6 and Fig. 7 respectively show a single-ended and fully-differential version of the filter using 3 digitally adjustable current amplifiers. That allows us to control both the pole frequency and quality filter independently of each other.

Parameter A_1 is used to adjust the quality factor. By common change of parameters A_2 and A_3 we can set the pole frequency of the filter.

The denominator of this filter is:

$$D = s^2 C_1 C_2 + sC_2 G_1 A_1 A_2 + G_1 G_2 A_2 A_3. \quad (30)$$

This equation gives the possibility of controlling of the pole frequency and quality factor independently of each other by adjusting A_1 in order to change the quality factor and simultaneous change of A_2 and A_3 when $A_2 = A_3 = A$ to control the pole frequency as is proven by:

$$f_0 = \frac{A}{2\pi}\sqrt{\frac{G_1 G_2}{C_1 C_2}}, \quad (31)$$

$$Q = \frac{1}{A_1}\sqrt{\frac{G_2 C_1}{G_1 C_2}}. \quad (32)$$

The transfer functions are described by:

$$I_{LP1} = -\frac{I_{O6}}{I_{IN1}} = \frac{I_{O5}}{I_{IN1}} = -\frac{I_{O6}}{I_{IN2}} = \frac{I_{O5}}{I_{IN2}} = \frac{G_1 G_2 A_2}{D}, \quad (33)$$

$$I_{LP2} = -\frac{I_{O6}}{I_{IN3}} = \frac{I_{O5}}{I_{IN3}} = \frac{G_1 G_2}{D}, \quad (34)$$

$$I_{LP3} = -\frac{I_{O3}}{I_{IN4}} = \frac{I_{O4}}{I_{IN4}} = -\frac{I_{O6}}{I_{IN5}} = \frac{I_{O5}}{I_{IN5}} = \frac{G_1 G_2 A_2 A_3}{D}, \quad (35)$$

$$I_{BP1} = -\frac{I_{O4}}{I_{IN1}} = \frac{I_{O3}}{I_{IN1}} = -\frac{I_{O4}}{I_{IN2}} = \frac{I_{O3}}{I_{IN2}} = \frac{sC_2 G_1 A_2}{D}, \quad (36)$$

$$I_{BP2} = -\frac{I_{O4}}{I_{IN3}} = \frac{I_{O3}}{I_{IN3}} = \frac{sC_2 G_1}{D}, \quad (37)$$

$$I_{BP3} = -\frac{I_{O2}}{I_{IN4}} = \frac{I_{O1}}{I_{IN4}} = \frac{sC_1 G_2 A_3}{D}, \quad (38)$$

$$I_{BP4} = -\frac{I_{O4}}{I_{IN5}} = \frac{I_{O3}}{I_{IN5}} = \frac{sC_2 G_1 A_2 A_3}{D}, \quad (39)$$

$$I_{HP1} = -\frac{I_{O2}}{I_{IN1}} = \frac{I_{O1}}{I_{IN1}} = \frac{s^2 C_1 C_2}{D}, \quad (40)$$

$$I_{HP2} = -\frac{I_{O2}}{I_{IN5}} = \frac{I_{O1}}{I_{IN5}} = \frac{s^2 C_1 C_2 A_3}{D}, \quad (41)$$

$$I_{BS1} = -\frac{I_{O2} + I_{O6}}{I_{IN1}} = \frac{I_{O1} + I_{O5}}{I_{IN1}} = \frac{s^2 C_1 C_2 + G_1 G_2 A_2}{D}, \quad (42)$$

$$I_{BS2} = -\frac{I_{O2} + I_{O6}}{I_{IN5}} = \frac{I_{O1} + I_{O5}}{I_{IN5}} = \\ = \frac{s^2 C_1 C_2 A_3 + G_1 G_2 A_2 A_3}{D}, \quad (43)$$

$$I_{AP} = -\frac{I_{O2} + I_{O3} + I_{O6}}{I_{IN1}} = \frac{I_{O1} + I_{O4} + I_{O5}}{I_{IN1}} = \\ = \frac{s^2 C_1 C_2 - sC_2 G_1 A_2 + G_1 G_2 A_2}{D}, \quad (44)$$

$$I_{AP} = -\frac{I_{O2} + I_{O3} + I_{O6}}{I_{IN5}} = \frac{I_{O1} + I_{O4} + I_{O5}}{I_{IN5}} = \\ = \frac{s^2 C_1 C_2 A_3 - sC_2 G_1 A_2 A_3 + G_1 G_2 A_2 A_3}{D}, \quad (45)$$

where A_1, A_2 and A_3 are current gains of $DACA_1$, $DACA_2$ and $DACA_3$.

Transfer functions which correspond with a specific term of the denominator of the filter have unity gain in pass-band area regardless values of A parameters, therefore, these transfer functions are most advantageous. That applies for transfer functions from equations (19), (24), (35) and (40). Band pass transfer functions containing C_1 capacitor instead of C_2 which is involved in both denominates of proposed filters have not unity gain and the smallest attenuation starts at -5 dB. That applies for equations (21), (22) and (38). Other transfer functions change their gain according values of parameter *A*. In case of proposed filters from Figs. 4 and 5 when comparing low pass transfer functions namely equations (17), (18) and (19), low pass transfer function from equation (17) using I_{IN2} has greater attenuation at higher frequencies.

The same applies for band pass transfer functions from equation (20) when using I_{IN2} and equation (21). Comparing high pass and band stop functions, transfer function from equations (24) and (26) have slightly greater attenuation at higher frequencies. Transfer functions of proposed filters from Figs. 6 and 7 provide greater attenuation at higher frequencies in case of low pass and band pass functions from equations (34), (37) and then (33) and (36) when I_{IN2} input is

used. High pass and band stop functions from equations (40) and (42) provide slightly greater attenuation at higher frequencies. Comparison has been carried out using starting values of specific filter parameters specified in chapter 4.

IV. SIMULATIONS

To verify appropriate functions of proposed filters, simulations of these circuits were carried out using simulating program OrCAD and Snap. Some simulation results are included in this paper for illustration. All output responses illustrated in Figs. 8, 9, 12, 13, 14, 17 and 18 are inverting filtering functions. Output responses illustrated in Figs. 10, 11, 15 and 16 are non-inverting. Models of active elements used in simulations are shown in Fig. 1 and 2 in chapter 1. Following values of specific filter parameters have been chosen for PSpice simulations the starting pole frequency f_0 = 1 MHz, Butterworth approximation Q = 0.707 (starting value), $C_1 = C_2$ = 100 pF and starting values of parameters $A_1 = A_2 = A_3$ = 1 (half values in case of F-D filters). Because a real part of DACA is still in the testing phase we are using alternative element which allows us to set any value of its gain in range of 0-5 continuously, therefore, values chosen to verify ability to change the pole frequency or quality factor of proposed filters are solely demonstrational and do not necessary correspond with values which can be obtained using a real element of DACA amplifier. Remaining values of passive elements were calculated according equation (46), (47) respectively.

$$R_1 = \frac{Q}{2\pi f_0 C_1} = 1125\Omega \tag{46}$$

$$R_2 = \frac{1}{4\pi^2 f_0^2 C_1 C_2 R_1} = 2252\Omega \tag{47}$$

Proposed fully-differential filters are designed that way they have almost the same transfer functions as proposed single-ended filters due to modified values of passive elements:

$$R_1 = \frac{1125}{2} = 563\Omega \tag{48}$$

$$R_2 = \frac{2252}{2} = 1126\Omega \tag{49}$$

In order to obtain particular transfer functions for the F-D filters factor A has to be replaced by 2A because of the differential gain of DACA, which is twice higher than in case of S-E structures as is demonstrated by equation (5).

Outputs of both S-E and F-D filter structures with 2 DACAs from Fig. 4 and Fig. 5 can be seen in Fig 8 when I_{IN1} input has been used and output responses are taken from outputs I_{O2} (blue line), I_{O4} (red line), I_{O6} (green line) and I_{O2} + I_{O6} (turquoise line) in case of S-E form of the filter and I_{O1} (blue line), I_{O2} (red line), I_{O3} (green line) and I_{O1} + I_{O3} (turquoise line) for F-D form.

Gain, delay and phase characteristics of all pass filter can be seen in Fig. 9 when outputs I_{O2} + I_{O3} + I_{O6} for S-E form and I_{O1} + I_{O2} + I_{O3} in case of F-D form were used. From the graph can be see that the filter is suitable only approximately up to frequency of 10 MHz because of bandwidth limitations of used active elements. The same applies for the second proposed filter.

Figure 10 shows the transient analysis of this all pass filter where blue line represents the input signal, red and green lines are the output responses of S-E form, F-D form respectively. Amplitude of the input signal has been set to 1 mA and frequency 1 MHz when the signal of non-inverting output should have its phase shifted of 180° opposed to the input signal. From the picture can be seen that the F-D filter is closer to the expected value.

Transient analysis of band-pass transfer functions of filters from Figs. 4 and 5 can be seen in Fig. 11. Graph shows the input signal and output responses of band-pass transfer functions of filters from Figs. 4 and 5 to a unit step of value of 1mA when I_{IN1} input and I_{O3} output in case of S-E filter and I_{O2} output in case of F-D filter have been used. It's important to note that used simulation models of active elements are designed mainly for AC analysis. That also applies for transient analysis of filters from Figs. 6 and 7.

Figure 12 demonstrates possibility of adjusting the pole frequency of proposed S-E filter by changing the current gain of DACAs when I_{IN1} input has been used and output responses are taken from output I_{O2} in case of S-E form and I_{O1} in case of F-D form. Values of parameter A have been set $A_1 = A_2 = \{0.5, 1, 2\}$. Calculated values of the pole frequency for both S-E and F-D solutions and for chosen values of parameter A were {499.95 kHz, 999.91 kHz, 1999.81 kHz}. Measured values obtained from simulation were {466.48 kHz, 921.54 kHz, 1816.23 kHz} for S-E form of proposed filter using 2 DACAs and {479.34 kHz, 942.31 kHz, 1846.38 kHz} in case of F-D form.

Figure 13 shows the transfer functions of S-E and F-D filters with 3 DACAs from Fig. 6 and Fig. 7. The input used in this case is I_{IN1} and output responses are taken from outputs I_{O2} (blue line), I_{O4} (red line), I_{O6} (green line) and I_{O2} + I_{O6} (turquoise line) in case of S-E form and I_{O1} (blue line), I_{O2} (red line), I_{O3} (green line) and I_{O1} + I_{O3} (turquoise line) for F-D form.

Figure 14 shows delay and phase characteristics of all pass filter when outputs I_{O2} + I_{O3} + I_{O6} for S-E form and I_{O1} + I_{O2} + I_{O3} in case of F-D form were used.

The transient analysis of this all pass filter can be seen in Fig. 15 where blue line represents the input signal, red and green lines are the output responses of S-E form, F-D form respectively. Parameters of the input signal have been chosen evenly like for the previous all pass filter, consequently, amplitude of the input was 1 mA and frequency 1 MHz. From the picture can be again seen that the output response of the F-D filter is closer to the expected value.

Figure 16 shows the input signal and output responses of band-pass transfer functions of filters from Figs. 6 and 7 to a unit step of value of 1mA when I_{IN1} input and I_{O3} output in case of S-E filter and I_{IN1} output in case of F-D filter have been used.

The ability of tuning parameters quality factor Q and pole frequency f_0 independently of each other can be seen in Fig. 17, 18 respectively. The input was I_{IN1} and the output responses were I_{O2} (S-E form), I_{O1} (F-D form) when the possibility of controlling f_0 has been analyzed and I_{O4} (S-E form) and I_{O2} (F-D form) in case of quality factor adjusting. Gains of DACAs were set as follow A_1 = {0.1, 0.5, 1} and A_2, A_3 = {0.5, 1, 2}. Calculated values of the pole frequency were the same as for previously described filter. Measured values obtained from simulation for the S-E form were

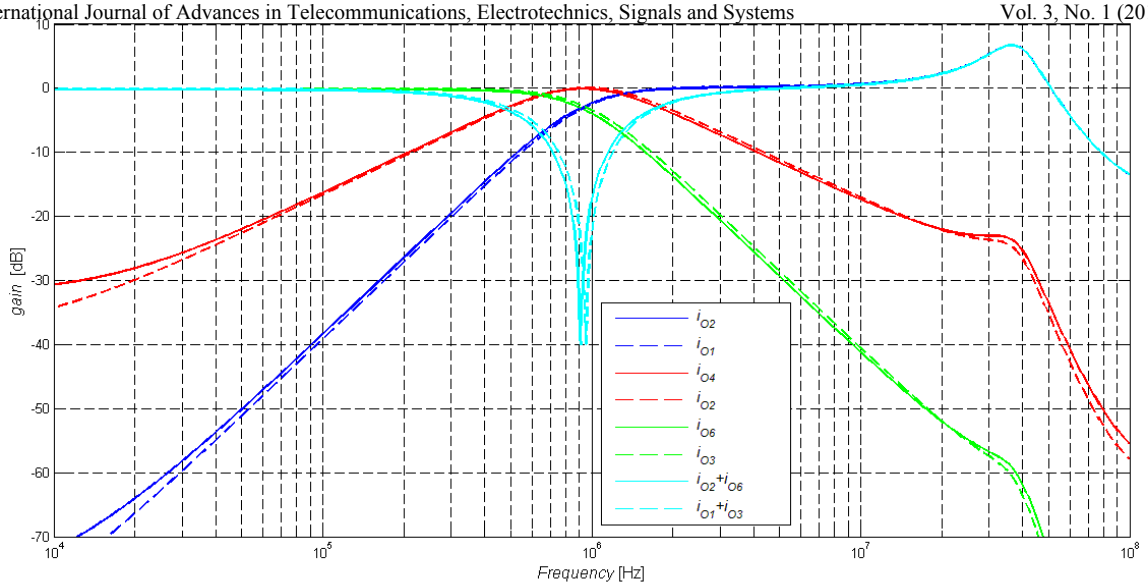

Fig. 8. Output responses of the S-E filter from Fig. 4 (solid lines) and of the F-D filter from Fig. 5 (dashed lines): high pass, band pass, low pass, band stop when I_{IN1} has been used

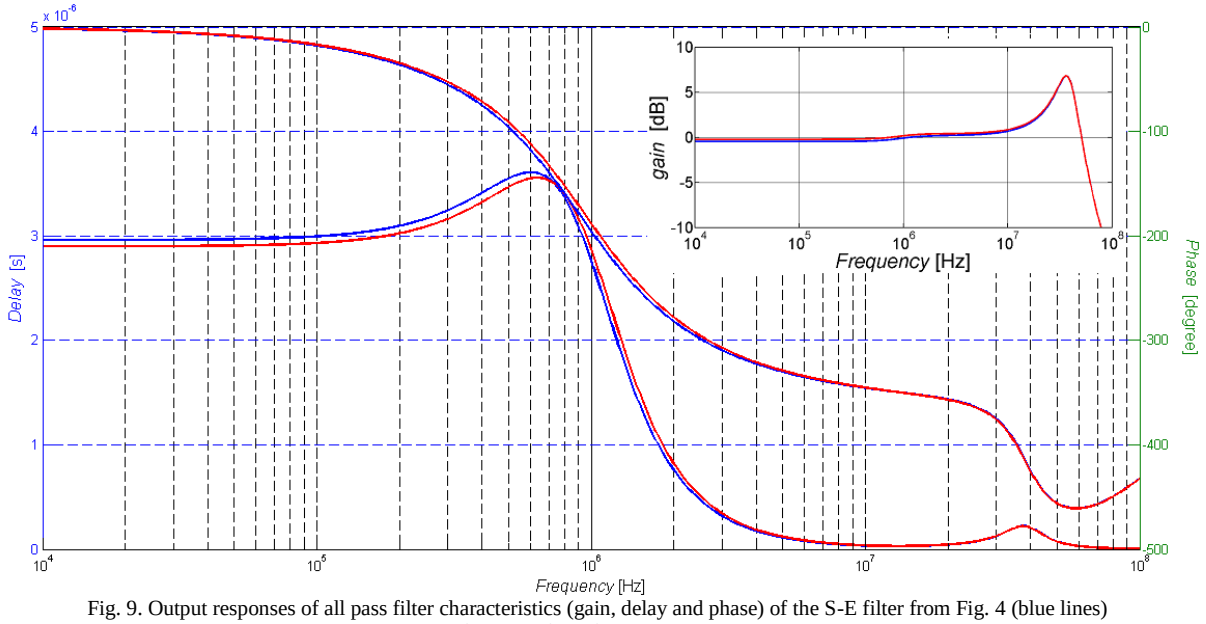

Fig. 9. Output responses of all pass filter characteristics (gain, delay and phase) of the S-E filter from Fig. 4 (blue lines) and of the F-D filter from Fig. 5 (red lines)

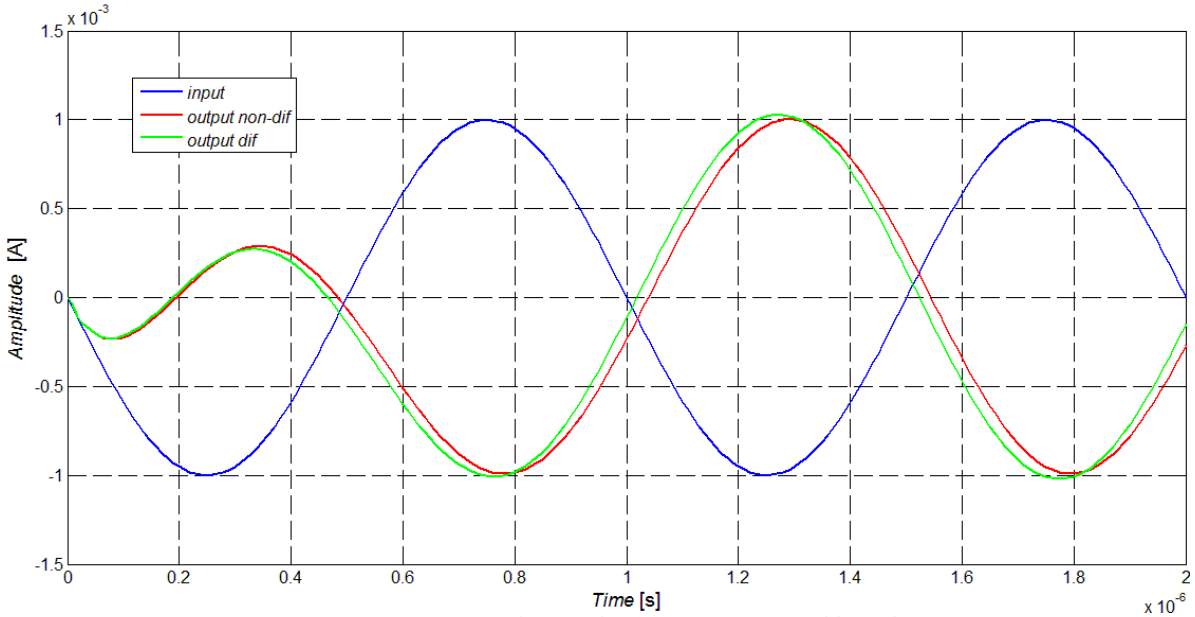

Fig. 10. Input signal and output responses of all pass filter (transient analysis) of filters from Figs. 4 and 5 when the input frequency was 1 MHz and amplitude 1 mA

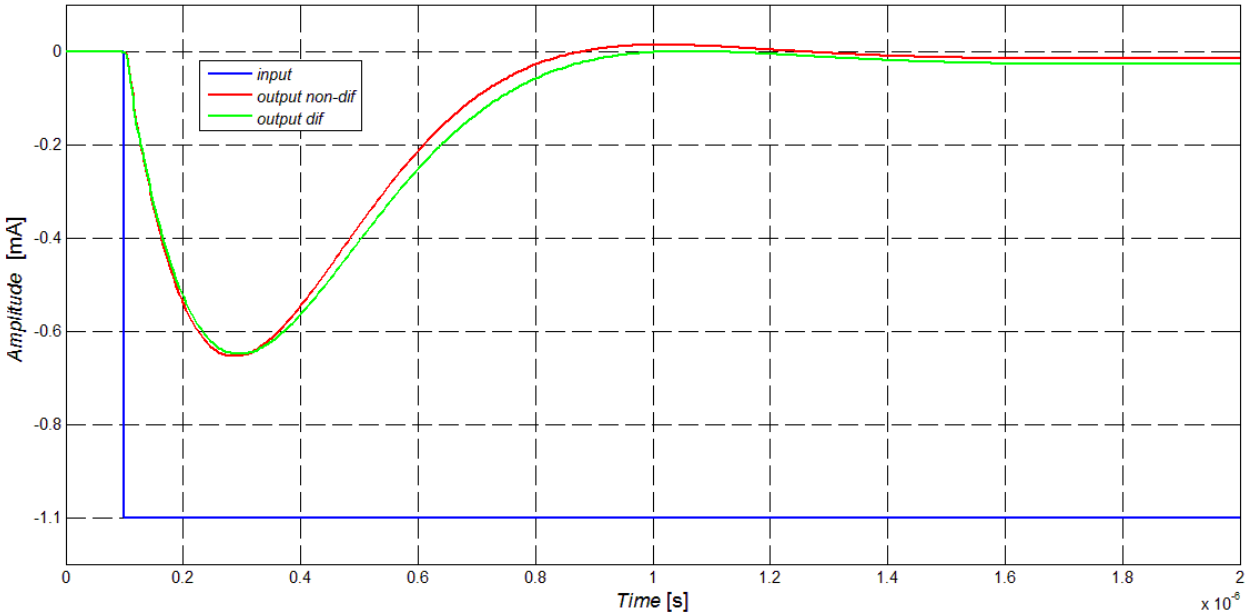

Fig. 11. Input signal and output responses of band-pass filtering functions of proposed filters from Figs. 4 and 5 to a unit step signal of value of 1mA

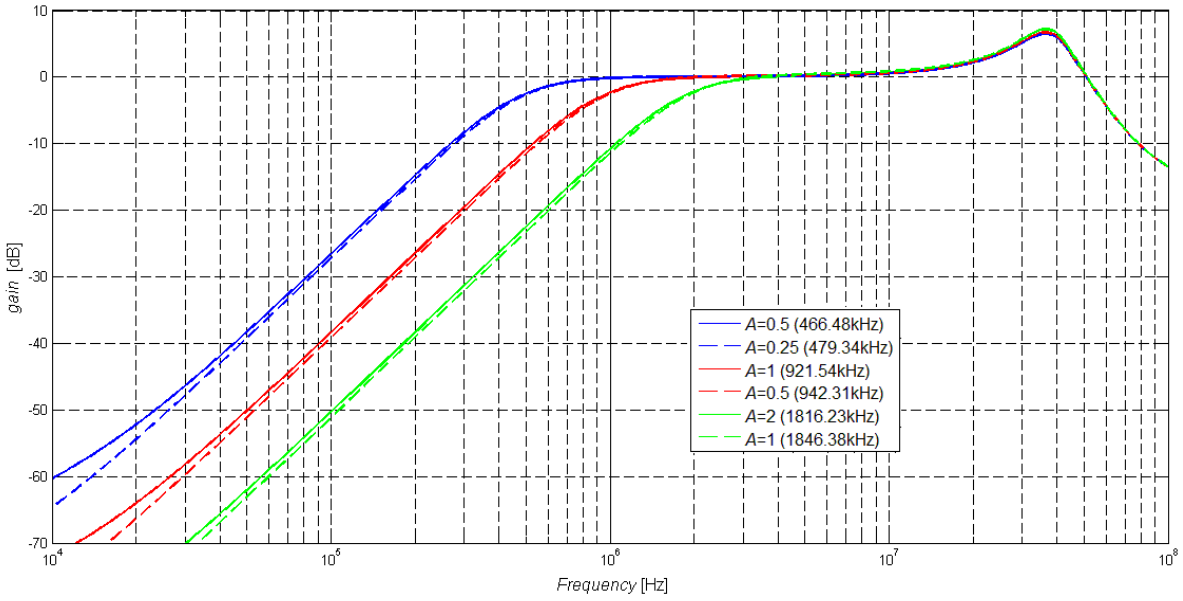

Fig. 12. Demonstration of controlling f_0 in case of the S-E filter from Fig. 4 (solid lines) and of the F-D filter from Fig. 5 (dashed lines) when $A_1 = A_2$ were set 0.5, 1, and 2

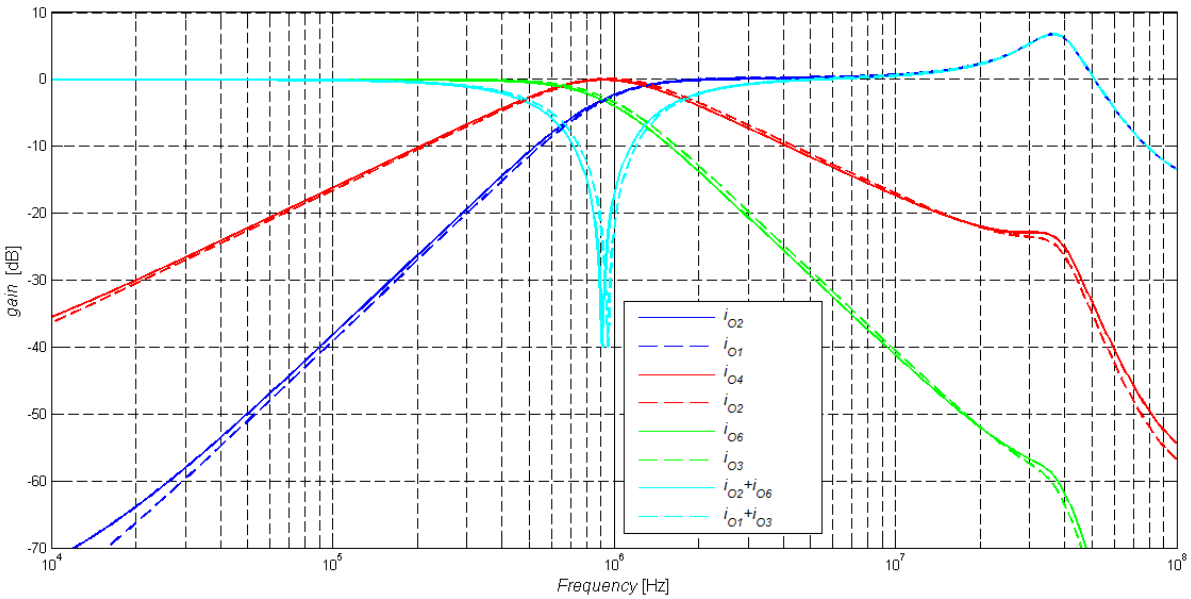

Fig. 13. Output responses of the S-E filter from Fig. 6 (solid lines) and pf the F-D filter from Fig. 7 (dashed lines): high pass, band pass, low pass, band stop when I_{IN1} has been used

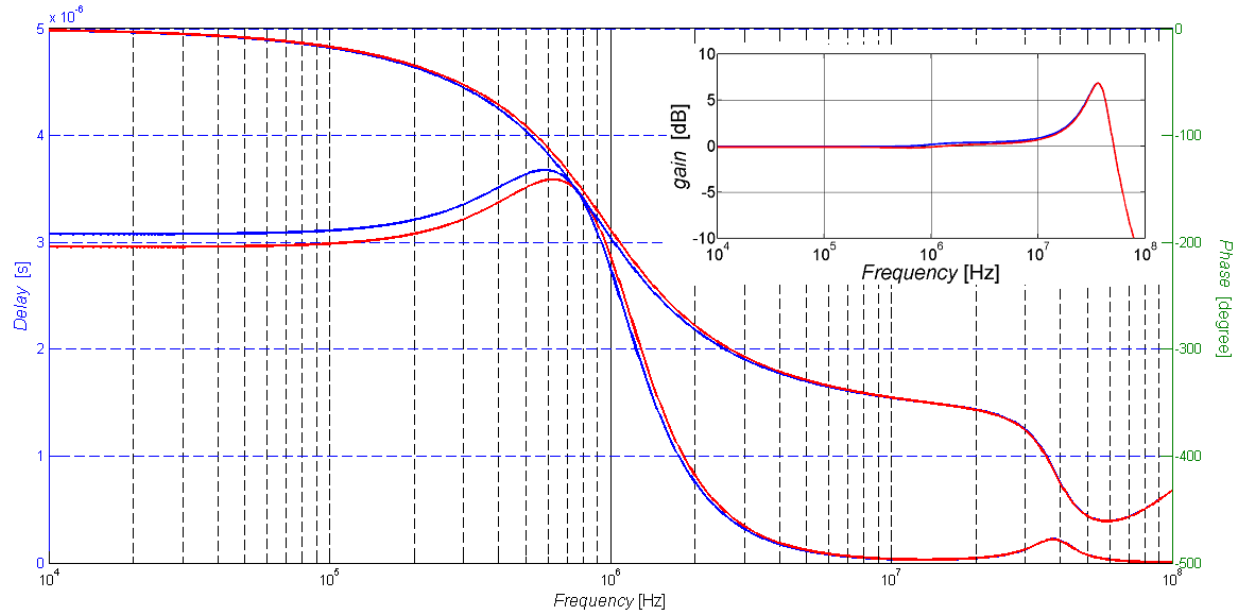

Fig. 14. Output responses of All pass filter characteristics (gain, delay and phase) of the S-E filter from Fig. 4 (blue lines) and of the F-D filter from Fig. 5 (red lines)

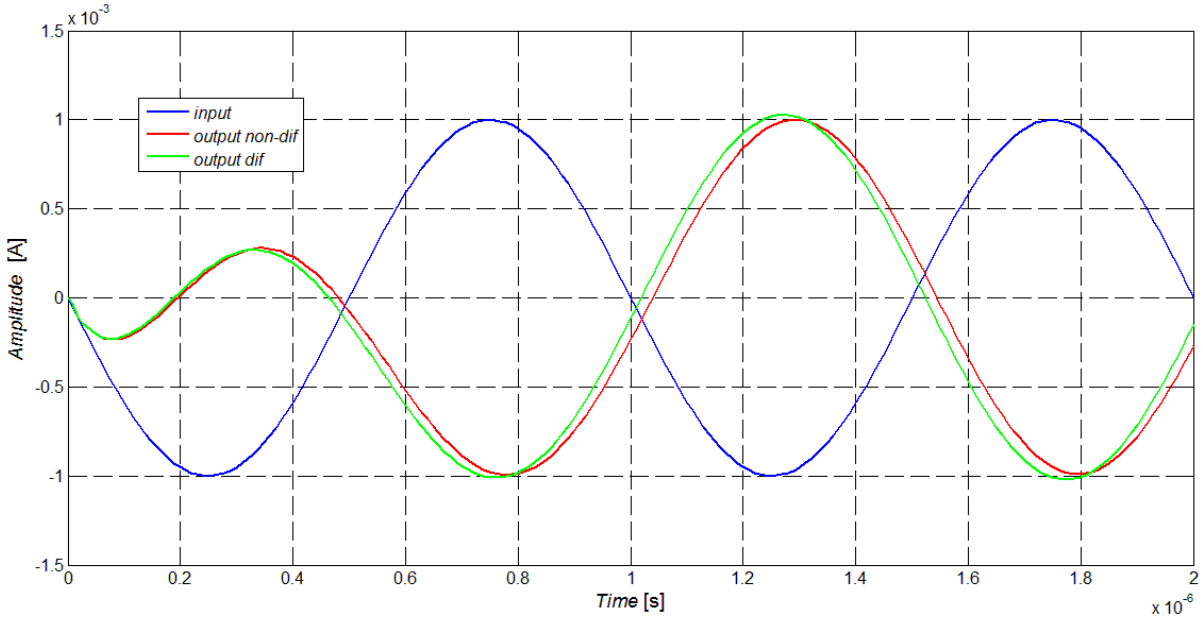

Fig. 15. Input signal and output responses of all pass filter (transient analysis) of filters from Figs. 6 and 7 when the input frequency was 1 MHz and amplitude 1 mA

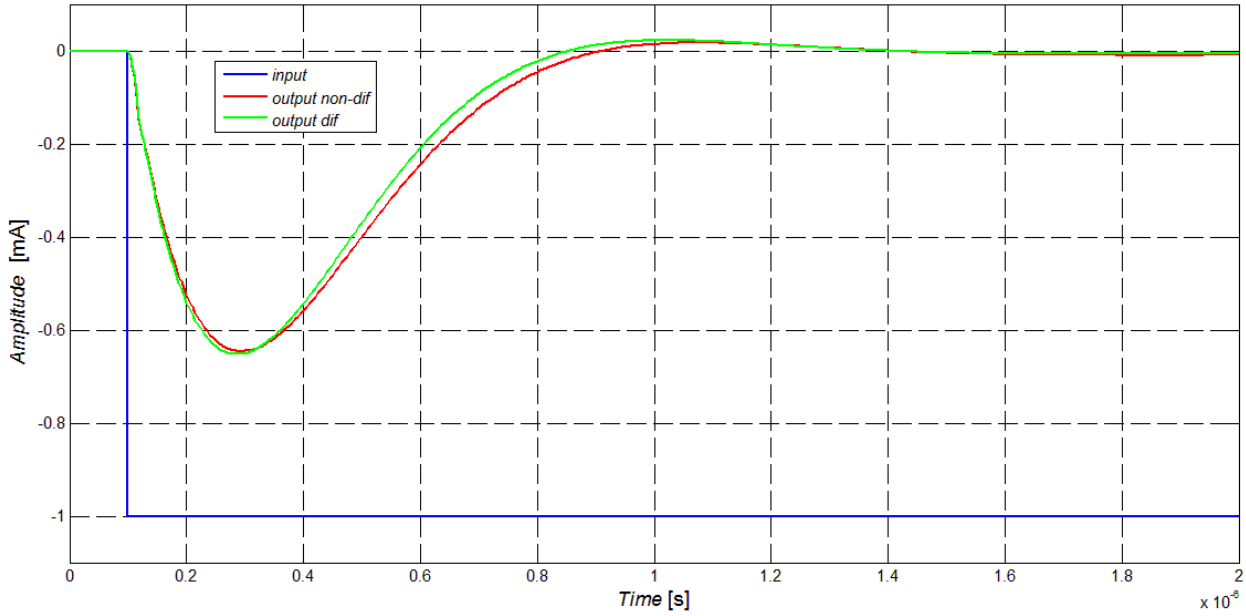

Fig. 16. Input signal and output responses of band-pass filtering functions of proposed filters from Figs. 6 and 7 to a unit step signal of value of 1mA

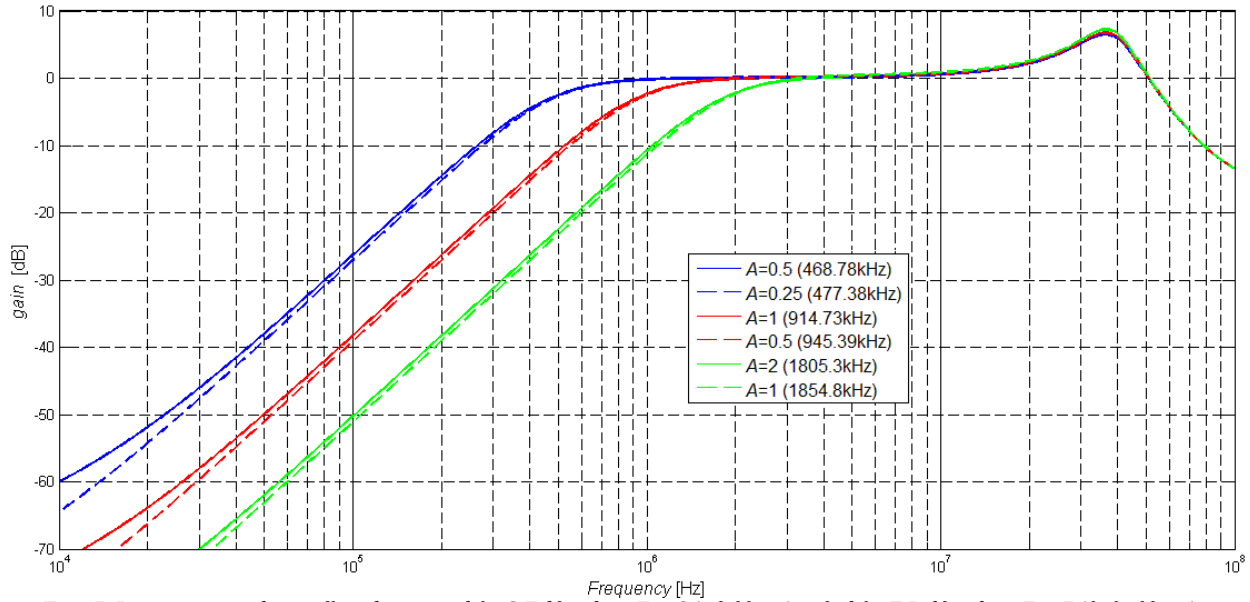

Fig. 17. Demonstration of controlling f_0 in case of the S-E filter from Fig. 6 (solid lines) and of the F-D filter from Fig. 7 (dashed lines) when $A_2 = A_3$ were set 0.5, 1, and 2

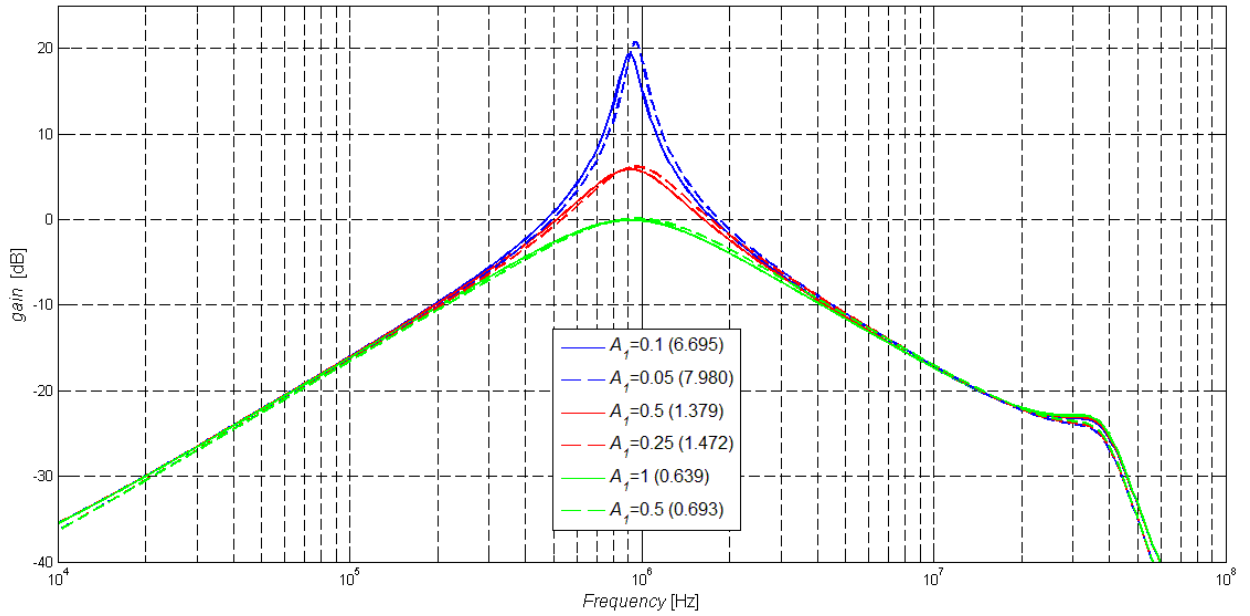

Fig. 18. Demonstration of controlling Q for the S-E filter from Fig. 6 (solid lines) and of the F-D filter from Fig. 7 (dashed lines) when A_1 was set 0.1, 0.5, and 1

{468.78 kHz, 914.73 kHz, 1805.3 kHz} and {477.38 kHz, 945.39 kHz, 1854.8 kHz} in case of the F-D form. Calculated values of the quality factor were {7.068, 1.414, 0.707} and simulated for the S-E form {6.695, 1.379, 0.639} and {7.980, 1.472, 0.693}.

From Figs. 8-18 we can compare S-E and F-D output responses of proposed filters. The graphs show magnitude responses of non-inverting low pass, band pass and high-pass transfer functions. The F-D filters provide a slightly higher attenuation than the S-E structures. In this case the difference is most probably caused by unequal values of resistors since the values of resistors used in F-D structures must be a half of resistance used for S-E structures to obtain the same transfer functions. The pole frequencies of F-D filters are also closer to calculated values. Simulation results shown in Fig. 12, Fig. 17 and Fig. 18 confirm the ability of controlling the pole frequency and quality factor of proposed filters.

V. Conclusion

Two new 2nd order universal filters proposed using signal-flow graphs method were presented in this paper. Both filters operate in the current-mode and both filters were proposed in single-ended and fully-differential form. In both proposals were placed digitally adjustable current amplifiers (DACAs) to control the pole frequency and quality factor of the filters. First designed filter uses 2 DACAs to adjust the pole frequency independently of the quality factor. In case of the second proposed filter there are used 3 DACAs to control both the pole frequency and quality factor independently of each other. From transfer functions of proposed circuits it is obvious that the filters are universal. Simulations verified functions of proposed circuits and some of them are included for illustration to compare S-E and F-D structures and illustrating possibility of controlling the pole frequency and quality factor.

ACKNOWLEDGEMENT

Research described in this letter is supported by Czech Science Foundation project 102/09/1681. The described research was performed in laboratories supported by the SIX project; the registration number CZ.1.05/2.1.00/03.0072, the operational program Research and Development for Innovation.

REFERENCES

[1] J. JERABEK, J. KOTON, K. VRBA, "A Generalized Method of Multifunctional Frequency Filter Design" (Zobecněná metoda návrhu multifunkčních kmitočtových filtrů), *Elektrorevue - Internet Journal* (http://www.elektrorevue.cz), No. 41, 2007, pp. 41-1 - 41-10.

[2] N. HERENCSAR, K. VRBA, " The Common Approach to Designing of Frequency Filters Based on Autonomous Circuits" (Obecný přístup k návrhu kmitočtových filtrů pomocí autonomních obvodů), *Elektrorevue - Internet Journal* (http://www.elektrorevue.cz), No. 40, 2006, pp. 40-1 - 40-17.

[3] J. KOTON, K. VRBA, "Designing of Frequency Filters Using Autonomous Circuit With a Full Admittance Network" (Návrh kmitočtových filtrů pomocí autonomního obvodu s úplnou sítí admitancí), *Elektrorevue - Internet Journal* (http://www.elektrorevue.cz), No. 33, 2005.

[4] J. KOTON, K. VRBA, "Zobecněné metody návrhu kmitočtových filtrů" (Generalized Methods of Frequency Filter Design), *Elektrorevue - Internet Journal* (http://www.elektrorevue.cz), No. 26, 2008, pp. 26-1 - 26-17.

[5] J. KOTON, K. VRBA, "Electronically Tunable Frequency Filters Based on Transformation Cells", In *The Third International Conference Systems*, Cancun, 2008, pp. 260-264.

[6] P. BRANDSTETTER, L. KLEIN, "Design of Frequency Filters by Method of Synthetic Immittance Elements with Current Conveyors", In Proc. *International Conference Applied Electronics (AE)*, Pilsen, Czech Republic, Sep. 2012, pp. 37 - 40.

[7] J. JERABEK, K. VRBA, " The Proposal of Tunable Frequency Filter With Current Active Elements Using Signal-Flow Graphs Method" (Návrh přeladitelného kmitočtového filtru s proudovými aktivními prvky za pomoci metody grafu signálových toků), *Elektrorevue - Internet Journal* (http://www.elektrorevue.cz), No. 42, 2009, pp. 42-1 - 42-7.

[8] K. INTAWICHAI, W. TANGSRIRAT, "Signal-Flow Graph Realization of nth-Order Current-Mode Allpass Filters Using CFTAs", In Proc. *The 10th International Conference Electrical Engineering/Electronics, Computer, Telecommunications and Information Technology (ECTI-CON)*, Krabi, Thailand, May 2013, pp. 1 - 6.

[9] E. YUCE, "Current-mode electronically tunable biquadratic filters consisting of only CCCIIs and grounded capacitors", *Microelectronics Journal*, Vol. 40, No. 12, Dec. 2009, pp. 1719-1725.

[10] M. KUMNGERN, "Multiple-input single-output current-mode universal filter using translinear current conveyors", *Journal of Electrical and Electronics Engineering Research*, Vol. 3(9), Nov. 2011, pp. 162-170.

[11] H. CHEN, "Current-mode dual-output ICCII-based tunable universal biquadratic filter with low-input and high-output impedances", *Int. J. Circuit Theory and Applications*, 2012, DOI: 10.1002/cta.1858.

[12] S. MINAEI', M. A. IBRAHIP, H. KUNTUAN, "A New Current-Mode KHN-Biquad Using Differential Voltage Current Conveyor Suitable for IF Stages", *In Proc. The Seventh International Symposium Signal Processing and Its Applications*, Paris, France, 2003, Vol. 1 , Jul. 2003, pp. 249 - 252.

[13] H. CHEN, "Tunable versatile current-mode universal filter based on plus-type DVCCs", *AEU - International Journal of Electronics and Communications*, Vol. 66, No. 4, Apr. 2012, pp. 332–339.

[14] M. T. ABUELMA'ATTI, A. BENTRCIA, "A novel mixed-mode OTA-C universal filter", *International Journal of Electronics*, Vol. 92, No. 7, 2005, pp. 375-383.

[15] CH. LEE, "Multiple-Mode OTA-C Universal Biquad Filters", Circuits, *Systems and Signal Processing* April 2010, Vol. 29, No. 2, pp. 263-274.

[16] D. R. DINESH PRASAD, A. K. S. BHASKAR, "Universal current-mode biquad filter using dual output current differencing transconductance amplifier", *AEU - International Journal of Electronics and Communications*, Vol. 63, No. 6, Jun. 2009, pp. 497–501.

[17] WORAPONG TANGSRIRAT, TATTAYA PUKKALANUN, "Structural generation of two integrator loop filters using CDTAs and grounded capacitors", *International Journal of Circuit Theory and Applications*,Vol. 39, No. 1, Jan. 2011, pp. 31–45.

[18] C. M. CHANG, B. M. AL-HASHIMI, C. L. WANG, C. W. HUNG, "Single fully differential current conveyor biquad filters", In Proc. IEE *Circuits, Devices and Systems*, Vol. 150, No.: 5 Oct. 2003, pp. 394-398.

[19] F. KACAR, B. METIN, H. KUNTAM, O. CICEKOGLU, "Current-Mode Multifunction Filters Using a Single FDCCII", In Proc. *International Conference Electrical and Electronics Engineering (ELECO)*, Nov. 2009, pp. II-54 - II-57.

[20] H. CHEN', S. WANG, P. LI, NIEN-HSIEN CHOU', CHIH-HAO CHANG, "Single FDCCII-based current-mode universal biquadratic filter", In Proc. *The 2nd International Conference Consumer Electronics, Communications and Networks (CECNet)*,Yichang, China, Apr. 2012, pp. 2076 - 2079.

[21] J. JERABEK, K. VRBA, "A Controllable Universal Filter Using Multi-Output Current Followers" (Řiditelný univerzální filtr s vícevýstupovými proudovými sledovači), *Elektrorevue - Internet Journal* (http://www.elektrorevue.cz), No. 35, 2008, pp. 35-1 - 35-10.

[22] R. SENANI, S. S. GUPTA, "Current-Mode Universal Biquad Using Current Followers: A Minimal Realization", *Radioengineering*, Vol. 20 No. 4, Dec. 2011, pp. 898-904.

[23] A. Ü. KESKIN, E. HANCIOGLU, "Current mode multifunction filter using two CDBAs", AEU - *International Journal of Electronics and Communications* Vol. 59, No. 8, 2005, pp. 495–498.

[24] T. TSUKUTANI, Y. SUMI, N. YABUKI, "Electronically tunable current-mode universal biquadratic filter using CCCDBAs", In Proc. *International Symposium Intelligent Signal Processing and Communications Systems ISPACS*, Bangkok, Thailand, 2008, pp. 1 - 4.

[25] J. KOTON, N. HERENCSAR, K. VRBA, J. JERABEK, "Digitally Adjustable Current Amplifier and its Application in Fully Differential Current-Mode Band- Pass Filter Design", *Elektrorevue - Internet Journal* (http://www.elektrorevue.cz), No. 90, 2010, pp. 47-52.

[26] J. JERABEK, K. VRBA, "Comparison of the Fully-Differential and Single-Ended Solutions of the Frequency Filter with Current Followers and Adjustable Current Amplifier", In Proc. *ICN2012 The Eleventh International Conference on Networks*. Reunion, France: IARIA, 2012, pp. 50-54.

[27] K. VRBA, J. JERABEK, "Filters Based on Active Elements with Current Mirrors and Inverters", *International Transactions Communication and Signal Processing*,, Vol. 1, No. 8, 2006.

[28] R. SPONAR, K. VRBA, "Measurements and Behavioral Modelling of Modern Conveyors", *International Journal of Computer Science and Network Security*, Vol. 3A, No. 6, 2006, pp. 57-63.

[29] K. VRBA, J. JERABEK, "Selected Features of The Universal Current Conveyor - application illustration" (Vybrané vlastnosti universálního proudového konvejoru - ukázka návrhu aplikace), *Elektrorevue - Internet Journal* (http://www.elektrorevue.cz), No. 33, 2006, pp. 1-9.

[30] J. KOTON, N. HERENCSAR, K. VRBA, I. KOUDAR, "Fully differential current-mode filters using digitally adjustable current amplifier", *Elektrorevue - Internet Journal* (http://www.elektrorevue.cz), No. 45, pp. 45-1–45-4.

[31] J. JERABEK, R. ŠOTNER, K. VRBA, I. KOUDAR, "A Fully Differential universal tunable filter with current active elements", (Plně diferenční univerzální a řiditelný filtr s proudovými aktivními prvky) *Elektrorevue - Internet Journal* (http://www.elektrorevue.cz), No. 7, 2010, pp. 7-1 - 7-6.

[32] J. JERABEK, K. VRBA, "The Proposal of Frequency Filters With Current Active Elements Based on Integrators", (Návrh kmitočtových filtrů pomocí integračních článků s proudovými aktivními prvky) *Elektrorevue - Internet Journal* (http://www.elektrorevue.cz), No. 9 2009, pp. 9-1 - 9-7.

Automatic detection of the macula in retinal fundus images using multilevel thresholding

Jiri Minar, Kamil Riha, Ales Krupka, Hejun Tong

***Abstract*—The paper proposes a novel method for detection of macula in medical image of human eye – retinal fundus images that can be used in ophthalmology for detecting various eye's diseases such glaucoma, diabetic retinopathy or macula oedema. The method utilizes an approach of multilevel thresholding of red channel of fundus retinal image. Subsequently, the thresholded layers are preprocessed by application of median blur filter. Algorithm for ellipse detection from OpenCV library is used on all thresholding level. Then proposed technique analyzes detection and evaluates position of macula in fundus image. The precision of the method is evaluated on dataset from public fundus image library DRIVE. The results were 90% (36 of 40). False detections ware only in images where macula was not visible.**

***Keywords*— Automatic, Fundus, Macula, Medical Image processing, Multilevel Segmentation, Thresholding.**

I. Introduction

THE human eye is one of most important part of human body and diseases like glaucoma, diabetic retinopathy and macular degeneration can irreversible damage human vision. Diabetic retinopathy is usually main reason for the blindness in elder age people if not treated in early stages [1]. Patient's retinal image has to be analyzed for detection of disease like a diabetic retinopathy.

Retinal images are usually known as Fundus images. These images have usually red tint due to rich blood supply. Fundus image contains optical disk, macula and blood vascular, which are important for diagnosis by ophthalmologist [2]. Macula is an oval shaped highly pigmented yellow spot usually located in the center of retina of the human eye. Near its center there is the fovea, a small pit that contains the largest concentration of cone cells in the eye and is responsible for central, high resolution vision. Macula is the darkest region in neighborhood of optical disk in Fundus image Fig. 1. There are also visible vessels and veins. Extraction of retinal vascular can be also used in some application related to secure area like personal identification .The main concern of this paper is to detect macula in Fundus imaged. Detection of macula is the most important step for the treatment of macula oedema. Patients with macula oedama have blood leakage in blood vessels in macula area, if detected it can be treated with laser [3].

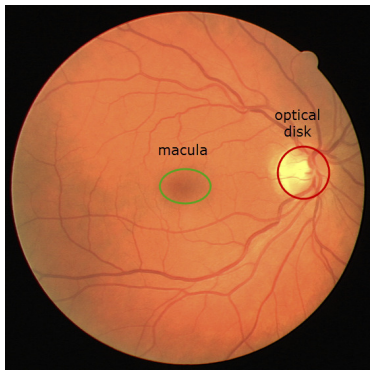

Fig. 1. Retinal image with marked macula and optic disk

II. Recent solution

Different approaches are presented in literature for macula detection. In [4], macula is detected using line operator. Paper [5] is presenting a method for macula detection using seeded mode tracking approach. Paper [6] presents the algorithm to detect macula using edge detection and region growing techniques. Ant Colony Optimization based hybrid method is presented in [7]. In paper [8] macula is localized first by making use of localized optic disc center and enhanced blood vessels. Finally, macula is detected by taking the distance from center of optic disk and thresholding then combining it with enhanced blood vessels image to locate the darkest pixel in this region, making clusters of these. The article [9] represents an approach of image segmentation on microscopic bone marrow images by using multilevel tresholding technique. This technique has been applied into two types of images which is normal bone marrow and Acute Lymphoblastic Leukemia (ALL) or this paper [10] introduces detection method based on multilevel-thresholding of input image and subsequent analysis of objects shape in each level. Detection algorithm focuses on path tracking of persons in video sequences correct evaluation of tailgating or piggybacking. This paper [11] introduces solution for localization of optic disc by using specialized template matching and segmentation by a deformable contour model. Difference approach of detection in medical images is

Jiri Minar is with Dept. of Telecommunications, Faculty of Electrical Engineering and Communication, Brno University of Technology, Technicka 12, 616 00 Brno, Czech Republic, email: jiri.minar@phd.feec.vutbr.cz

Kamil Riha received his M.Sc. degree in Electronics & Communication in 2003 and the Ph.D. degree in 3D Scene Acquisition for Auto-Stereoscopic Display in 2007. Presently, he is employed at Brno University of Technology, Faculty of Electrical Engineering, Department of Telecommunications, as the academic employee (since 2006). His research interests include in particular areas of digital image processing and electronics. email: rihak@feec.vutbr.cz

Ales Krupka is with Dept. of Telecommunications, Faculty of Electrical Engineering and Communication, Brno University of Technology, Technicka 12, 616 00 Brno, Czech Republic,

described in this article [12], where is described method for highly accurate and effective localization of the transverse section of the carotis communis artery in ultrasound images using Viola-Jones detector.

The presented solution focuses on macula detection using multi-level thresholding without any supporting detection of area in fundus image. Proposed algorithm should be very accurate with detection of macula center with non-complex algorithm.

III. Proposed Technique

The proposed macula detection algorithm using multilevel thresholding and ellipse detection from all level is described in flow chart in Fig. 2. The technique consists of three main parts: Layer selection and image preprocessing, multilevel thresholding and position detection algorithm.

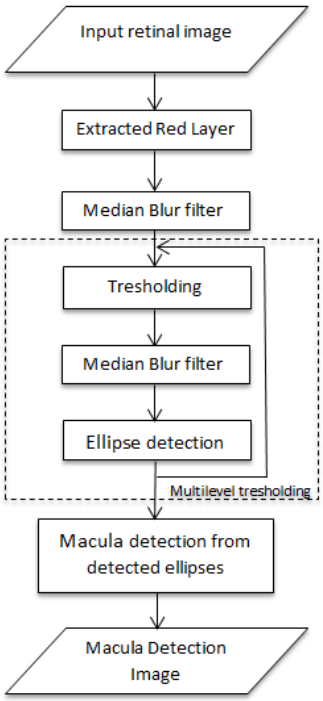

Fig. 2. Complete algorithm for macula detection

A. Layer selection

The proposed technique uses multilevel thresholding of Fundus image and ellipse detection using OpenCV[1] (Open Computer Vision) framework. OpenCV contains various libraries for image processing and object detection.

All color channels from Fundus image (red, green, blue) (as seen in Fig. 3) were extracted. Green channel is usually used for vessels and veins segmentation, because there is most image information with veins and vessels. We used red channel as an input point of our algorithm. This decision was made after an analysis of RGB channels. Red channel contains mostly information about macula and less information about veins and vessels (Fig. 3c), which can negatively influence algorithm for ellipse detection.

[1] Available from URL: `http://opencv.org`

B. Preprocessing

Macula does not have usually perfect rounded circle or ellipse shape, but it has ellipse with craggy perimeter. For this reason is red channel of fundus image preprocessed by application of blur function using normalized box filter. Thus preprocessed image is used as input to multilevel segmentation and ellipse detection algorithm.

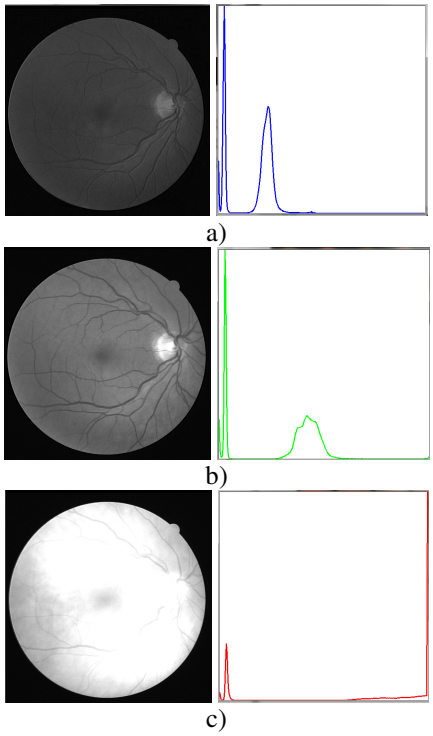

Fig. 3. RGB channels of fundus retinal image with histograms a) Blue b) Green c) Red

C. Multilevel thresholding

Consequently the fundus image is segmented in the loop, where loop is created over all threshold level. This multilevel thresholding is computed for all 256 levels, because red channel is processed as grey image with 8-bit information about grey shade. Thresholding levels from 100 to 230 usually return the most useful and quality output for next contour and ellipse detection (as shown in Fig.4).

Thresholding layers are blur again to increase roundness of shape on images to increase change of detection of contour and after that detection of ellipses from this contour.

Fig. 4. Thresholding of red channel from fundus image.

D. *Ellipse detection*

Ellipse contours and shapes is finding in all thresholds level by functions from OpenCV framework. Function for contour detection using algorithm described in this paper [13]. All detected ellipses are evaluated for shape and ellipses eccentricity value lower than 0.5 or greater than 1.5 are eliminated. This elimination is essential for elimination of false detection, because macula is circle shaped or ellipse with small eccentricity as shown in Fig. 5. All ellipses detected in each thresholding level are stored in buffer for consequence processing.

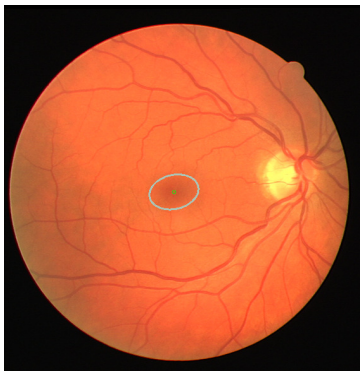

Fig. 5. Detected ellipse from one thresholding level (fig. 4.) and displayed in original fundus image with marked center.

E. *Ellipse detection evaluation*

Next step in proposed technique for macula detection is evaluation of all detected ellipses and decision where macula is situated in fundus image. The algorithm 1 shows principle of this detection. First all detected ellipses (Fig. 7) are split into group with the same coordinates of centroid (center of ellipse) with some toleration. We have used toleration of 15 pixels. The group with the biggest amount of detection is marked as group with possible macula location. The biggest ellipse in this group is marked as final detection and shape and centroid is drawn into original image (Fig. 5).

foreach *threshold level* **do**
  | apply blur filter;
  | detect contours;
  | detect ellipse;
  | eliminate ellipses with wrong eccentricity;
  | store in buffer;
end
for *k = 0* **to** *numbers of all detected ellipses* **do**
  | collect ellipse to group with similar centroid;
end
evaluate group with most ellipse detection;
get coordinates of the biggest ellipse in group;
get perimeter of the biggest ellipse in group;

Algorithm 1: Evaluation of macula location

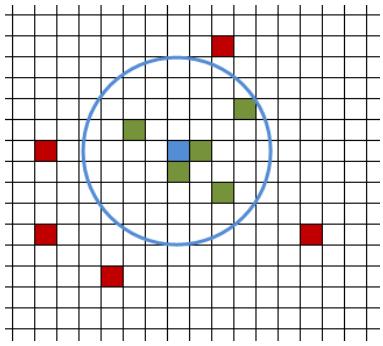

Fig. 7. Grouping of detected ellipses by centroid – with radius evaluation ±4 pixels. Blue pixel – initial centroid, green pixels – coordinates of centroids in radius, red pixels – centroids outside radius

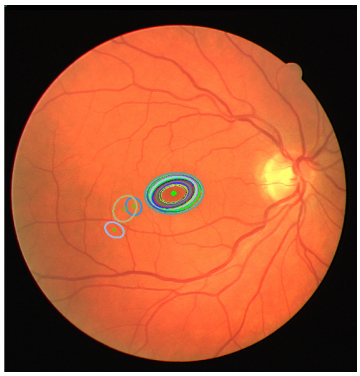

Fig. 8. All ellipses detected for all thresholding levels and displayed in original fundus image with marked center.

IV. Experimental Results

To evaluate the performance of proposed algorithm, a dataset of 40 images are used. Evaluation is applied on DRIVE (Digital Retinal Images for Vessel Extraction) that is publically available. 40 images of size 565x584, each pixel having eight bits are included in DRIVE database [14].

Fig. 9. One of four picture removed from dataset due macula is not presented in this image.

Four images were manually eliminated from this DRIVE dataset of 40 images, because macula is not visible on these images (can even not be seen by human eyes). This can be cause by some eye disease in advanced stage or wrongly focused of fundus image with optical disc in the middle as can be seen in Fig. 8. In this picture there is also marked position,

where macula is detected – it is false detection – because macula is not presented in image. The algorithm has to designate best detection in the image.

Detection results are very promising. Overall results for whole DRIVE database are 90% of accurate detection macula in fundus image. Macula was detected in 36 fundus images out of 40. Macula was marked on random places in 4 images. The reason of this false detection macula was caused that macula was not visible at all on these 4 images also by human eye, thus algorithm marked place with the most false detection. This is the place for improvement of algorithm.

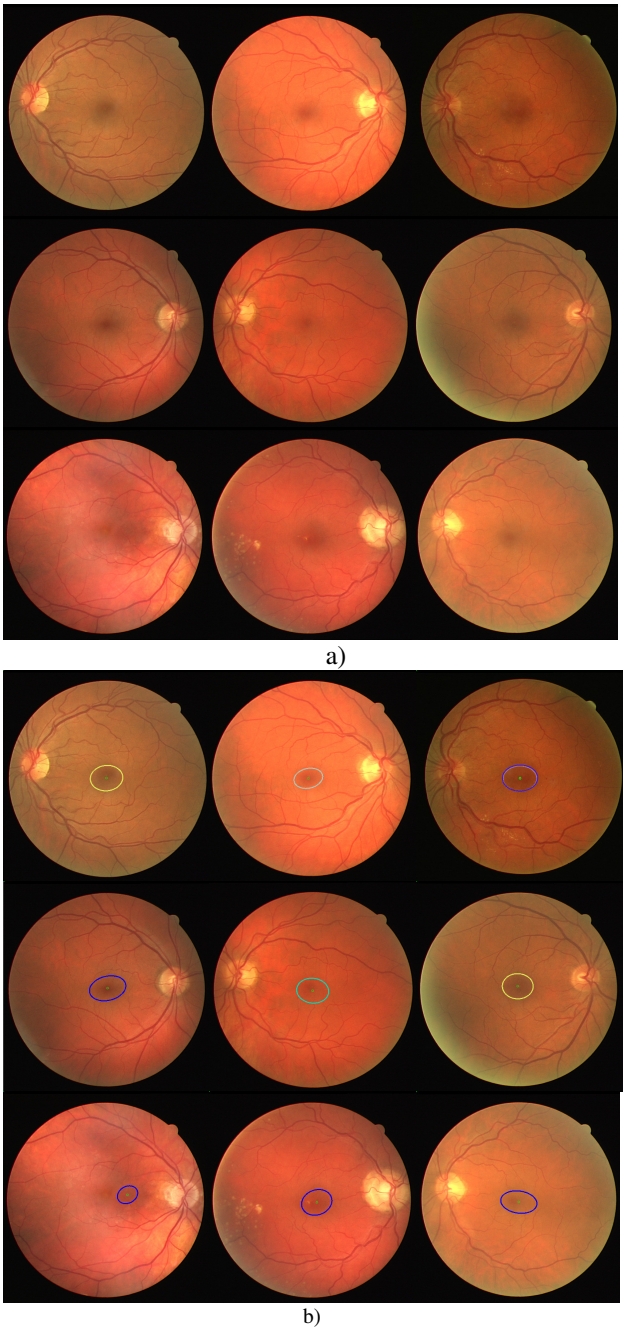

a)

b)

Fig. 10. Nine examples of fundus images from DRIVE database
a) Original Fundus images
b) Fundus images with marked detection of macula

V. Conclusion

We have presented technique for detection of macula position in fundus images. This technique is using multilevel thresholding, contour, and ellipse detection. Proposed method was very successful on test dataset from DRIVE database (40 fundus images). Macula was successfully located on all images where was presented and we detected macula area with 90% effectivity (36 of 40). False detection were only in images where macula was not visible, thus area where most ellipses were detected, was marked as macula. However, this false detection can be avoided by suitable technique of fundus image collection or enhance of the algorithm by not displaying "weak" detection e.g. area with very small ellipse detection.

References

[1] G.E. Lang, "Diabetic retinopathy", *Development in Ophthalmology,* Vol. 39, 2007.

[2] K. Akita, H. Kuga, "A computer method of understanding ocular fundus image," *Pattern Recognition,* vol. 15, no. 6, pp 431-443, 1982.

[3] Chinenye, "Discover the amazing way to treat and handle sickness & diseases", Vol.2, 2007.

[4] Shijian Lu, Joo Hwee Lim, Automatic macula detection from retinal images by a line operator", *Proceedings of 2010 IEEE 17th International Conference on Image Processing*, pp. 4073-4076, 2010.

[5] Damon W.K. Wong, Jiang Liu, Ngan-Meng Tan, Fengshou Yin, Xiangang Cheng, Ching-You Cheng, Gemmy C.M. Cheung, Tien Yin Wong, "Automatic Detection of the Macula in Retinal Fundus Images using Seeded Mode Tracking Approach", *34th Annual International Conference of the IEEE EMBS,* pp. 4950-4953, 2012

[6] C.Marin, S. PenaA, M.G.Penedo, M. Ortega, J. Rouco, A. P. Reino, M. Pena, "Macula Precise Localization Using Digital Retinal Angiographies", *WSEAS Transactions on Computer Research,* Issue 1, vol 3., pp.21-33, January 2008.

[7] Kavitha, G. Ramakrishnan, "Identification and analysis of macula in retinal images using Ant Colony Optimization based hybrid method", *World Congress on Nature & Biologically Inspired Computing*, pp: 1174 – 1177, Dec 2009.

[8] Maryam Mubbashar, Anam Usman, M. Usman Akram, Automated System for Macula Detection in Digital Retinal Images", *Information and Communication Technologies (ICICT)*, 2011 International Conference, pp. 1-5, 2011

[9] R. Adollah, E. U. Francis, M. Y. Mashor, N. H. Harun, "Bone Marrow Image Segmentation Based on Multilevel Thresholding", *2012 International Conference on Biomedical Engineering (ICoBE)*, pp. 458 – 61, 2012

[10] Minar J., Riha K., Tong H., "Intruder detection for automated access control system with Kinect device", *36th International Conference on Telecommunications and Signal Processing (TSP)*, pp. 826-829, 2012

[11] Lowell, J., Hunter, A., Steel, D., Ryder, B., Fletcher, E. "Optic Nerve Head Segmentation" *IEEE Transactions on Medical Imaging*, 23 (2), Feb 2004.

[12] Riha K., Masek J., Burget R., Benes R., Zavodna E., "Novel Method for Localization of Common Carotid Artery Transverse Section in Ultrasound Images Using Modified Viola- Jones Detector", *Ultrasound in medicine and biology*, vol. 39, pp. 1887-1902, 2013

[13] Suzuki, S. and Abe, K., "Topological Structural Analysis of Digitized Binary Images by Border Following", *CVGIP 30 1*, pp 32-46 (1985)

[14] J.J. Staal, M.D. Ambramoff, M. Niemeijer, M.A. Viergever, B. van Ginneken, "Ridge based vessel segmentation in color images of the retina", *IEEE Transactions on Medical Imaging,* vol. 23, pp. 501-509, 2004

A Robust Pre-Filter and Power Loading Design for Time Reversal UWB Systems over Time-Correlated MIMO Channels

Sajjad Alizadeh, Hossein Khaleghi Bizaki and Reza Saadat

***Abstract*—Conventional Time Reversal (TR) technique suffers from performance degradation in time varying Multiple-Input Multiple-Output Ultra-Wideband (MIMO-UWB) systems due to outdating Channel State Information (CSI) over time progressions. That is, the outdated CSI degrades the TR performance significantly in time varying channels. The correlation property of time correlated channels can improve the TR performance against other traditional TR designs. Based on this property, at first, we propose a robust TR-MIMO-UWB system design for a time-varying channel in which the CSI is updated only at the beginning of each block of data where the CSI is assumed to be known. As the channel varies over time, pre-processor blindly pre-equalizes the channel during the next symbol time by using the correlation property. Then, a novel recursive power allocation strategy is derived over time-correlated time-varying TR-MIMO-UWB channels. We show that the proposed power loading technique, considerably improves the Bit Error Rate (BER) performance of TR-MIMO-UWB system in imperfect CSI with robust pre-filter. The proposed algorithms lead to a cost-efficient CSI updating procedure for the TR optimization. Simulation results are provided to confirm the new design performance against traditional method.**

***Keywords*—Time Reversal (TR) technique, MIMO channel, Ultra-Wideband (UWB) system, Temporal Correlation, Imperfect CSI, MMSE pre-equalizer.**

I. Introduction

Ultra-wide band (UWB) communication systems have recently received much interest from both research community and industry [1]-[2]. However, due to the wide bandwidth property, UWB systems suffer from a very long delay spread of the multipath channels in indoor environments. Different types of the receiver structure such as RAKE, Transmitted Reference or the Decision Feedback Autocorrelation receivers can be implied [3]-[5] in which each technique has different complexities. To reduce the receiver complexity, non-coherent scheme is developed to bypass the complicated treatments on the UWB channel [6]-[7]. Accordingly, based on the idea of moving the complexity from the receiver to the transmitter, the Time Reversal (TR) preprocessing technique also referred to as the full pre-RAKE combining, which is originated from underwater acoustics and ultra sonic system [8], has been extended to the UWB applications. As a result, the TR technique can be used to reduce the long delay spread of the UWB channel. Multiple-Input Multiple-Output (MIMO) solution, employing multiple antennas at the transmitter and receiver, is capable of increasing the data transmission rate by the spatial multiplexing without expanding the bandwidth and power [9]. In order to transmit parallel data streams simultaneously (spatial multiplexing), the Multi-Stream Interference (MSI) of the MIMO channel must be mitigated. The TR solution in the MIMO-UWB systems can mitigate not only the Inter-Symbol Interference (ISI) but also the MSI caused by transmitting several data streams, simultaneously [10]. The main bottleneck in the TR implementation is the necessity of the CSI at the transmitter, because in the TR technique we use the time-reversed version of the estimated CSI as pre-filter. In practice, perfect CSI is not available in transmitter side due to the channel estimation error in time varying channels. In spite of TR's good performance, it is very sensitive to erroneous CSI due to imperfect channel estimation especially in time varying channel. Recently, the TR-based UWB system and its variations have been investigated in some literatures. We have sorted them into two categories:

First category of the researches on the TR pre-coding assumes that perfect CSI is given at the transmitter side [11]-[15]. Authors of [11] proposed an antenna selection scheme for the TR-MIMO-UWB communication system in a perfect CSI case to reduce the number of transmit antenna. Also, a Minimum Mean Square Error (MMSE) equalizer is used for the TR-UWB system with perfect CSI in [12] to mitigate the residual ISI and increase the transmission data rate. An ultra-high data rate TR-MIMO-UWB system with space-time pre-coding has been proposed in [13] based on the Zero-Forcing (ZF) criterion in which the imperfect CSI has not been considered. Similar solution has been provided in [14] with the assumption of the spatial correlation among transmit and receive antenna. Also, the impact of spatial correlation on the TR-MIMO-UWB system has been investigated in [15] where several data streams can be transmitted by using only one antenna in a system named virtual TR-MIMO-UWB. Unfortunately, these methods suffer from the effects of the imperfect CSI in the transmitter, because the time variant channels and imperfect CSI have not been taken into account in these literatures.

Second category of the researches on the TR pre-coding assumes that imperfect CSI is available at the transmitter side [10], [16]-[22]. The effect of channel imperfection on the TR-MIMO-UWB system performance has been evaluated in [10]

Sajjad Alizadeh and Reza Saadat are with the Department of Electrical and Computer Engineering, Yazd University, Yazd, 89195-741, Iran, (e-mail: s.alizadeh@stu.yazd.ac.ir, rsaadat@yazd.ac.ir).

Hossein Khaleghi Bizaki is with the Electrical and Electronic Engineering University Complex, Malek Ashtar University of Technology, Tehran, Iran, (e-mail: bizaki@ee.iust.ac.ir).

Manuscript received March 14, 2014; revised April 28, 2014.

for low and high data rate transmissions. Unfortunately, an optimization scheme has not been provided in this literature to overcome the effects of the channel imperfection. In [16]-[19], we had provided the pre-filtering solutions for the channel estimation error compensation in which the time variant channel is not considered. Especially, a power allocation scheme was proposed in [18] to improve the robust pre-filtered TR-MIMO-UWB systems in an imperfect CSI for the quasi-static channels. On the other hand, the robustness of TR technique in imperfect CSI caused by a time varying channel environment has been studied in [20] by experimental results. It has been shown that, if the channel maintains some partial correlation with its previous ensembles, the TR method give a better performance even if the total correlation of the channels is very low. Authors of [20] gave to us an idea to develop our previous works [18] (pre-filtering and power loading in the quasi-static TR-MIMO-UWB systems) for the temporal correlated time varying TR-MIMO channels in an imperfect CSI. Also, a post-time-reversed MIMO-UWB transmission scheme has been proposed in [21] which improves the TR robustness against imperfect CSI caused by channel estimation error when compared with the conventional TR scheme. Finally, an analysis without any improvement solution has been provided in [22] on the effect of the channel estimation error on the performance of the TR-UWB systems.

As it is observed from previous literatures, all of them assume the quasi-static channels in their analysis. In order to increase the TR performance in time varying channels, the pre-processors should be optimized approximately in some symbol duration [23]. On the other hand, the generation of reliable channel feedback in some short symbol time is complicated in time-varying channel and can be led to high bandwidth overhead. From practical implementation point of view, most of the TRs have been designed assuming that the wireless channel can be regarded as constant over a block of data. In mobile applications where the channel is time-varying, the assumption that the channel is constant over some periods only holds approximately and will affects the TR performance that are designed based on this assumption. Hence, a judicious and innovative TR system design that takes the time-varying nature of the channel into account is the key to solve the above problems.

Based on mentioned researches on the TR pre-coding and also, works of [18] and [23], we extend and unify the TR concepts to time varying MIMO channels in an imperfect CSI, which will allow us to improve mobile systems performance, as well as to provide guidelines for future pre-coder designs employing low feedback overhead. On the other hand, a recursive power allocation strategy is proposed to more improve the performance of the proposed robust TR-MIMO-UWB system. According to authors best knowledge, no research has been reported so far about time varying and time correlated TR-MIMO-UWB systems. Therefore, it is essential to analyze and improve the TR-MIMO-UWB systems in mobile applications with imperfect CSI. Our current works can be used for the mobile communication networks, such as Ad Hoc networks and so on. The rest of the paper is organized as follows; we introduce the system model in Section II. A novel solution based on a MMSE criterion and a novel recursive power allocation scheme are derived for TR-MIMO-UWB system over time varying channels in Section III and IV, respectively. Numerical and simulation results characterizing the performance of the proposed methods are presented in Section V, and finally, conclusions are drawn in Section VI.

II. System Description in Time Correlated Channels

A TR-MIMO-UWB communication system includes a transmitter equipped with antennas and a receiver equipped with antennas is depicted in Fig. 1. Let us consider an impulsive (Impulse Radio) UWB (IR-UWB) system using Binary Pulse Amplitude Modulation (BPAM) with pulse shaping according to the Federal Communications Commission (FCC) desired power spectral density [1]-[2]. The transmitted signal for every input of the MIMO system is represented as,

$$x(t) = \sqrt{E_b} \sum_{k=-\infty}^{+\infty} d_k p(t - kT) \tag{1}$$

where $d_k = \{\pm 1\}$ is the binary transmit symbol, E_b is the bit energy, $p(t)$ is the desired pulse shape, and T denotes the symbol duration. According to Fig. 1, at first, the input signal is converted into N_r streams, pre-equalized with an optimized MMSE pre-equalizer, pre-coded with TR pre-filter, and then sent to N_r transmitting antennas, simultaneously. The resultant signal passes through the multipath MIMO channel and then, is corrupted by an Additive White Gaussian Noise (AWGN). Thus, there are $N_t \times N_r$ multipath channel between transmit and receive antennas. For simplicity of our analysis, we use the tapped delay line (TDL) model with maximum L_g taps [10]-[11]. If τ_d and T are the delay spread of the channel and the symbol duration, respectively, then $L_g \cong \frac{\tau_d}{T}$. In fact, we use a TDL model with equal tap spacing of T. Note that in our application, $\tau_d \gg T$ then we have a frequency-selective model for each multipath channel between transmit and receive antennas. Furthermore, because of using the very short duration pulses, IR-UWB meets extremely resolvable multipath components (MPC) leading to long delay spread τ_d, in that, two multipath components (taps) with delays τ_m and τ_n are resolvable if $|\tau_m - \tau_n| \geq T$. We assume $|\tau_m - \tau_n| \geq T$. Also, the UWB channels are assumed to be time correlated across blocks [23]. The TR pre-filter is used in the spatial multiplexing UWB system in order to cope with the ISI and MSI problems. Since the ultra-high data rate UWB transmission usually requires extremely short symbol time, thus ISI and MSI are very strong. These interferences, especially MSI, are not absolutely eliminated by TR pre-filter [13]. Therefore, to completely eliminate the residual ISI and MSI, a MMSE pre-equalizer, i.e. $\mathbf{F}_{MMSE}$ in Fig. 1, is needed in transmitter as will be considered in Section 3. Both MMSE pre-equalizer and TR pre-filter require the perfect CSI. The CSI can be estimated using the training symbols. The training pattern employed for channel estimation is similar to what is considered in [24], in which at the beginning of every block, the first N_t symbols are assigned as training sequence, once in every $T_f = NT$ seconds, where every block includes

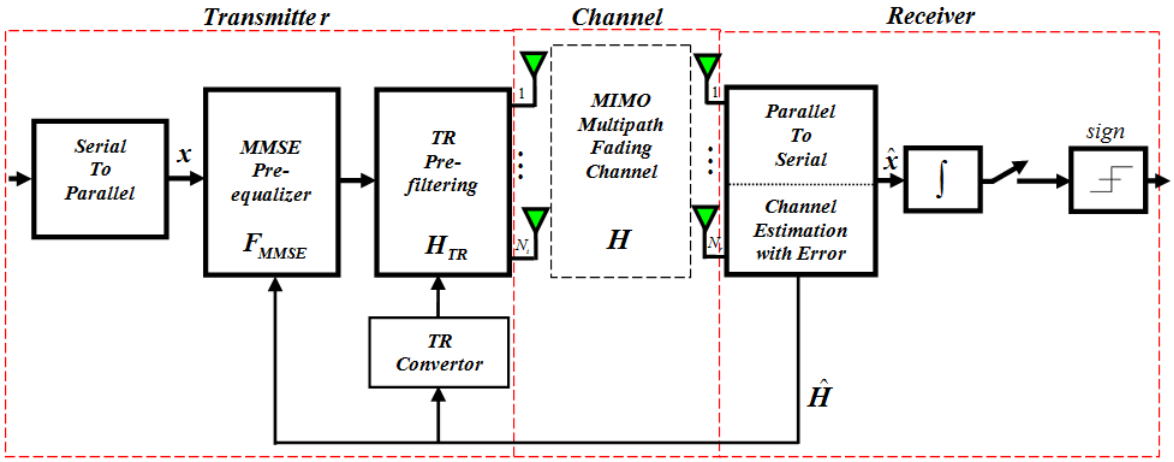

Fig. 1. TR-MIMO-UWB system model.

N symbols. As in [24], the MMSE channel estimation is assumed in this paper. Then, the estimated CSI is fedback to transmitter through the feedback channel. In practice, perfect CSI is not available in the transmitter side due to non-ideal channel estimator. Pre-processors (TR pre-filtering and MMSE pre-equalizing) are influenced by the imperfect CSI effects. Finally, the data stream is detected based on a simple integrate-and-dump receiver with the sampling rate of $\frac{1}{T}$.

The effect of channel estimation error in a time varying channel can be considered as $\mathbf{H}_t = \hat{\mathbf{H}}_t + \mathbf{\Delta H}_t$ where $\mathbf{H}_t$, $\hat{\mathbf{H}}_t$ and $\mathbf{\Delta H}_t$ are the true value, estimated value and estimation error of the CIR at the time instant t, respectively. It is assumed that the entries of $\mathbf{\Delta H}_t$ are i.i.d. random variables with zero mean complex Gaussian noise. The estimated value $\hat{\mathbf{H}}_t$ is converted to the TR pre-filter, as $\mathbf{H}_{TR,t}$, by the TR convertor. This function will be exactly explained after some following basic definitions in next paragraphs of this section. The estimated CIR between i^{th} transmit antenna and j^{th} receive antenna ($i = 1, ..., N_t, \quad j = 1, ..., N_r$) at the time instant t can be denoted as,

$$\hat{h}_{ij,t}(t) = \sum_{l=0}^{L_g-1} \hat{\alpha}_l^{ij,t} \delta(t - \hat{\tau}_l^{ij,t}) \qquad (2)$$

where $\hat{\alpha}_l$ is the estimated fading coefficient of the l^{th} multipath components (MPC), $\hat{\tau}_l$ is the corresponding delay of the l^{th} tap and L_g is the number of resolvable MPCs. The discrete time vector form of CIR in reversed order at the time instant t is denoted as: $\hat{\mathbf{h}}_{ij,t} = [\hat{h}_{ij,t}^{L_g-1}, \cdots, \hat{h}_{ij,t}^{l}, \cdots, \hat{h}_{ij,t}^{0}]_{1\times L_g}$ where $\hat{h}_{ij,t}^{l}$ is the amplitude of the l^{th} path for the channel between i^{th} transmit antenna and j^{th} receive antenna at time instant t. Also, the estimation error vector of the CIR is defined as: $\mathbf{\Delta h}_{ij,t} = [\Delta h_{ij,t}^{L_g-1}, \cdots, \Delta h_{ij,t}^{l}, \cdots, \Delta h_{ij,t}^{0}]_{1\times L_g}$ where $i = 1, ..., N_t$, $j = 1, ..., N_r$ and $l = 0, ..., L_g - 1$. The probability distribution of the error coefficients are considered as: $\Delta h_{ij,t}^{l} \sim CN(0, \sigma_e^2)$ where σ_e^2 is the estimation error variance. As in [10]-[11], the estimated CIR and estimation error matrices of size in the time instant t, can be written as:

$$\hat{\mathbf{H}}_t = \begin{pmatrix} \hat{\mathbf{h}}_{11,t} & \hat{\mathbf{h}}_{21,t} & \cdots & \hat{\mathbf{h}}_{N_t1,t} \\ \hat{\mathbf{h}}_{12,t} & \hat{\mathbf{h}}_{22,t} & \cdots & \hat{\mathbf{h}}_{N_t2,t} \\ \vdots & \vdots & \vdots & \vdots \\ \hat{\mathbf{h}}_{1N_r,t} & \hat{\mathbf{h}}_{2N_r,t} & \cdots & \hat{\mathbf{h}}_{N_tN_r,t} \end{pmatrix}$$

$$\mathbf{\Delta H}_t = \begin{pmatrix} \mathbf{\Delta h}_{11,t} & \mathbf{\Delta h}_{21,t} & \cdots & \mathbf{\Delta h}_{N_t1,t} \\ \mathbf{\Delta h}_{12,t} & \mathbf{\Delta h}_{22,t} & \cdots & \mathbf{\Delta h}_{N_t2,t} \\ \vdots & \vdots & \vdots & \vdots \\ \mathbf{\Delta h}_{1N_r,t} & \mathbf{\Delta h}_{2N_r,t} & \cdots & \mathbf{\Delta h}_{N_tN_r,t} \end{pmatrix}$$

Note that the size of matrices $\hat{\mathbf{H}}_t$ and $\mathbf{\Delta H}_t$ is $N_r \times N_t L_g$. Also, $\mathbf{C}_{\mathbf{\Delta H}_t} = E\{\mathbf{\Delta H}_t \mathbf{\Delta H}_t^H\}$ is the estimation error covariance matrix and $E\{\mathbf{\Delta H}_t\} = 0$ is assumed. For simplicity of analysis, we assume that the estimation errors of the different sub-channels are statistically independent, that is, they have a common error variance σ_e^2. Thus, we have $\mathbf{C}_{\mathbf{\Delta H}_t} = E\{\mathbf{\Delta H}_t \mathbf{\Delta H}_t^H\} = \sigma_e^2 \mathbf{I}$ where $\mathbf{I}$ is the identity matrix. If the estimated CIR of all sub-channels, i.e. $\hat{\mathbf{h}}_{ij,t}$, are known at the transmitter side, time reversed version of them are used to TR pre-filter to pre-equalize the transmitted data. Thus, we can construct the pre-filter matrix based on the time reversed form of the estimated sub-channels by the TR convertor which is a $N_t L_g \times N_r(2L_g - 1)$ matrix in [10]-[11] as

$$\mathbf{H}_{TR,t} = \begin{pmatrix} \overline{\mathbf{H}}_{11,t} & \overline{\mathbf{H}}_{12,t} & \cdots & \overline{\mathbf{H}}_{1N_r,t} \\ \overline{\mathbf{H}}_{21,t} & \overline{\mathbf{H}}_{22,t} & \cdots & \overline{\mathbf{H}}_{2N_r,t} \\ \vdots & \vdots & \vdots & \vdots \\ \overline{\mathbf{H}}_{N_t1,t} & \overline{\mathbf{H}}_{N_t2,t} & \cdots & \overline{\mathbf{H}}_{N_tN_r,t} \end{pmatrix}$$

where each sub-matrix $\overline{\mathbf{H}}_{ij,t}$ is an $L_g \times (2L_g - 1)$ Toeplitz matrix defined by [10]-[11] as

$$\overline{\mathbf{H}}_{ij,t} = \begin{pmatrix} \hat{h}_{ij,t}^{0} & \cdots & \hat{h}_{ij,t}^{L_g-1} & 0 & \cdots & 0 \\ 0 & \hat{h}_{ij,t}^{0} & \cdots & \hat{h}_{ij,t}^{L_g-1} & 0 & \vdots \\ \vdots & & \ddots & & \ddots & 0 \\ 0 & \cdots & 0 & \hat{h}_{ij,t}^{0} & \cdots & \hat{h}_{ij,t}^{L_g-1} \end{pmatrix}$$

In fact, for each sub-matrix $\overline{\mathbf{H}}_{ij,t}$, we have

$\overline{\mathbf{H}}_{ij,t} = Toeplitz(TR(\hat{\mathbf{h}}_{ij,t}))$ where $Toeplitz(.)$ and $TR(.)$ are the Toeplitz matrix maker and the time reversed order of a vector, respectively. Therefore, the TR pre-filter by the TR convertor can be written as $\mathbf{H}_{TR,t} = Toeplitz(TR(\hat{\mathbf{H}}_t^H)) = \mathcal{F}(\hat{\mathbf{H}}_t^H)$ where the TR operation is applied on the vectors $\hat{\mathbf{h}}_{ij,t}$ of the matrix $\hat{\mathbf{H}}_t^H$. Also, $(.)^H$ denotes the complex conjugate transpose of the matrix $\hat{\mathbf{H}}_t$. The equivalent TR channel response matrix of size $N_r \times N_r(2L_g - 1)$ is given by

$$\mathbf{H}_t\mathbf{H}_{TR,t} = \begin{pmatrix} \overline{\mathbf{h}}_{11,t} & \overline{\mathbf{h}}_{21,t} & \cdots & \overline{\mathbf{h}}_{N_r1,t} \\ \overline{\mathbf{h}}_{12,t} & \overline{\mathbf{h}}_{22,t} & \cdots & \overline{\mathbf{h}}_{N_r2,t} \\ \vdots & \vdots & \vdots & \vdots \\ \overline{\mathbf{h}}_{1N_r,t} & \overline{\mathbf{h}}_{2N_r,t} & \cdots & \overline{\mathbf{h}}_{N_rN_r,t} \end{pmatrix}$$

where each sub-channel $\overline{\mathbf{h}}_{ij,t}$ is a $1 \times (2L_g - 1)$ auto-correlation ($i = j$) or cross-correlation ($i \neq j$) vector. The received symbols vector at the MIMO channel output with MMSE pre-equalizer and TR pre-filter can be written as $\hat{\mathbf{x}}_t = \mathbf{H}_t\mathbf{H}_{TR,t}\mathbf{F}_{MMSE,t}\mathbf{x}_t + \mathbf{n}_t$ where $\mathbf{x}_t$, $\hat{\mathbf{x}}_t$, and $\mathbf{n}_t$ are the transmitted symbols, the received symbols and AWGN, respectively. The vector $\mathbf{x}_t$ contains i.i.d. random variables with zero mean $E\{\mathbf{x}_t\} = \mathbf{0}$ and variance $E\{\mathbf{x}_t\mathbf{x}_t^H\} = \sigma_{\mathbf{x}}^2\mathbf{I}$ with antipodal modulation. Also, we assume $\mathbf{n}_t \sim CN(\mathbf{0}, \sigma_{\mathbf{n}}^2\mathbf{I})$ where $\sigma_{\mathbf{n}}^2 = E\{\mathbf{n}_t\mathbf{n}_t^H\}$. Summarily, the size of the input and output vectors or matrices of each block of Fig. 1 can be presented as follows; the transmitted and received symbol vectors $\mathbf{x}$ and $\hat{\mathbf{x}}$ as well noise vector $\mathbf{n}$ are of size $N_r \times 1$. Also, the MMSE pre-coding matrix $\mathbf{F}_{MMSE}$ and the TR pre-filter matrix $\mathbf{H}_{TR}$ are of size $N_r(2L_g - 1) \times N_r$ and $N_tL_g \times N_r(2L_g - 1)$, respectively. The true value $\mathbf{H}$ and the estimated value $\hat{\mathbf{H}}$ of the channel matrix are of size $N_r \times N_tL_g$. Therefore, the total pre-coding $\mathbf{H}_{TR}\mathbf{F}_{MMSE}$ is a $N_tL_g \times N_r$ matrix.

To analysis the TR-MIMO-UWB system in the time correlated channels, we define $\hat{\mathbf{H}}_{t-\tau}$ as the estimated CIR matrix at the time instant $t - \tau$. In fact, $\hat{\mathbf{H}}_{t-\tau}$ corresponds to the channel state τ seconds earlier than $\hat{\mathbf{H}}_t$. We assume that $\hat{\mathbf{H}}_t$ and $\hat{\mathbf{H}}_{t-\tau}$ are correlated realizations of the estimated channels. Thus, given the outdated CSI, i.e. $\hat{\mathbf{H}}_{t-\tau}$, we can characterize the unknown current CSI, i.e. $\hat{\mathbf{H}}_t$, as introduced in [23],

$$\hat{\mathbf{H}}_t = \rho\hat{\mathbf{H}}_{t-\tau} + \sigma_h\sqrt{1-\rho^2}\mathbf{E}_t = \rho\hat{\mathbf{H}}_{t-\tau} + \mathbf{\Delta E} \quad (3)$$

where $\sigma_h^2 = E\{\|\hat{\mathbf{h}}_{ij,t}\|^2\}$ is the variance of the channel coefficients. Note that the different sub-channels are statistically independent assumed, that is, they have a common variance. The entries of the matrix $\mathbf{E}_t$ in (3) are assumed to be i.i.d. zero-mean complex Gaussian random variables, i.e. $\mathbf{E}_t \sim CN(\mathbf{0}, \mathbf{I})$. Also, the matrix $\mathbf{\Delta E}$ is the $CN(\mathbf{0}, \sigma_h^2(1-\rho^2)\mathbf{I})$-distributed uncertainty on the true estimated channel given the outdated CSI, $\hat{\mathbf{H}}_{t-\tau}$. The time correlation coefficient ρ between the time instants t and $t - \tau$ is defined in [23] as,

$$\rho = \frac{E\{\hat{\mathbf{h}}_{ij,t}\hat{\mathbf{h}}_{ij,t-\tau}^H\}}{\sqrt{E\{\|\hat{\mathbf{h}}_{ij,t}\|^2\}E\{\|\hat{\mathbf{h}}_{ij,t-\tau}\|^2\}}} \quad (4)$$

The similar discussion can be presented for the estimation error matrix $\mathbf{\Delta H}_t$, i.e., we have,

$$\mathbf{\Delta H}_t = \rho\mathbf{\Delta H}_{t-\tau} + \sigma_e\sqrt{1-\rho^2}\mathbf{E'}_t = \rho\mathbf{\Delta H}_{t-\tau} + \mathbf{\Delta E'} \quad (5)$$

where $\mathbf{E'}_t \sim CN(\mathbf{0}, \mathbf{I})$ and $\mathbf{\Delta E'} \sim CN(\mathbf{0}, \sigma_e^2(1-\rho^2)\mathbf{I})$. Because the matrix $\mathbf{H}_{TR,t}$ is a function of the matrix $\hat{\mathbf{H}}_t$ as $\mathbf{H}_{TR,t} = \mathcal{F}(\hat{\mathbf{H}}_t^H)$, it can be written as,

$$\begin{aligned} \mathbf{H}_{TR,t} &= \rho\mathbf{H}_{TR,t-\tau} + \sigma_{h_{eq}}\sqrt{1-\rho^2}\mathbf{E}_{t_{eq}} \\ &= \rho(Toeplitz(TR(\hat{\mathbf{H}}_{t-\tau}^H))) + \mathbf{\Delta E}_{eq} \end{aligned} \quad (6)$$

where $\mathbf{E}_{t_{eq}} \sim CN(\mathbf{0}, \mathbf{I})$ and it is different from $\mathbf{E}_t$ in (3) and $\mathbf{E'}_t$ in (5), even though they have the same statistical properties. Also, $\sigma_{h_{eq}}^2$ is the variance of the TR channel coefficients and $\mathbf{\Delta E}_{eq} \sim CN(\mathbf{0}, \sigma_{h_{eq}}^2(1-\rho^2)\mathbf{I})$. Finally, we define the conventional TR as the time reversal based MIMO-UWB system in an imperfect CSI without any optimizations. Also, the proposed pre-filter optimization means the application of the conventional TR (time reversal based MIMO-UWB system in an imperfect CSI) with the MMSE optimized pre-filter.

III. Robust Pre-filter Optimization

It is worthwhile to note that the interferences (ISI and MSI) are not absolutely eliminated by TR pre-filter. Especially in ultra-high data rate UWB transmission, we need to extremely short symbol in which leads to strong ISI and MSI. On the other hands, a TR pre-filter works in time domain to raise the SNR, but simultaneously leads to a BER performance floor caused by the ISI and MSI [13]. In this section, we derive a MMSE pre-equalization solution in the presence of the estimation error in time varying channels. The error vector that is needed to be considered for the system illustrated in Fig. 1 should be the difference between the transmitted symbols and the detected symbols, i.e.,

$$\begin{aligned} \mathbf{e}_t &= \hat{\mathbf{x}}_t - \mathbf{x}_t \\ &= ((\hat{\mathbf{H}}_t + \mathbf{\Delta H}_t)\mathbf{H}_{TR,t}\mathbf{F}_{MMSE,t}\mathbf{x}_t + \mathbf{n}_t) - \mathbf{x}_t \end{aligned} \quad (7)$$

where the TR matrix $\mathbf{H}_{TR,t}$ is constructed based on $\hat{\mathbf{H}}_t$ as presented in Section II. The MMSE solution should minimize the cost function $E\{\|\mathbf{e}_t\|^2\} = E\{\|\hat{\mathbf{x}}_t - \mathbf{x}_t\|^2\}$ with respect to $\mathbf{F}_{MMSE,t}$. Therefore, the linear MMSE pre-equalizer can be obtained by solving of (8). Calculation of the conditional expectation, as required in (8), seems to be difficult. We consider an approximately solution to solve it. To do this, we use the correlation model presented in (3), (5) and (6). According to [23], this model describes the time correlation coefficient function of the estimated CSI between the time instants $t - \tau$ and t as $\rho = J_0(2\pi f_d\tau)$ in which f_d is the maximum Doppler frequency. Also, $J_0(.)$ denotes the zero order Bessel function and $\tau = kT; k \leq N$ where k denotes as number of symbol and T is the data symbol duration. Knowledge of the Doppler spread is assumed in the design of the above proposal filter. Derivation of linear MMSE pre-equalization has been carried out in [25], Appendix E and also, an imperfect CSI based derivation has been provided in section 6.2.2 of [25]. Clearly, at first we take the conditional expectation over $\mathbf{\Delta H}_t$, $\mathbf{\Delta E}$ and $\mathbf{\Delta E}_{eq}$ similar to [23], because of using conditional CSI

$$\begin{aligned}\mathbf{F}_{MMSE,t} = \quad & \arg\min_{\tilde{\mathbf{F}}_{MMSE,t}} E_{\hat{\mathbf{H}}_t|\hat{\mathbf{H}}_{t-\tau}}\{E_{\mathbf{H}_{TR,t}|\mathbf{H}_{TR,t-\tau}}\{E_{\mathbf{x},\mathbf{\Delta H}_t}\{\|((\hat{\mathbf{H}}_t+\mathbf{\Delta H}_t)\mathbf{H}_{TR,t}\tilde{\mathbf{F}}_{MMSE,t}\mathbf{x}_t+\mathbf{n}_t)-\mathbf{x}_t\|^2\}\}\} \\ & \text{subject to } E_{\hat{\mathbf{H}}_t|\hat{\mathbf{H}}_{t-\tau}}\{E_{\mathbf{H}_{TR,t}|\mathbf{H}_{TR,t-\tau}}\{E_{\mathbf{x},\mathbf{\Delta H}_t}\{\|\tilde{\mathbf{F}}_{MMSE,t}\mathbf{x}_t\|^2\}\}\}=\sigma_{\mathbf{x}}^2\end{aligned} \tag{8}$$

$$\begin{aligned}\mathbf{F}_{MMSE,t} = \rho^2(\hat{\mathbf{H}}_{t-\tau}\mathbf{H}_{TR,t-\tau})^H \quad & \{\rho^4(\hat{\mathbf{H}}_{t-\tau}\mathbf{H}_{TR,t-\tau})(\hat{\mathbf{H}}_{t-\tau}\mathbf{H}_{TR,t-\tau})^H \\ & +\mathbf{C}_{\mathbf{\Delta H}_t}+\mathbf{C}_{\mathbf{\Delta E}}+\mathbf{C}_{\mathbf{\Delta E}_{eq}}+\mathbf{C}_{\mathbf{\Delta E},\mathbf{\Delta E}_{eq}}+(\tfrac{1}{SNR})\mathbf{I}\}^{-1}\end{aligned} \tag{9}$$

model as described in (3), (5) and (6) similar to Equation (2) of [23], and then, substitute $\rho\hat{\mathbf{H}}_{t-\tau}$, $\rho\mathbf{H}_{TR,t-\tau}$ and the mutually covariance matrices $\mathbf{C}_{\mathbf{\Delta H}_t}$, $\mathbf{C}_{\mathbf{\Delta E}}$, $\mathbf{C}_{\mathbf{\Delta E}_{eq}}$ and $\mathbf{C}_{\mathbf{\Delta E},\mathbf{\Delta E}_{eq}}$ as the channel imperfections in the Equation 6.24b of [25]. Accordingly, we get the MMSE solution as (9) in which $SNR=\frac{\sigma_{\mathbf{x}}^2}{\sigma_{\mathbf{n}}^2}$ and $\mathbf{C}_{\mathbf{\Delta H}_t}$ is the channel estimation error covariance matrix as $\mathbf{C}_{\mathbf{\Delta H}_t}=E_{\mathbf{\Delta H}_t}\{\mathbf{\Delta H}_t\mathbf{\Delta H}_t^H\}=\sigma_e^2\mathbf{I}$ in which σ_e^2 is the common estimation error variance for all of the sub-channels. Note that we assumed $\mathbf{\Delta E}$, $\mathbf{\Delta H}_t$ and also, $\mathbf{\Delta E}_{eq}$ and $\mathbf{\Delta H}_t$ are statistically independent. Also, according to (6), $\hat{\mathbf{H}}_t$ and $\mathbf{H}_{TR,t}$ are statistically dependent. The covariance matrices can be obtained as,

$$\begin{aligned}&\mathbf{C}_{\mathbf{\Delta E}}=E\{\mathbf{\Delta E}\mathbf{\Delta E}^H\}=\sigma_h^2(1-\rho^2)\mathbf{I}\\&\mathbf{C}_{\mathbf{\Delta E}'}=E\{\mathbf{\Delta E}'\mathbf{\Delta E}'^H\}=\sigma_e^2(1-\rho^2)\mathbf{I}\\&\mathbf{C}_{\mathbf{\Delta E}_{eq}}=E\{\mathbf{\Delta E}_{eq}\mathbf{\Delta E}_{eq}^H\}=\sigma_{h_{eq}}^2(1-\rho^2)\mathbf{I}\\&\mathbf{C}_{\mathbf{\Delta E},\mathbf{\Delta E}_{eq}}=E\{\mathbf{\Delta E}\mathbf{\Delta E}_{eq}^H\}=\sigma_h\sigma_{h_{eq}}(1-\rho^2)\mathbf{I}\end{aligned} \tag{10}$$

With respect to (5), $\mathbf{C}_{\mathbf{\Delta H}_t}=\rho^2\mathbf{C}_{\mathbf{\Delta H}_{t-\tau}}+\mathbf{C}_{\mathbf{\Delta E}'}$ in which $\mathbf{C}_{\mathbf{\Delta H}_{t-\tau}}=E_{\mathbf{\Delta H}_{t-\tau}}\{\mathbf{\Delta H}_{t-\tau}\mathbf{\Delta H}_{t-\tau}^H\}$ is the estimation error covariance matrix at the time instant $t-\tau$. If the perfect CSI is available (ideal channel estimation), Equation (9) is referred to as MMSE pre-filter optimization design in which $\mathbf{C}_{\mathbf{\Delta H}_t}=\mathbf{C}_{\mathbf{\Delta E}'}=0$.

IV. Proposed Power Allocation Scheme

In transmission over sub-channels $\overline{\mathbf{h}}_{ij,t}$, it can happen that we are faced with sub-channels that would require enormous transmit power to achieve acceptable bit error rates, especially in an imperfect CSI case. In this case it is beneficial, given the fixed amount of transmit power available, not to aim for equal error rates in all sub-channels, but perform an optimum power loading by minimizing the average bit error rate [25]. Some power allocation schemes are proposed in [26] to reduce the delay spread of the channel impulse response in the TR-MISO-UWB systems. Authors in [26] did not consider imperfect CSI case and also ISI and MSI effects on system performance in which their analysis is true for the ideal and quasi-static channels. Therefore, based on previous findings such as [25] and [27], we propose a new power loading scheme for TR-MIMO-UWB systems by minimizing the average bit error rate (BER) at the receiver in an imperfect CSI scenario and the time varying channels. This novel approach is a development of our previous power allocation work in the quasi-static MIMO channels [18]. The received signal at the MIMO channel output with TR pre-filtering and MMSE pre-equalizing in the time instant t, according to Fig. 1 can be written as

$$\mathbf{y}_t=(\hat{\mathbf{H}}_t+\mathbf{\Delta H}_t)\mathbf{H}_{TR,t}\mathbf{F}_{MMSE,t}\mathbf{x}_t+\mathbf{n}_t \tag{11}$$

where $\mathbf{\Delta H}_t$ and $\mathbf{n}_t$ are assumed mutually independent and uncorrelated matrices. Also, $\mathbf{x}_t=\frac{1}{\sqrt{N_t}}[x_{1,t},x_{2,t},...,x_{N_r,t}]^T$, $\mathbf{y}_t=\frac{1}{\sqrt{N_r}}[y_{1,t},y_{2,t},...,y_{N_r,t}]^T$ and $\mathbf{n}_t=[n_{1,t},n_{2,t},...,n_{N_r,t}]^T$ are the $N_r\times 1$ transmitted symbols, received symbols and AWGN vectors, respectively. The $N_r(2L_g-1)\times N_r$ MMSE pre-equalizing matrix $\mathbf{F}_{MMSE,t}$ is given by (9). For simplicity of our analysis, we define the $N_r(2L_g-1)\times 1$ MMSE pre-equalized transmitted symbols vector $\mathbf{x}_t'$ as $\mathbf{x}_t'=\mathbf{F}_{MMSE,t}\mathbf{x}_t$. Then, the received signal at j^{th} receive antenna in the time instant t can be expressed by (12). The first part of the received signal is the desired data symbol. In this part, the equivalent channel is the autocorrelation of channels. Also, $v_{j,t}$ and $w_{j,t}$ are the interference from other symbols and the interference from the channel estimation error in the time instant t, respectively. In $v_{j,t}$ and $w_{j,t}$ parts, the equivalent channel is the cross-correlation of channels. Therefore, the values of these terms are less than the former (first part of the received signal). Also, $v_{j,t}$ and $w_{j,t}$ terms in (12) appears as interference which degrades the performance of TR-MIMO-UWB system, especially in imperfect CSI. Some of this interference can be reduced by a MMSE pre-equalizer, but, we try to maximize the Signal to Interference plus Noise Ratio (SINR) more than ever by a power allocation scheme. If we define the conditional expectations as,

$$\begin{aligned}&E_{\hat{\mathbf{h}}_{ij,t}|\hat{\mathbf{h}}_{ij,t-\tau}}\{E_{\overline{\mathbf{H}}_{ij,t}|\overline{\mathbf{H}}_{ij,t-\tau}}\{.\}\}=E_{con}\{.\}\\&E_{\mathbf{\Delta h}_{ij,t}|\mathbf{\Delta h}_{ij,t-\tau}}\{E_{\overline{\mathbf{H}}_{ik,t}|\overline{\mathbf{H}}_{ik,t-\tau}}\{.\}\}=E_{con-error}\{.\}\end{aligned} \tag{13}$$

Then, the SINR at the j^{th} receive antenna in the time instant t is given by (14) in which $\|.\|_F$ denotes the Frobenius norm. By applying the above conditional expectations and using the approximate solution exploited for calculation of (9), also according to (3), (5) and (6), the SINR at the j^{th} receive antenna in the time instant t can be calculated as (15). If we define $\mathbf{R}_{ij,t-\tau}:=\hat{\mathbf{h}}_{ij,t-\tau}\overline{\mathbf{H}}_{ij,t-\tau}$ as auto-correlation vector of the channel vector $\hat{\mathbf{h}}_{ij,t-\tau}$ and, $\mathbf{C}_{ik,t-\tau}:=_{k\neq j}\hat{\mathbf{h}}_{ij,t-\tau}\overline{\mathbf{H}}_{ik,t-\tau}$ as cross-correlation vector of $\hat{\mathbf{h}}_{ij,t-\tau}$ with other sub-channels then, the SINR at the j^{th} receive antenna is expressed as (16) in which the estimation errors of the different sub-channels are assumed to be mutually independent, i.e., $\mathbf{\Delta h}_{ij,t}\amalg\mathbf{\Delta h}_{mn,t}$ where $\amalg$ is standing for mutual independence. Performance of the TR-MIMO-UWB system depends on transceiver structure and the received signal properties, e.g., its probability density

$$y_{j,t} = \underbrace{\sum_{i=1}^{N_t} \hat{\mathbf{h}}_{ij,t}\overline{\mathbf{H}}_{ij,t}\mathbf{x}'_{j,t}}_{Signal} + \underbrace{\underbrace{\sum_{i=1}^{N_t}\sum_{k=1,k\neq j}^{N_r} \hat{\mathbf{h}}_{ij,t}\overline{\mathbf{H}}_{ik,t}\mathbf{x}'_{k,t}}_{v_{j,t}} + \underbrace{\sum_{i=1}^{N_t}\sum_{k=1}^{N_r} \boldsymbol{\Delta}\mathbf{h}_{ij,t}\overline{\mathbf{H}}_{ik,t}\mathbf{x}'_{k,t}}_{w_{j,t}}}_{Interference} + \underbrace{n_{j,t}}_{Noise} \tag{12}$$

$$SINR_{j,t} = \frac{E_{con}\{\| \sum_{i=1}^{N_t} \hat{\mathbf{h}}_{ij,t}\overline{\mathbf{H}}_{ij,t}\|_F^2\}}{E_{con}\{\| \sum_{i=1}^{N_t}\sum_{k=1,k\neq j}^{N_r} \hat{\mathbf{h}}_{ij,t}\overline{\mathbf{H}}_{ik,t}\|_F^2\} + E_{con-error}\{\| \sum_{i=1}^{N_t}\sum_{k=1}^{N_r} \boldsymbol{\Delta}\mathbf{h}_{ij,t}\overline{\mathbf{H}}_{ik,t}\|_F^2\} + E\{\|\mathbf{n}_{j,t}\|_F^2\}} \tag{14}$$

$$SINR_{j,t} = \frac{\rho^4\left(\| \sum_{i=1}^{N_t} \hat{\mathbf{h}}_{ij,t-\tau}\overline{\mathbf{H}}_{ij,t-\tau}\|_F^2\right) + \sigma_h^2\sigma_{h_{eq}}^2(1-\rho^2)^2}{\rho^4\left(\| \sum_{i=1}^{N_t}\sum_{k=1,k\neq j}^{N_r} \hat{\mathbf{h}}_{ij,t-\tau}\overline{\mathbf{H}}_{ik,t-\tau}\|_F^2 + \| \sum_{i=1}^{N_t}\sum_{k=1}^{N_r} \boldsymbol{\Delta}\mathbf{h}_{ij,t-\tau}\overline{\mathbf{H}}_{ik,t-\tau}\|_F^2\right) + \sigma_{h_{eq}}^2(1-\rho^2)^2(\sigma_h^2+\sigma_e^2) + \sigma_n^2} \tag{15}$$

$$SINR_{j,t} = \frac{\rho^4\left(\sum_{i=1}^{N_t}\sum_{l=0}^{2L-2} |\mathbf{R}_{ij,t-\tau}(l)|^2\right) + \sigma_h^2\sigma_{h_{eq}}^2(1-\rho^2)^2}{\rho^4\left(\sum_{i=1}^{N_t}\sum_{k=1,k\neq j}^{N_r}\sum_{l=0}^{2L-2} |\mathbf{C}_{ik,t-\tau}(l)|^2 + L\sigma_e^2\sum_{i=1}^{N_t}\sum_{k=1}^{N_r}\sum_{l=0}^{L-1} |\hat{\mathbf{h}}_{ik,t-\tau}(l)|^2\right) + \sigma_{h_{eq}}^2(1-\rho^2)^2(\sigma_h^2+\sigma_e^2) + \sigma_n^2} \tag{16}$$

function (PDF). For $L_g t_s \geq 5nsec$ where t_s is the time resolution of the channel, the average numbers of paths is high, so using central limit theorem, the sum of a large number of independent, zero-mean random variables form a Gaussian PDF for the path gain [28]-[29]. But for $L_g t_s < 5nsec$, path gain PDF is not Gaussian and as the $L_g t_s$ increases, the non-Gaussian shape tends more to Gaussian, and the densities become more bell shaped [29]. According to the above discussion, the average BER of the TR-MIMO-UWB system at the j^{th} receive antenna, assuming BPAM modulation, can be derived approximately from Eq. (16) as [27-29],

$$BER_{j,t} \approx \frac{1}{N_t}\sum_{i=1}^{N_t} Q\left(\sqrt{2SINR_{j,t}p_{i,j}}\right) \tag{17}$$

where $p_{i,j}$, $P_{T,j} = \sum_{i=1}^{N_t} p_{i,j}$ and $Q(.)$ are the transmit power assigned to i^{th} transmit antenna, the total transmitted available power for the j^{th} receive antenna and the Marcum Q-function, respectively. $Q(x)$ is defined as,

$$Q(x) = \frac{1}{\sqrt{2\pi}}\int_x^{+\infty} \exp(\frac{-t^2}{2})dt \tag{18}$$

For simplicity of our analysis we assume $\sigma_{\mathbf{x}}^2 = 1$, so that $P_{T,j} = N_t$. The optimum power allocation vector $\mathbf{P}_j = [p_{1,j}, \cdots, p_{N_t,j}]^T$ that minimizes the average BER at the j^{th} receive antenna, when an imperfect CSI is presented, can be obtained by introducing the Lagrange function as [25],

$$L_G = \frac{1}{N_t}\sum_{i=1}^{N_t} Q\left(\sqrt{2SINR_{j,t}p_{i,j}}\right) - \lambda\left(N_t - \sum_{i=1}^{N_t} p_{i,j}\right) \tag{19}$$

With partial derivative we obtain,

$$\frac{\partial L_G}{\partial p_{i,j}} = \frac{-1}{2N_t\sqrt{\pi}}\sqrt{\frac{SINR_{j,t}}{p_{i,j}}}\exp(-SINR_{j,t}p_{i,j}) + \lambda \tag{20}$$

Solving $\frac{\partial L_G}{\partial p_{i,j}} = 0$ for $p_{i,j}$, we can allocate the power to each transmit antenna in a manner that,

$$\left(\frac{1}{SINR_{j,t}}\right)p_{i,j}\exp(SINR_{j,t}p_{i,j}) = \frac{1}{4N_t^2\lambda^2\pi} \tag{21}$$

and finally,

$$p_{i,j}(\lambda) = \left(\frac{1}{SINR_{j,t}}\right)W\left((SINR_{j,t})^2\frac{1}{4N_t^2\lambda^2\pi}\right) \tag{22}$$

where $W(.)$ is the real valued Lambert's W-function defined as the inverse of the function $f(x) = x\exp(x)$ for $x \geq 0$, i.e., $W(x) = a \Leftrightarrow a\exp(a) = x$ [30]. Since the $W(x)$ function is real and concave, the unique solution for power allocation vector to minimize the average BER at the j^{th} receive antenna can be found by the following simple iterative procedure [31].

1. Choose a positive λ, which fulfils,

$$(SINR_{j,t})\left(\frac{1}{4N_t^2\lambda^2\pi}\right) \leq P_{T,j} \tag{23}$$

2. Calculate,

$$\hat{P}_{T,j} = \left(\frac{1}{SINR_{j,t}}\right)W\left((SINR_{j,t})^2\frac{1}{4N_t^2\lambda^2\pi}\right) \tag{24}$$

3. If $\hat{P}_{T,j}$ is not yet sufficiently close to $P_{T,j}$ then multiply λ by $\frac{P_{T,j}}{\hat{P}_{T,j}}$ and go back to step (2).

4. Compute $\mathbf{P}_j = [p_{1,j}, \cdots, p_{N_t,j}]^T$ according to (22).

Note that since $W(x)$ for $x > \frac{-1}{e}$ is a monotonic function then according to (22) the highest powers (max $p_{i,j}$) are assigned to the weakest signals so the SINR values approximately stay constant for all sub-channels. The above algorithm should be iterated for all of N_r receive antenna and then, we achieve the total optimized power allocation vector as $\mathbf{P} = \sum_{j=1}^{N_r}\mathbf{P}_j$. Note that the total available power for data transmission is $P_T = \frac{1}{N_r}\sum_{j=1}^{N_r} P_{T,j}$.

V. Simulation Results and Discussion

To evaluate the performance of the proposed solutions for the TR-MIMO-UWB system, Monte Carlo simulations are conducted in this section. As in [11], the second-order derivative of Gaussian pulse has been used as the transmitted pulse $p(t)$, which is mathematically defined as,

$$p(t) = \left(1 - 4\pi \left(\frac{t - t_c}{T_p}\right)^2\right) \exp\left(-2\pi \left(\frac{t - t_c}{T_p}\right)^2\right) \quad (25)$$

where T_p is a parameter corresponding to pulse width, and t_c is a time shifting of the pulse. In the following simulations, we consider $T_p = 5nsec$, and $t_c = 2.5nsec$. Also, one pulse per symbol is assumed, i.e., symbol duration T is assumed $5nsec$ where is equal to transmission rate of $200Mbps$ and also, sampling time $t_c = 0.167nsec$ is considered. We assume that the signal is transmitted over UWB channel. As in [11], we use the IEEE 802.15.3a CM4 channel model [32]-[33] as a worst case for each channel realization in simulations. Although the channel model CM4 is designed for Single-Input Single-Output (SISO) scenario, the extension to a MIMO configuration is achieved by assuming that the MIMO channel parameters are independent and identically distributed realizations from the same statistical model. We further consider the case of a 2×2 TR-MIMO-UWB system set-up with BPAM modulated data streams. In our simulations, we use the normalized Doppler frequency $f_dT = 0.001$, $f_dT = 0.005$ and $f_dT = 0.01$. Also, the channel estimation error variance $\sigma_e^2 = 0.1$ is assumed. At first, it is necessary that we clarify some phrases mentioned in some simulation results. Phrase "Perfect CSI" means the conventional TR-MIMO-UWB system in perfect CSI. Clearly, this scenario does not need to the optimization schemes. We provide a benchmark curve according to [11]. Phrase "Conventional TR-MIMO-UWB" means the time reversal based MIMO-UWB system in an imperfect CSI without any optimization. Also, "proposed MMSE TR-MIMO-UWB" means the application of the conventional TR (time reversal based MIMO-UWB system in an imperfect CSI) with the MMSE optimized pre-filter. Phrase "Proposed with loading" means the application of the proposed MMSE TR-MIMO-UWB with the power allocation scheme. Finally, "Proposed without loading" is referred to the proposed MMSE TR-MIMO-UWB.

To optimize the TR-MIMO-UWB system performance of Fig. 1 and to mitigate the imperfect CSI effects, we use the proposed robust MMSE solution mentioned in Section 3. Figs. 2 and 3 plot the average BER performances of the 2×2 TR-MIMO-UWB system with proposed optimization for N=5, 10, respectively. Clearly, it can be seen from Figs. 2 and 3 that, our robust MMSE solution exhibits a lower average BER performance when compared to the conventional TR-MIMO-UWB system design. More specifically, from the figures, it can be observed that the proposed method have more advantage for shorter N where the channel time correlation is noticeable, in that, as N increases, the correlation coefficient $\rho = J_0(2\pi f_d \tau) = J_0(2\pi f_d NT)$ decreases and so, the optimized solutions performance is diminished.

Figs. 4 and 5 plot the average BER performances of the 2×2 TR-MIMO-UWB system with proposed optimization for $f_dT = 0.001$ and $f_dT = 0.005$, respectively. As it can be observed from Figs. 4 and 5 that, for lower normalized Doppler frequency, our proposed method has good performance over all values of N while in the higher normalized Doppler frequency, the performance is noticeable for shorter Ns where the channel time correlation is noticeable.

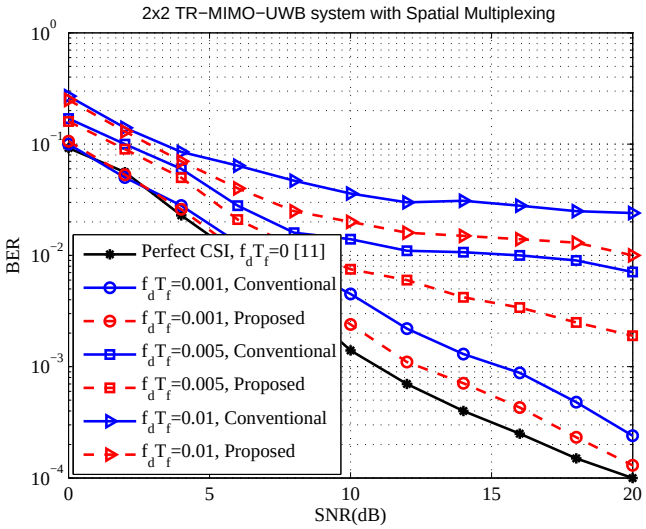

Fig. 2. BER performance of the 2×2 TR-MIMO-UWB system with proposed MMSE optimization for $N = 5$, $\sigma_e^2 = 0.1$ and different Doppler values.

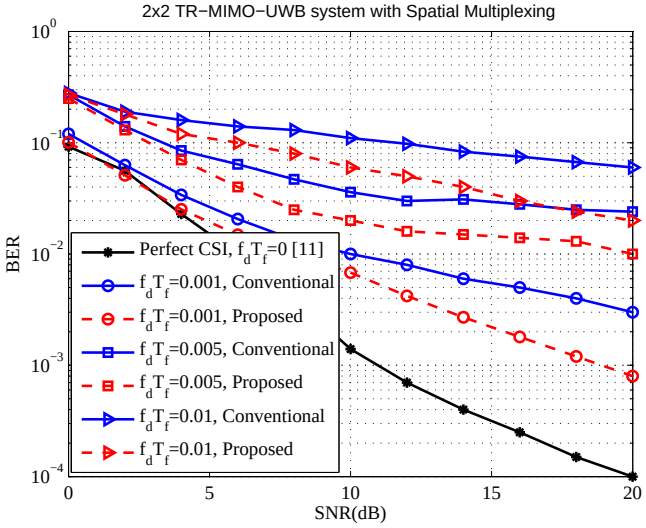

Fig. 3. BER performance of the 2×2 TR-MIMO-UWB system with proposed MMSE optimization for $N = 10$, $\sigma_e^2 = 0.1$ and different Doppler values.

In addition to the MMSE robust optimization scheme, we use the proposed power loading solution mentioned in Section IV to improve the TR-MIMO-UWB system performance more than ever. In Figs. 6-9, we can observe the performance of the proposed power loading for the MMSE robust optimization. As can be seen from these figures, the performance of power

loading is noticeable, especially for high SNR values. Such as, according to Figs. 6-7, for $f_dT = 0.001$, the power loading scheme substantially outperforms the robust optimization method about 2dB SNR in Fig. 6 and 4dB SNR in Fig. 7 both at the average BER=10^{-3}. Also, according to Figs. 8-9, the power loading scheme can be used to increase the TR-MIMO-UWB system performance, considerably. Furthermore, the system performance is mitigated as N increases. Therefore, our proposed method significantly depends on the values of N or the time-correlation coefficient ρ.

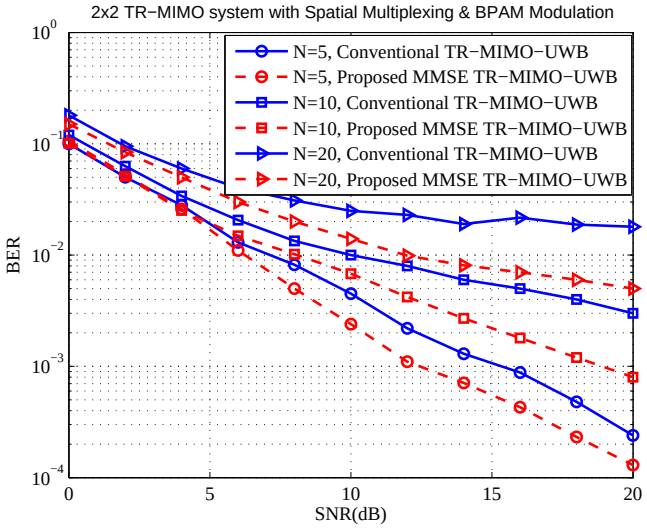

Fig. 4. BER performance of the 2×2 TR-MIMO-UWB system with proposed MMSE optimization for $f_dT = 0.001$, $\sigma_e^2 = 0.1$ and different N values.

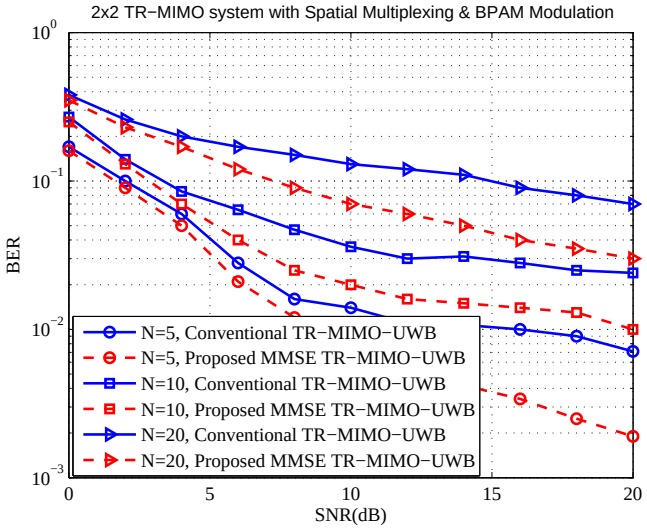

Fig. 5. BER performance of the 2×2 TR-MIMO-UWB system with proposed MMSE optimization for $f_dT = 0.005$, $\sigma_e^2 = 0.1$ and different N values.

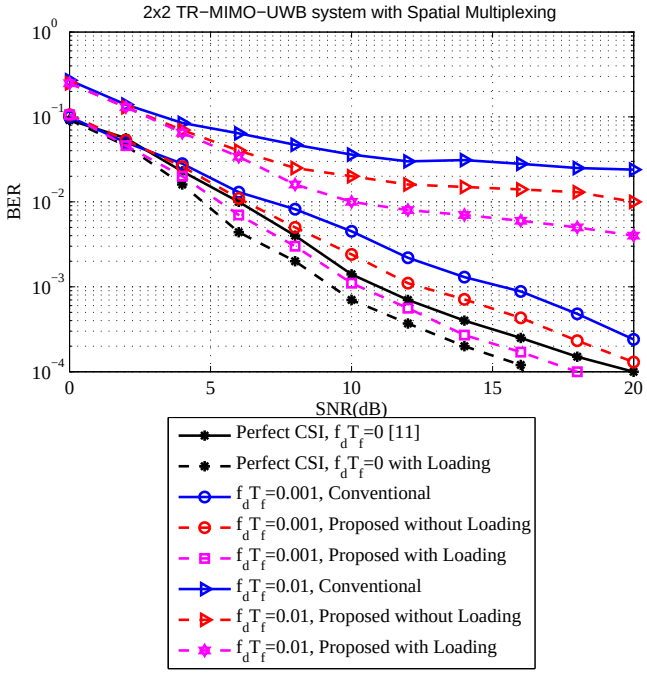

Fig. 6. BER performance of the 2×2 TR-MIMO-UWB system with proposed MMSE optimization and power loading for $N = 5$, $\sigma_e^2 = 0.1$ and different Doppler values.

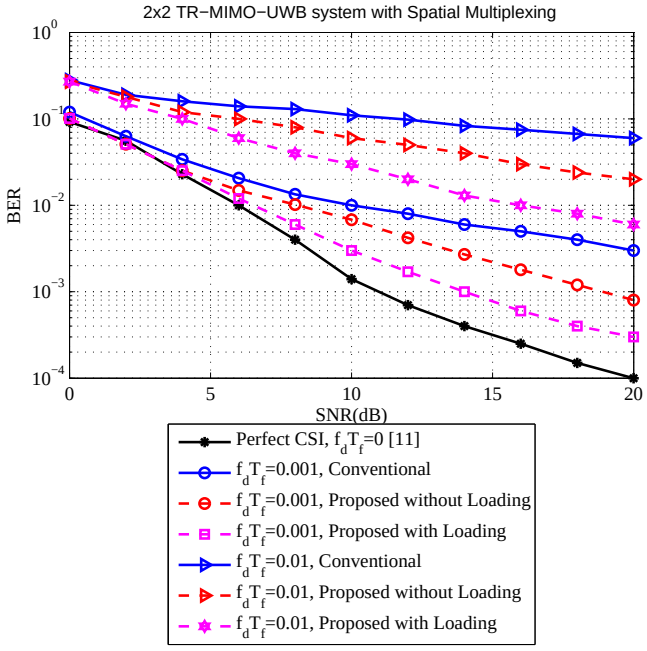

Fig. 7. BER performance of the 2×2 TR-MIMO-UWB system with proposed MMSE optimization and power loading for $N = 10$, $\sigma_e^2 = 0.1$ and different Doppler values.

As we observed from the simulation results, we will confront the weak performance of our methods as the speed of the user or vehicle increases, in that by increasing f_d, the correlation coefficient decreases (it depends by zero-order Bessel function) and so, SINR decreases. As a result, the

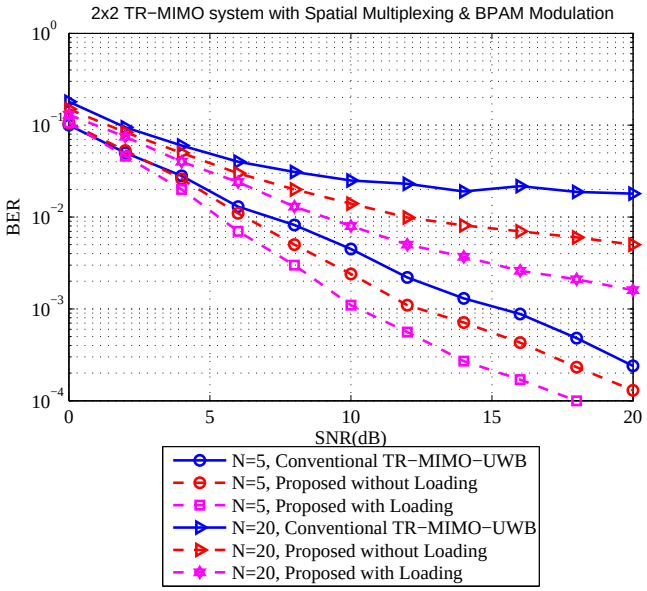

Fig. 8. BER performance of the 2×2 TR-MIMO-UWB system with proposed MMSE optimization and power loading for $f_d T = 0.001$, $\sigma_e^2 = 0.1$ and different N values.

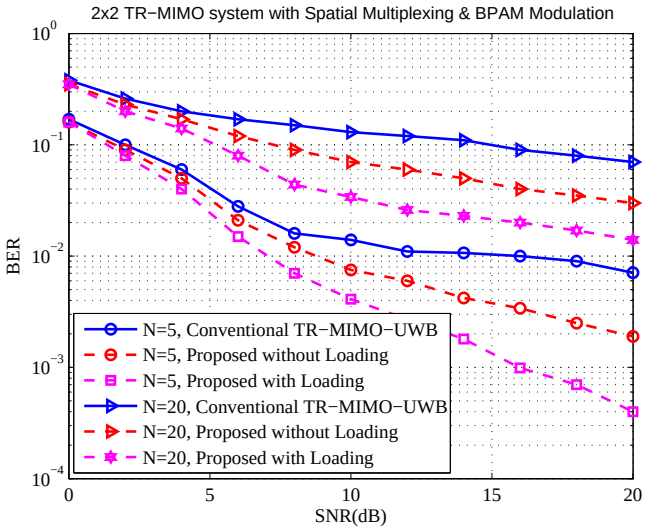

Fig. 9. BER performance of the 2×2 TR-MIMO-UWB system with proposed MMSE optimization and power loading for $f_d T = 0.005$, $\sigma_e^2 = 0.1$ and different N values.

BER increases. Similar discussions can be presented for N. Therefore, the best performance of our solutions is in lower speed of user or lower N values.

VI. Conclusions

A robust MMSE TR-MIMO-UWB system design that exploits the knowledge of the conditional channel distribution, given the available outdated CSI in τ second ago was proposed in this paper. In proposal solution, once the channel estimation error covariance matrix $\mathbf{C}_{\mathbf{\Delta H}_t}$, outdated CSI and the time correlation coefficient ρ is transmitted from the receiver to the transmitter in the beginning of a data block and then, they are used during that block. This solution mitigates the feedback overhead in time varying channel significantly than traditional method in which we used to feedback the CSI during a data block. We have also shown that our robust approach outperforms the traditional design in terms of BER plots in time varying scenario, especially for high SNR and shorter data block length where the time correlation of the channel is noticeable. Then, the power loading strategy was proposed for the imperfect CSI in the robust optimized MMSE TR-MIMO-UWB system. It was observed that it brought a performance gain in the 2×2 TR-MIMO-UWB system in an imperfect CSI scenario and the robust optimized system.

References

[1] F. Nekoogar, *Ultra-wideband communications: fundamentals and applications*, Pearson Education, First printing, September, 2005.

[2] J. H. Reed, *An Introduction to Ultra Wideband Communication Systems*, Prentice Hall PTR, April 05, 2005.

[3] R. Hoctor and H. Tomlinson, *Delay-Hopped Transmitted-Reference RF Communications*, Proc. IEEE 2nd Ultra Wideband Systems and Technologies (UWBST02), Baltimore, MD, pp. 265-269, May 2002.

[4] R. J. Fontana, E. Richley, and J. Barney, *Commercialization of an Ultra Wideband Precision Asset Location System*, Proc. IEEE Conference UWB systems and Technologies, Reston, VA, 2003.

[5] J. D. Choi and W. E. Stark, *Performance of Ultra-Wideband Communications with Suboptimal Receivers in Multipath Channels*, IEEE Journal on Selected Areas in Communications, vol. 20, pp. 1754-1766, Dec. 2002.

[6] K. Witrisal, G. Leus, G. J. M. Janssen et al., *Noncoherent ultra-wideband systems: an overview of recent research activities*, IEEE Signal Processing Magazine, vol. 26, no. 4, pp. 4866, 2009.

[7] J. Zhang, P. V. Orlik, Z. Sahinoglu, A. F. Molisch, and P. Kinney, *UWB systems for wireless sensor networks*, Proceedings of the IEEE, vol. 97, no. 2, pp. 313331, 2009.

[8] M. Fink, *Time-reversed acoustic*, Scientific Amer., pp. 67-73, Nov.1999.

[9] G. Foschini and M. Gans, *On limits of wireless communications in a fading environment when using multiple antennas*, Wireless Pers. Commun, 1998, 6, (3), pp.311-335.

[10] T. Kaiser and F. Zheng, *Ultra Wideband Systems with MIMO*, John Wiley Sons Ltd.,UK, 2010.

[11] H. Nguyen, F. Zheng and T. Kaiser, *Antenna selection for time reversal MIMO UWB systems*, In IEEE 69th Vehicular Technology Conf., Barcelona, Spain, 2629 April 2009.

[12] T. Strohmer, M. Emami, J. Hansen, G. Papanicolaou, and A. J. Paulraj, *Application of time reversal with MMSE equalizer to UWB Communications*, Proc. IEEE Global Telecommunications Conference, Dallas, Texas, Nov.29-Dec.3, 2004, pp.3123-3127.

[13] T. Wang, and T. Lv, *Canceling Interferences for High Data Rate Time Reversal MIMO UWB System: A Precoding Approach*, EURASIP Journal on Wireless Communications and Networking, vol. 2011, pp.1-10.

[14] T. K. Nguyen, H. Nguyen, F. Zheng, and T. Kaiser, *Spatial correlation in SM-MIMO-UWB systems using a pre-equalizer and pre-Rake filter*, in Proceedings of the IEEE International Conference on Ultra-Wideband (ICUWB '10), pp. 540543, September 2010.

[15] H. Nguyen, V. D. Nguyen, T. K. Nguyen, K. Maichalernnukul, F. Zheng, and T. Kaiser, *On the Performance of the Time Reversal SM-MIMO-UWB System on Correlated Channels*, International Journal of Antennas and Propagation, , doi:10.1155/2012/929018, Volume 2012.

[16] H. Khaleghi Bizaki, S. Alizadeh, *Mitigation of Channel Estimation Error in TR-UWB system Based on a Novel MMSE Equalizer*, Springer Annals of Telecommunication, DOI 10.1007/s12243-012-0325-8, published online: 6 Oct. 2012.

[17] S. Alizadeh, H. Khaleghi Bizaki and M. Okhovvat, *Effect of Channel Estimation Error on Performance of Time Reversal-UWB Communication System and its Compensation by Pre-filter*, IET Communications, vol. 6, no. 12, pp.17811794, Nov. 2012.

[18] S. Alizadeh, and H. Khaleghi Bizaki, *Novel Robust Optimization and Power Allocation of Time Reversal-MIMO-UWB Systems in an Imperfect CSI*, The International Journal of Advances in Telecommunications, Electrotechnics, Signals and Systems (IJATES2), Vol. 2, No. 2 (2013), pp. 84-91.
[19] S. Alizadeh, and H. Khaleghi Bizaki, *An Enhanced MMSE based Pre-processing Scheme for Time Reversal MIMO-UWB Systems in an Imperfect CSI*, Proceedings of the 21st IEEE Iranian Conference on Electrical Engineering (ICEE'2013), Mashhad, Iran, doi: 10.1109/IranianCEE.2013.6599663, 14-16 May 2013.
[20] I. H. Naqvi, P. Besnier and G. El Zein, *Robustness of a time-reversal ultra wideband system in non-stationary channel environment*, IET Microwaves, Antennas and Propagation, March 2011, Vol. 5, No. 4, pp. 468-475.
[21] X. Liu, B. Z. Wang, S. Xiao and S. Lai, *Post-Time-Reversed MIMO Ultra wideband Transmission Scheme*, IEEE Transactions on Antennas and Propagation, May 2010, vol. 58, no.5, pp.1731-1738.
[22] D. Abbasi-Moghadam, V. T. Vakili, *Effect of Channel Estimation Error on Time Reversal UWB Communication System*, Springer Wireless Personal Communications, DOI: 10.1007/s11277-011-0460-y, published online: 25 Nov. 2011.
[23] H. Khaleghi Bizaki, *Tomlinson-Harashima Precoding Optimization over Correlated MIMO Channels*, IEEE International Conference on Wireless Communications, Networking, and Information Security (WCNIS), pp. 207-211, Jun. 2010.
[24] B. Hassibi and B. M. Hochwald, *How much training is needed in multiple antenna wireless links?*, IEEE Trans. Inf. Theory, vol. 49, no. 4, pp. 951-963, Apr. 2003.
[25] C. Windpassinger, *Detection and Precoding for Multiple Input Multiple Output Channels*, PhD dissertation, Erlangen University, Jan. 2004.
[26] P. Kyristi, G. Panicolaou, and A. Oprea, *MISO time reversal and 918 delay-spread compression for FWA channels at 5 GHz*, IEEE Antennas 919 Wireless Propag. Lett., Dec. 2004, vol. 3, pp. 9699.
[27] H. K. Bizaki and A. Falahati, *Tomlinson-Harashima precoding with imperfect channel state information*, IET. Communication journal, vol.2, no.1, pp.151-158, January 2008.
[28] K. Witrisal, *Statistical analysis of the IEEE 802.15.4a UWB PHY over Multipath Channels*, IEEE Wireless Communications and Networking Conference, WCNC2008, March 31April 3 2008.
[29] D. Abbasi-moghadam, V. Tabataba Vakili, *Characterization of Indoor Time Reversal UWB Communication Systems: Spatial, Temporal and Frequency Properties*, Wiley International Journal of Communication Systems, doi:10.1002/dac.1140, published online 28 April 2010.
[30] R. M. Corless, G. H. Gonnet, D. E. G. Hare, D. J. Jeffrey, and D. E. Knuth, *On the Lambert W Function*, Advances in Computational Mathematics, volume 5, 1996, pp. 329-359.
[31] T. Hunziker, D. Dahlhaus, *Optimal Power Adaptation for OFDM Systems with Ideal Bit-Interleaving and Hard-Decision Decoding*, IEEE International Conference on Communications (ICC), vol. 5, 2003, pp:3392-3397.
[32] J. Foerster et al., *Channel modeling sub-committee report final*, IEEE P802.15 Wireless Personal Area Networks, P802.15-02/490r1-SG3a, Feb. 2003.
[33] A. F. Molisch, K. Balakrishnan, D. Cassioli, C. Chong, S. Emami, A. Fort, J. Karedal, J. Kunisch, H. Schantz, U. Schuster, and K. Siwiak, *IEEE 802.15.4a Channel model final report*, Tech. Rep., 2004.

Sajjad Alizadeh was born in Roudsar, Guilan Province, Iran on November 3, 1983. He received the Associate Degree (A.D.) from Electronics Engineering College (Electronics Industry University) of Shiraz University (Shiraz University of Technology (SUTECH) today), Shiraz, Iran, in 2005 and the B.Sc. degree from Shahid Rajaee Teacher Training University (SRTTU), Tehran, Iran, in 2007, both in electronics. Also he received the M.Sc. degree in Communication Engineering from Imam Hossein University (IHU), Tehran, Iran, in 2011. He is currently working toward the Ph.D. degree in Electrical Engineering (Communication Systems) at Yazd University, Yazd, Iran. He has served as a referee in IET Communications journal. His current research interests are in the area of UWB wireless communications with special emphasis on digital and statistical signal processing, Time Reversal signaling, propagation channels modeling, multiple-antenna (MIMO) schemes, Cognitive Radio networks, Detection and Estimation theory, Convex Optimizations and Interference Modeling in Wireless Communications.

Hossein Khaleghi Bizaki received his Ph.D. degree in Electrical Engineering, Communication system, from Iran University of Science and Technology (IUST), Tehran, Iran, in 2008. Dr. Bizaki started his work as assistant professor in 2008. Now, he is author or co-author of more than 30 publications. His research interests include Information Theory, Coding Theory, Wireless Communication, MIMO Systems, Space Time Processing, and other topics on Communication System and Signal Processing.

Reza Saadat (M'11) received the B.Sc. degree in electronics engineering, the M.Sc. degree in communication systems engineering, and the Ph.D. degree in electrical engineering from Isfahan University of Technology, Isfahan, Iran, in 1992, 1996, and 1999, respectively. Since 1999, he has been an Assistant Professor with the Department of Electrical and Computer Engineering, Yazd University, Yazd, Iran. His research interests include received signal strength positioning, resource allocation, and wireless sensor networks.

Blind Identification and Equalization of MC-CDMA Systems Using Higher Order Cumulants

Mohammed ZIDANE, Said SAFI, Mohamed SABRI, Ahmed BOUMEZZOUGH, and Miloud FRIKEL

***Abstract*—In this work we propose an algorithm based on fourth order cumulants for identification of the linear system (Finite Impulse Response (FIR)) with Non Minimum Phase (NMP) excited by non-Gaussian sequences, independent identically distributed (i.i.d). In order to test its efficiency, we have compared with the Safi et al. algorithm, for that we considered three practical frequency-selective fading channel, called Broadband Radio Access Network (BRAN A, BRAN B, and BRAN D), normalized for MC−CDMA systems. In the part of MC−CDMA, we use the zero forcing (ZF) and the minimum mean square error (MMSE) equalizers to perform our algorithms. The simulation results show that the bit error rate (BER) performances of the downlink MC−CDMA systems, using proposed algorithm (AlgoZ) is more accurate compared with the results obtained with the Safi et al. (Alg−CUM) algorithm.**

***Keywords*—NMP channel, Blind System Identification and Equalization, Higher Order Statistics, MC−CDMA systems.**

I. Introduction

In this work, identification of a finite impulse response (FIR) linear system driven by a non gaussian in noisy environment is considered. When the process is Gaussian, the autocorrelation sequence of the observed process is used to identify the system, but the autocorrelation sequence is insensitive to the phase characteristics of the system, and a non minimum phase system cannot be identified correctly using the autocorrelation sequence [1]. Further, the autocorrelation sequence fails to provide a complete statistical description for a non Gaussian process [2], it was shown that consistent estimates of the parameters of any FIR system can be obtained by using higher order statistics or cumulants of the observed process [2],[3]. This is because the higher order cumulants preserve the phase characteristics, unlike the autocorrelation sequence.

Many algorithms exist, in the literature for the identification of the non-minimum phase FIR system using higher order cumulants [2],[4],[8],[9],[10].

In this paper, we have, principally, focussed in channels impulse response estimation with non minimum phase and selective frequency such as: BRAN A, BRAN B, and BRAN D normalized for MC-CDMA systems. In most wireless environments, there are many obstacles in the channels, such as buildings, mountains and walls between the transmitter and the receiver. Reections from these obstacles cause many different propagation paths. The problem encountered in communication is the synchronization between the transmitter and the receiver, due to the echoes and reection between the transmitter and the receiver. To solve the problem of phase estimation we will use, the Higher order cumulants (HOC) to test whats the robustness of those techniques if the channel is affected by a gaussian noise.

In this paper, we propose an algorithm based, only, on fourth order cumulants. In order to test its efciency, we have compared with the Safi et al. algorithm [2], for that we considered three practical frequency-selective fading channel, called Broadband Radio Access Network (BRAN A, BRAN B, and BRAN D), normalized by the European Telecommunications Standards Institute (ETSI) in [12] and [13]. The simulation results show that the bit error rate (BER) performances of the downlink MC-CDMA systems (transmission from the base station to the mobile systems), using proposed algorithm (AlgoZ) is more accurate compared with the results obtained with the Safi et al (Alg−CUM) algorithm.

II. Preliminaries and problem statement

A. Model and assumptions

We consider the single-input single-output (SISO) model (figure 1) of the Finite Impulse Response (FIR) system described by the following relationships:

Noise free case :

$$y(k) = \sum_{i=1}^{q} x(i)h(k-i) \tag{1}$$

With noise :

$$r(k) = y(k) + n(k) \tag{2}$$

Where $x(i)$ is the input sequence, is the impulse response coefficients, q is the order of FIR system, is $r(k)$ the mesured output of system and $n(k)$ is the noise sequence.

In order to simplify the construction of the algorithm we

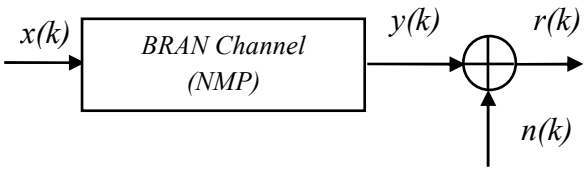

Fig. 1. Channel model

assume that: The input sequence, $x(k)$, is independent and

M. ZIDANE and S. SAFI are with the Department of Mathematics and Informatics, Polydisciplinary Faculty, Sultan Moulay Slimane University, Morocco.

M. SABRI, A. BOUMEZZOUGH are with Department of Physics, Faculty of Sciences and technology, Sultan Moulay Slimane University, Morocco.

M. FRIKEL is with GREYC laboratory, ENSICAEN School, Caen University, France.

doi: 10.11601/ijates.v3i1.73

identically distributed $(i.i.d)$ zero mean, and non-Gaussian. The system is causal and truncated, i.e. $h(k) = 0$ for $i < 0$ and $i > q$, where $h(0) = 1$. The system order q is known. The measurement noise sequence $n(k)$ is assumed zero mean, i.i.d, Gaussian and independent of $x(k)$ with unknown variance.

B. Basic relationships

In this section, we present the general fundamental relations which permit to identify the FIR linear systems using Higher Order Cumulants (HOC).

The mth order cumulants of the $y(n)$ can be expressed as a function of impulse response coefficients $h(i)$ as follows [2],[4],[7],[9],[10]:

$$C_{my}(t_1, t_2, ..., t_{m-1}) = \xi_{mx} \sum_{i=0}^{q} h(i)h(i+t_1)...h(i+t_{m-1}). \tag{3}$$

Where ξ_{mx} represents the m^{th} order cumulants of the excitation signal $x(i)$ at origin.
If $m = 2$ into Eq. (3) we obtain the second order cumulant (AutoCorrelation Function (ACF)):

$$C_{2y}(t) = \xi_{2x} \sum_{i=0}^{q} h(i)h(i+t) \tag{4}$$

For $m = 4$, Eq. (3) becomes:

$$C_{4y}(t_1, t_2, t_3) = \xi_{4x} \sum_{i=0}^{q} h(i)h(i+t_1)h(i+t_2)h(i+t_3). \tag{5}$$

The Fourier transforms of the 2^{nd} and 4^{rd} order cumulants are given respectively by the following equations [6],[11]:

$$\begin{aligned} S_{2y}(\omega) = TF\{C_{2y}(t)\} &= \xi_{2x} \sum_{i=0}^{q} \sum_{t=-\infty}^{+\infty} h(i)h(i+t) \exp(-j\omega t) \\ &= \xi_{2x} H(-\omega)H(\omega) \end{aligned} \tag{6}$$

With

$$H(\omega) = \sum_{i=0}^{+\infty} h(i) \exp(-j\omega t) \tag{7}$$

$$\begin{aligned} S_{4y}(\omega_1, \omega_2, \omega_3) &= TF\{C_{4y}(t_1, t_2, t_3)\} \\ &= \xi_{4x} H(-\omega_1 - \omega_2 - \omega_3)H(\omega_1)H(\omega_2)H(\omega_3) \end{aligned} \tag{8}$$

So, if we take $\omega = \omega_1 + \omega_2 + \omega_3$, the equation (8) becomes:

$$S_{2y}(\omega_1 + \omega_2 + \omega_3) = \xi_{2x} H(-\omega_1 - \omega_2 - \omega_3)H(\omega_1 + \omega_2 + \omega_3) \tag{9}$$

Then, from the Eqs, (8) and (9) we construct a relationship between the spectrum, the bispectrum and the parameters of the output system:

$$S_{4y}(\omega_1, \omega_2, \omega_3)H(\omega_1+\omega_2+\omega_3) = \mu H(\omega_1)H(\omega_2)H(\omega_3)S_{2y}(\omega_1+\omega_2+\omega_3) \tag{10}$$

With
$\mu = \frac{\xi_{4x}}{\xi_{2x}}$
The inverse Fourier transform of the Eq. (10) is:

$$\sum_{i=0}^{q} C_{4y}(t_1-i, t_2-i, t_3-i)h(i) = \mu \sum_{i=0}^{q} h(i)h(t_2-t_1+i)h(t_3-t_1+i)C_{2y}(t_1-i). \tag{11}$$

Based on the relationship (11) we can develop the following algorithm based on the Higher Order Statistics (HOC).

III. Proposed algorithm: AlgoZ

if we take $t_1 = t_2$ into Eq. (11) we obtain:

$$\sum_{i=0}^{q} C_{4y}(t_1-i, t_1-i, t_3-i)h(i) = \mu \sum_{i=0}^{q} h(i)h(i)h(t_3-t_1+i)C_{2y}(t_1-i). \tag{12}$$

If we use the ACF property of the stationary process such as $C_{2y(t)} \neq 0$ only for $-q \leq t \leq q$ and vanishes elsewhere if we suppose that $t_1 = -q$ the Eq. (11) becomes:

$$\sum_{i=0}^{q} C_{4y}(-q-i, -q-i, t_3-i)h(i) = \mu h^2(0)h(t_3+q)C_{2y}(-q) \tag{13}$$

If we suppose that the system is causal and truncated (i.e. $h(i) = 0$ for $i < 0$ and $i > q$), the choice of t_3 imposes that $t_3 \geq -q$. So, this implies $0 \leq t_3 + q \leq q$. For this reason, we have $t_3 = -q, -q + 1, , 0$.
Else if we take $t_1 = t_3 = -q$ into the Eq. (12), we obtain the following equation:

$$\sum_{i=0}^{q} C_{4y}(-q-i, -q-i, -q-i)h(i) = \mu \sum_{i=0}^{q} h(i)h(i)h(i)C_{2y}(-q-i). \tag{14}$$

According to the ACF property the relation (14) becomes:

$$C_{4y}(-q, -q, -q)h(0) = \mu h^3(0)C_{2y}(-q) \tag{15}$$

With $h(0) = 1$ we obtain:

$$C_{4y}(-q, -q, -q) = \mu C_{2y}(-q) \tag{16}$$

So, we based on Eq. (16) for eliminating $C_{2y}(-q)$ in Eq. (13), we obtain the equation constituted of only the fourth order cumulants:

$$\sum_{i=0}^{q} C_{4y}(-q-i, -q-i, t_3-i)h(i) = h(t_3+q)C_{4y}(-q, -q, -q) \tag{17}$$

Where $t_3 = -q, -q + 1, ..., 0$. The system of Eq. (17) can be written under the matrix form as follows:

$$\begin{pmatrix} C_{4y}(-q-1,-q-1,-q-1) & ... & C_{4y}(-2q,-2q,-2q) \\ C_{4y}(-q-1,-q-1,-q)-\alpha & ... & C_{4y}(-2q,-2q,-2q+1) \\ . & . & . \\ . & . & . \\ . & . & . \\ C_{4y}(-q-1,-q-1,-1) & ... & C_{4y}(-2q,-2q,-q)-\alpha \end{pmatrix}$$

$$\times \begin{pmatrix} h(1) \\ . \\ . \\ . \\ h(i) \\ . \\ . \\ . \\ h(q) \end{pmatrix} = \begin{pmatrix} 0 \\ -C_{4y}(-q,-q,-q+1) \\ . \\ . \\ . \\ . \\ -C_{4y}(-q,-q,0) \end{pmatrix} \quad (18)$$

Where
$\alpha = C_{4y}(-q,-q,-q)$
Or in more compact form, the Eq. (18) can be written as follows:

$$Mh_e = d \quad (19)$$

With M the matrix of size $(q+1,q)$ elements, h a column vector of size $(q,1)$ and d is a column vector of size $(q+1,1)$. The Least Square (LS) solution of the system of equation (19) is given by:

$$\widehat{h}_e = (M^T M)^{-1} M^T d \quad (20)$$

IV. Safi et al Algorithm: Alg-CUM [2]

Safi et al.[2] demonstrates that the coefficients $h(j)$for an FIR system can be obtained by the relationship, based on three order cumulants following:

$$\sum_{i=0}^{q} C_{3y}(-q-i,t_2-i)h(i) = C_{3y}(-q,-q)h(t_2+q) \quad (21)$$

With $t_2 = -q,...,0$ The system of Eq. (20) can be written under the matrix form as follows:

$$\begin{pmatrix} C_{3y}(-q-1,-q-1) & ... & C_{3y}(-2q,-2q) \\ C_{3y}(-q-1,-q)-\alpha & ... & C_{3y}(-2q,-2q+1) \\ . & . & . \\ . & . & . \\ . & . & . \\ C_{3y}(-q-1,-1) & ... & C_{3y}(-2q,-q)-\alpha \end{pmatrix}$$

$$\times \begin{pmatrix} h(1) \\ . \\ . \\ . \\ h(i) \\ . \\ . \\ . \\ h(q) \end{pmatrix} = \begin{pmatrix} 0 \\ -C_{3y}(-q,-q+1) \\ . \\ . \\ . \\ . \\ -C_{3y}(-q,0) \end{pmatrix} \quad (22)$$

Where
$\alpha = C_{3y}(-q,-q)$
The Eq. (22) can be written as follows:

$$Mh_e = d \quad (23)$$

Where M is the matrix of size $(q+1)\times(q)$ elements, h_e is a column vector constituted by the unknown impulse response parameters $h(k) = k = 0,...,q$ and d is a column vector of size $(q+1)$ as indicated in the Eq. (23).

The least squares (LS) solution of the system of Eq. (23), will be written under the following form

$$\widehat{h}_e = (M^T M)^{-1} M^T d \quad (24)$$

V. Application: identification and equalization of MC-CDMA system

The MC−CDMA modulator spreads the data of each user in frequency domain, the complex symbol a_j of each user j is, firstly, multiplied by each chips $c_(j,k)$ of spreading code, and then applied to the modulator of multicarriers. Each subcarrier transmits an element of information multiplied by a code chip of that subcarrier. In figure 2 we have represented the principle of MC−CDMA modulator:

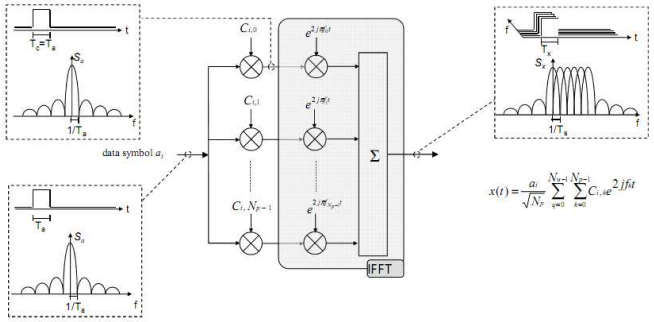

Fig. 2. Principle of MC−CDMA modulator the symbol a_j of each user j

A. MC−CDMA Transmitter

Figure 3 explains the principle of the transmitter for down-link MC−CDMA systems. The MC−CDMA signal is given by

$$x(t) = \frac{a_i}{\sqrt{N_p}} \sum_{q=0}^{N_u-1} \sum_{k=0}^{N_p-1} c_{i,k} e^{2jf_k t} \quad (25)$$

Where $f_k = f_0 + \frac{k}{T_c}$, N_u is the user number and N_p is the number of subcarriers.
The optimum space between two adjacent subcarriers is equal to inverse of duration T_c of chip of spreading code in order to guarantee the orthogonality between subcarriers.

We assumed that the channel is time invariant and its impulse response is characterized by P paths of magnitudes β_p and phases θ_p. the impulse response is given by the following equation

$$h(\tau) = \sum_{p=0}^{P-1} \beta_p e^{\theta_p} \delta(\tau - \tau_p) \quad (26)$$

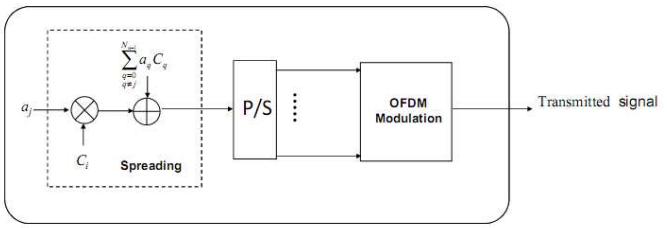

Fig. 3. The transmitter for downlink MC-CDMA systems

The relationship between the emitted signal $x(t)$ and the received signal $r(t)$ is given by:

$$\begin{aligned} r(t) &= \int_{-\infty}^{+\infty} \sum_{p=0}^{P-1} \beta_p e^{\theta_p} \delta(\tau - \tau_p) x(t-\tau) d\tau + n(t) \\ &= \sum_{p=0}^{P-1} \beta_p e^{\theta_p} x(t-\tau_p) + n(t) \end{aligned} \tag{27}$$

Where $n(t)$ is an additive white Gaussian noise (AWGN).

B. MC−CDMA Receiver

The downlink received MC−CDMA signal at the input receiver is given by the following equation

In Figure 4 we represent the receiver for downlink MC-CDMA systems.

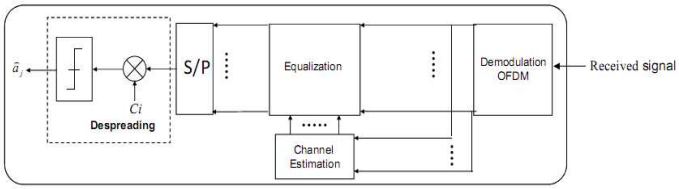

Fig. 4. The receiver for downlink MC-CDMA systems

$$\begin{aligned} r(t) = \frac{1}{\sqrt{N_p}} \sum_{p=0}^{P-1} \sum_{k=0}^{N_p-1} \sum_{i=0}^{N_u-1} \times \\ \times Re\left\{ \beta_p e^{j\theta} a_i c_{i,k} e^{2j\pi(f_0 + k/T_c)(t-\tau_p)} \right\} + n(t) \end{aligned} \tag{28}$$

At the reception, we demodulate the signal according the N_p subcarriers, and then we multiply the received sequence by the code of the user. After the equalization and the spreading operation, the estimation $\widehat{a_i}$ of the emitted user symbol a_i, of the i^{th} user can be written by the following equation

$$\begin{aligned} \widehat{a_i} &= \sum_{q=0}^{N_u-1} \sum_{k=0}^{N_p-1} c_{i,k}(g_k h_k c_{q,k} a_q + g_k n_k) \\ &= \underbrace{\sum_{k=0}^{N_p-1} c_{i,k}^2 (g_k h_k a_i)}_{I \quad (i=q)} \\ &+ \underbrace{\sum_{q=0}^{N_u-1} \sum_{k=0}^{N_p-1} c_{i,k} c_{q,k} g_k h_k a_q}_{II \quad (i \neq q)} \\ &+ \underbrace{\sum_{k=0}^{N_p-1} c_{i,k}(g_k n_k)}_{III} \end{aligned} \tag{29}$$

C. Equalization for MC−CDMA

1) Zero forcing (ZF): The principle of the ZF, is to completely cancel the distortions brought by the channel. The gain factor of the ZF equalizer,is given by the equation

$$g_k = \frac{1}{|h_k|} \tag{30}$$

By that manner, each symbol is multiplied by a unit magnitude. So, the estimated received symbol, $\widehat{a_i}$ of symbol a_i of the user i is described by:

$$\widehat{a_i} = \underbrace{\sum_{k=0}^{N_p-1} c_{i,k}^2 a_i}_{I \quad (i=q)} + \underbrace{\sum_{q=0}^{N_u-1} \sum_{k=0}^{N_p-1} c_{i,k} c_{q,k} a_q}_{II \quad (i \neq q)} + \underbrace{\sum_{k=0}^{N_p-1} c_{i,k} \frac{1}{h_k} n_k}_{III} \tag{31}$$

If we suppose that the spreading code are orthogonal, $i.e.$,

$$\sum_{k=0}^{N_p-1} c_{i,k} c_{q,k} = 0 \qquad \forall i \neq q \tag{32}$$

Eq. (31) will become

$$\widehat{a_i} = \sum_{k=0}^{N_p-1} c_{i,k}^2 a_i + \sum_{k=0}^{N_p-1} c_{i,k} \frac{1}{h_k} n_k \tag{33}$$

2) Minimum Mean Square Error, (MMSE): The MMSE techniques minimize the mean square error for each subcarrier k between the transmitted signal x_k and the output detection

$$E[|\varepsilon|^2] = E[|x_k - g_k r_k|^2] \tag{34}$$

The minimization of the function $E[|\varepsilon|^2]$, gives us the optimal equalizer coefficient, under the minimization of the mean square error criterion, of each subcarrier as

$$g_k = \frac{h_k^*}{|h_k|^2 + \frac{1}{\zeta_k}} \tag{35}$$

Where $\zeta_k = \frac{E[|r_k h_k|^2]}{E[|n_k|^2]}$
The estimated received symbol, $\widehat{a_i}$ of symbol a_i of the user i is described by

$$\widehat{a_i} = \underbrace{\sum_{k=0}^{N_p-1} c_{i,k}^2 \frac{|h_k|^2}{|h_k|^2 + \frac{1}{\zeta_k}} a_i}_{I \quad (i=q)} + \underbrace{\sum_{q=0}^{N_u-1} \sum_{k=0}^{N_p-1} c_{i,k} c_{q,k} \frac{|h_k|^2}{|h_k|^2 + \frac{1}{\zeta_k}} a_q}_{II \quad (i \neq q)} + \underbrace{\sum_{k=0}^{N_p-1} c_{i,k} \frac{h_k^*}{|h_k|^2 + \frac{1}{\zeta_k}} n_k}_{III} \tag{36}$$

The same, if we suppose that the spreading code are orthogonal, $i.e.$,

$$\sum_{k=0}^{N_p-1} c_{i,k} c_{q,k} = 0 \qquad \forall i \neq q \tag{37}$$

Eq.(36) will become

$$\widehat{a_i} = \sum_{k=0}^{N_p-1} c_{i,k}^2 \frac{|h_k|^2}{|h_k|^2 + \frac{1}{\zeta_k}} a_i + \sum_{k=0}^{N_p-1} c_{i,k} \frac{h_k^*}{|h_k|^2 + \frac{1}{\zeta_k}} n_k \tag{38}$$

VI. Simulation results

In order to evaluate the performance of the proposed algorithm, we consider the BRAN A, BRAN B and BRAN D model representing the fading radio channels, the data corresponding to this model are measured for multicarrier code division multiple access (MC−CDMA) systems. The following equation describes the impulse response $h(k)$ of BRAN radio channel.

$$h(k) = \sum_{i=0}^{N_T} A_i \delta(k - \tau_i) \tag{39}$$

Where $\delta(k)$ is Dirac function, h_i the magnitude of the targets i, $N_T = 18$ the number of target and τ_i is the time delay (from the origin) of target i.
In order to estimates the parameters constituting the BRAN channels impulse response with maximum information, because the BRAN channels is constituted by $N_T = 18$ parameters and seeing that the latest parameters are very small, we have taking the following procedure:

- We decompose the BRAN channel impulse response into four sub-channel as follow:

$$h(k) = \sum_{j=1}^{3} h_j(k) \tag{40}$$

- We estimate the parameters of each sub-channel independently, using the proposed algorithm.

- We add all sub channel parameters, to construct the full BRAN C channel impulse response.

A. Bran A radio channel

In Table 1 we have summarized the values corresponding the BRAN A radio channel impulse response [14].

Delay $\tau_i[ns]$	Mag.$A_i[dB]$	Delay $\tau_i[ns]$	Mag.$A_i[dB]$
0	0	90	−7.8
10	−0.9	110	−4.7
20	−1.7	140	−7.3
30	−2.6	170	−9.9
40	−3.5	200	−12.5
50	−4.3	240	−13.7
60	−5.2	290	−18
70	−6.1	340	−22.4
80	−6.9	390	−26.7

Table 1: Delay and magnitudes of 18 targets of BRAN A channel

In Figure 5 we represent the estimation of the impulse response of BRAN A channel using the proposed and safi et al. algorithms in the case of SNR = 20 dB and data length N = 4096.

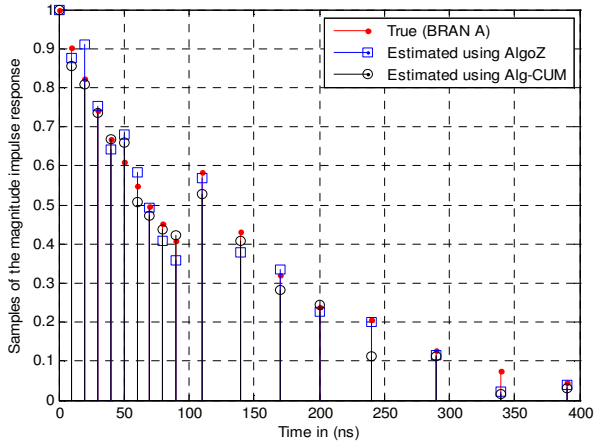

Fig. 5. Estimated of the BRAN A channel impulse response, for an SNR = 20 dB and a data length N=4096.

From Figure 5, we can conclude that the estimated BRAN A channel impulse response, using the proposed algorithm (AlgoZ), is very closed to the true one, for data length $N = 4096$ and $SNR = 20dB$. If we observe the estimated values of BRAN A impulse response, using the Safi et al. algorithm (Alg−CUM) shown in Figure 5, we remark, the same results given by the proposed method.
In the following figure (fig. 6) we have represented the estimated magnitude and phase of the impulse response BRAN A using all target, for an data length $N = 4096$ and $SNR = 20dB$, obtained using proposed algorithm (AlgoZ), compared with the safi et al. algorithm (Alg−CUM).

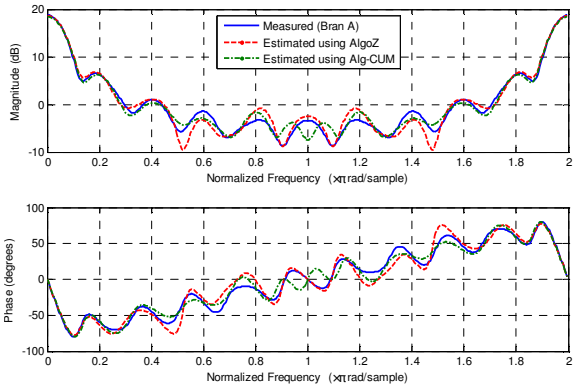

Fig. 6. Estimated of the BRAN A channel impulse response using all target, for an $SNR = 20dB$ and a data length N=4096

B. Bran B radio channel

In Table 2 we have represented the values corresponding to the BRAN B radio channel impulse response [14].

Delay $\tau_i[ns]$	Mag.$A_i[dB]$	Delay $\tau_i[ns]$	Mag.$A_i[dB]$
0	-2.6	230	-5.6
10	-3.0	280	-7.7
20	-3.5	330	-9.9
30	-3.9	380	-12.1
50	0.0	430	-14.3
80	-1.3	490	-15.4
110	-2.6	560	-18.4
140	-3.9	640	-20.7
180	-3.4	730	-24.6

Table 2: Delay and magnitudes of 18 targets of BRAN B channel

In Figure 7 we represent the estimation of the impulse response of BRAN B channel using the (AlgoZ) and (Alg$-$CUM) algorithms in the case of $SNR = 20dB$ and data length $N = 4096$.

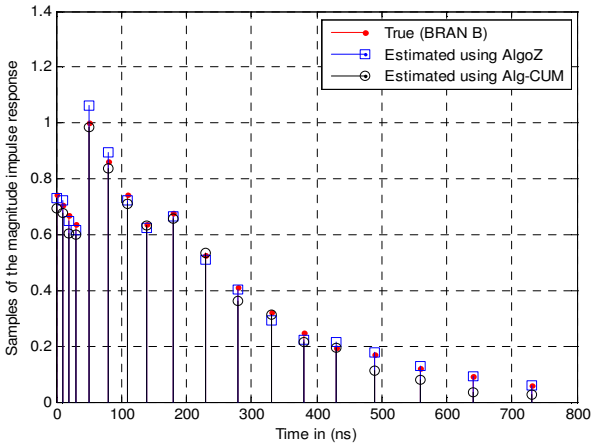

Fig. 7. Estimated of the BRAN B channel impulse response, for an $SNR = 20dB$ and a data length $N = 4096$.

From Figure 7, we can conclude that the estimated BRAN B channel impulse response, using (AlgoZ) algorithm, is very closed to the true one, for data length $N = 4096$ and $SNR = 20dB$. Using the algorithm (Alg$-$CUM) shown in Figure 7, we remark, approximately, the same results given by the AlgoZ except the last four parameters we have a minor difference between the estimated and the measured ones.

In the following figure (fig. 8) we have represented the estimated magnitude and phase of the impulse response BRAN B using all target, for an data length $N = 4096$ and $SNR = 20dB$, obtained using (AlgoZ) algorithm, compared with the Safi et al. algorithm (Alg$-$CUM).

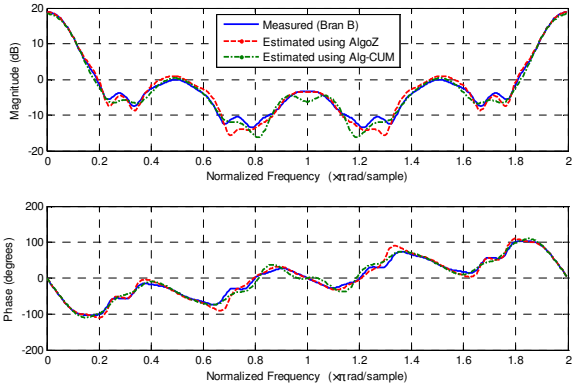

Fig. 8. Estimated of the BRAN B channel impulse response using all target, for an SNR = 20 dB and a data length N=4096

From the figure 8 we observe that the estimated magnitude and phase, using (AlgoZ) and (Alg$-$CUM) algorithms, have the same form and we have not more difference between the estimated and the true ones.

C. Bran D radio channel

In Table 3 we have represented the values corresponding to the BRAN D radio channel impulse response [14].

Delay $\tau_i[ns]$	Mag.$A_i[dB]$	Delay $\tau_i[ns]$	Mag.$A_i[dB]$
0	0.0	230	-9.4
10	-10.0	280	-10.8
20	-10.3	330	-12.3
30	-10.6	400	-11.7
50	-6.4	490	-14.3
80	-7.2	600	-15.8
110	-8.1	730	-19.6
140	-9.0	880	-22.7
180	-7.9	1050	-27.6

Table 3: Delay and magnitudes of 18 targets of BRAN D channel

In time domain we have represented the BRAN D channel impulse response parameters (Fig. 9)

From the gure (Fig. 9) we ca can conclude that the estimated BRAN D channel impulse response, using (AlgoZ) and (Alg$-$CUM), are very closed to the true ones, principally for high data length $(N = 4096)$, and for $SNR \geq 20dB$.

In the following figure (Fig. 10) we have represented the estimated magnitude and phase of the impulse response BRAN

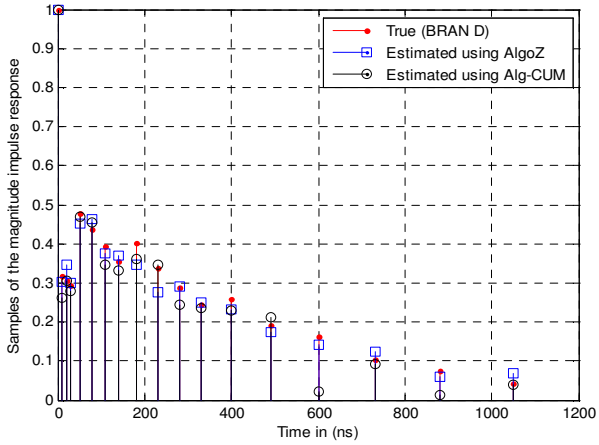

Fig. 9. Estimated of the BRAN D channel impulse response, for an SNR = 20 dB and a data length N=4096.

D using all target for an $N = 4096$ and $SNR = 20dB$.

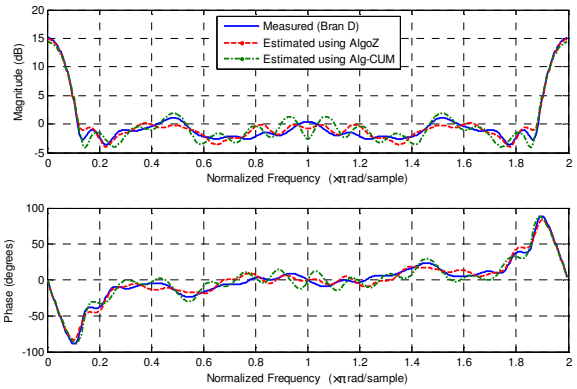

Fig. 10. Estimated of the BRAN D channel impulse response, for an SNR = 20 dB and a data length N=4096

From the gure 10 we observe that the estimated magnitude and phase, using (AlgoZ), have the same form between the estimated and the true ones, but using (Alg−CUM) we remark a faible difference between the estimated and the true ones.

VII. M-CDMA SYSTEM PERFORMANCE

In this subsection we consider the BER, for the two equalizers ZF and MMSE, using measured and estimated BRAN A, BRAN B, and BRAN D channel impulse responses.

A. ZF and MMSE Equalizers: Case of BRAN A Channel

In Figure 11, we represent the BER for different SNR, obtained using proposed algorithm (AlgoZ), compared with the (Alg−CUM) algorithm, using the ZF equalizer.

Figure 12 represents the BER for different SNR, obtained using proposed algorithm (AlgoZ), compared with the (Alg−CUM) algorithm, using the MMSE equalizer.

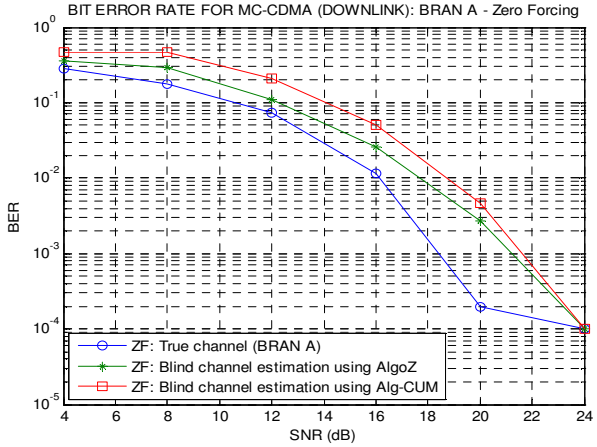

Fig. 11. BER of the estimated and measured BRAN A channel using the ZF equalizer

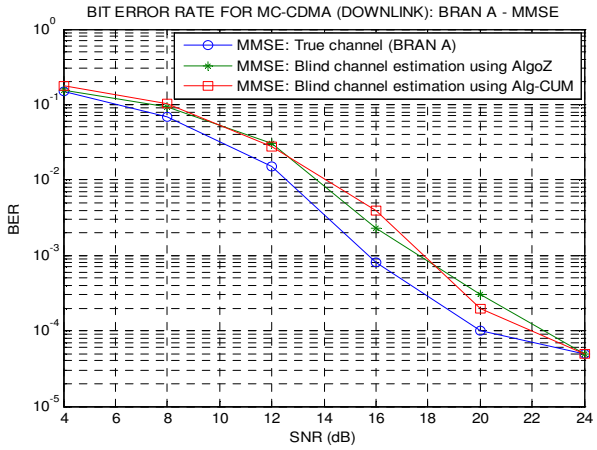

Fig. 12. BER of the estimated and measured BRAN A channel using the MMSE equalizer.

The BER simulation for different SNR, demonstrates that the estimated values by the (AlgoZ) algorithm are more close to the measured value than those estimated by (Alg−CUM) algorithm, we have a faible difference, for ZF and MMSE equalization. From the figure 12, we conclude that: if the SNR=24dB we have 1 bit error occurred when we receive 10^5 bit using MMSE equalizer.

B. ZF and MMSE Equalizers: Case of BRAN B Channel

In Figure 13, we represent the BER for different SNR, obtained using proposed algorithm (AlgoZ), compared with the (Alg−CUM) algorithm, using the ZF equalizer.

Figure 14 represents the BER for different SNR, obtained using proposed algorithm (AlgoZ), compared with the (Alg−CUM) algorithm, using the MMSE equalizer.

The BER simulation for different SNR, demonstrates that the estimated values by the (AlgoZ) algorithm are more close to the measured value than those estimated by (Alg−CUM) algorithm. From the figure 14, we conclude that: if the

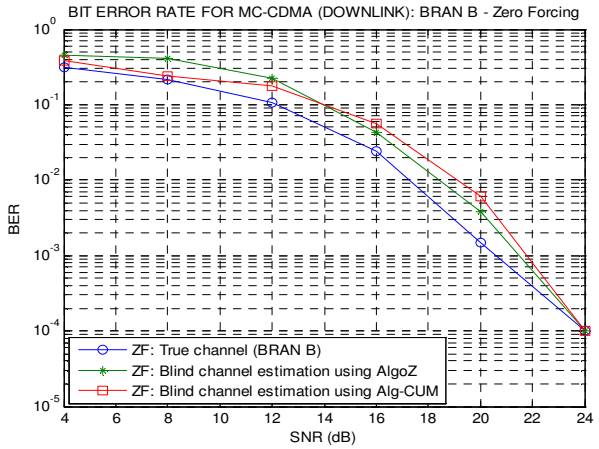

Fig. 13. BER of the estimated and measured BRAN B channel using the ZF equalizer.

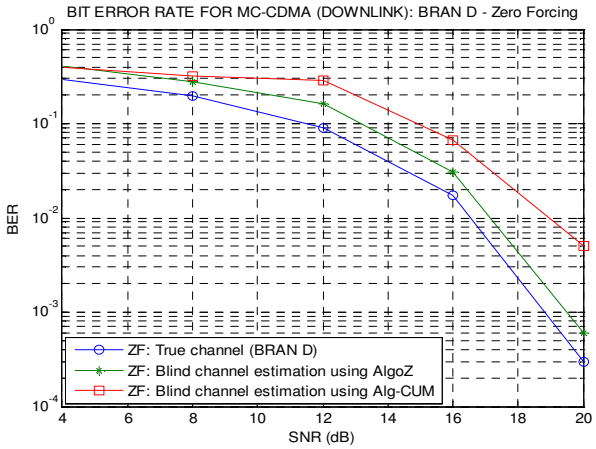

Fig. 15. BER of the estimated and measured BRAN D channel using the ZF equalizer

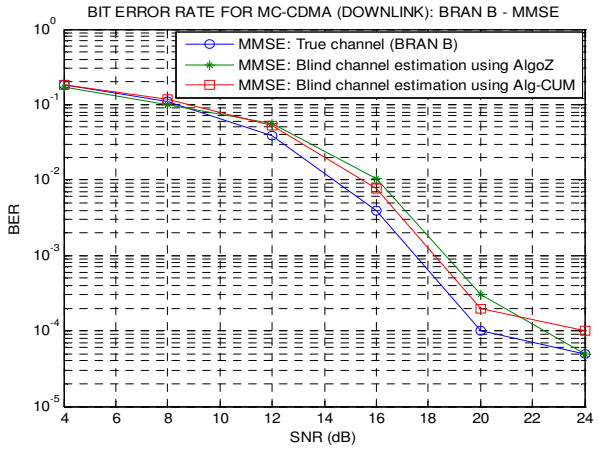

Fig. 14. BER of the estimated and measured BRAN B channel using the MMSE equalizer

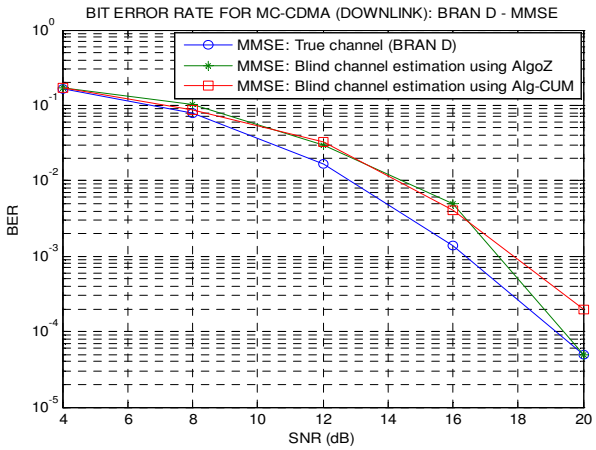

Fig. 16. BER of the estimated and measured BRAN D channel using the MMSE equalizer

$SNR = 24dB$, we observe that 1 bit error occurred when we receive 10^4 bit with the (Alg−CUM), but using (AlgoZ) we obtain only one bit error for 10^5 bit received.

C. ZF and MMSE Equalizers: Case of BRAN D Channel

In the figure 15, we represent the BER for different SNR, using the measured and estimated BRAN D channel, using the ZF equalizer.

From the figure 15, we observe that the blind ZF equalization gives approximately the same results obtained by the measured BRAN D values using AlgoZ, than those obtained by (Alg−CUM) algorithm, we have a difference between the estimated and the measured ones. If the $SNR = 20dB$ we have a BER less than 10^{-3} using (AlgoZ), but using the (Alg−CUM) we have only the BER less than 10^{-2}.

Figure 16 represents the BER for different SNR, using the measured and estimated BRAN D channel, using the MMSE equalizer.

Figure 16 demonstrates clearly that the estimated values by the rst algorithm (AlgoZ) are close to the measured value than those estimated by second algorithm (Alg−CUM), So, if the $SNR = 20dB$, we observe that 1 bit error occurred when we receive 10^4 bit with the (Alg−CUM), but using (AlgoZ) we obtain only one bit error for 10^5 bit received.

VIII. Conclusion

In this paper we have proposed an new algorithm (AlgoZ) based on fourth order cumulants, compared with the Safi et al algorithm (Alg−CUM), to identify the parameters of the impulse response of the frequency selective channel such as the experimental channels, BRAN A, BRAN B, and BRAN D, normalized for MC−CDMA systems. The simulation results show the effciency of the proposed algorithm (AlgoZ) than those obtained using (Alg−CUM), mainly if the input data are suffcient. The magnitude and phase of the impulse response is estimated with an acceptable precision in noisy environment principally if we use the rst algorithm (AlgoZ). In part of three experimental channels for MC−CDMA systems application, we have obtained very important results on bit error rate using the proposed algorithm (AlgoZ), than those obtained by (Alg−CUM) algorithm.

REFERENCES

[1] L. Srinivas and K. V. S. Hari, "FIR System Identification Based on Subspaces of a Hight Order Cumulant Matrix", IEEE Transactions on signal processing, 44(6) (1996).

[2] S. Safi, M. Frikel, M. M'Saad and A. Zeroual, "Blind Impulse Response Identification of frequency Radio Channels: Application to Bran A Channel", Int. J. Sig. Proces., 4(1) 201-206 (2007).

[3] M. Bakrim and D. Aboutajdine, "Cumulant-based identification of non gaussian moving average signals", Traitement du Signal, 16(3) 175-186 (1999).

[4] S. Safi and A. Zeroual, "Blind non-minimum phase channel identification using 3^{rd} and 4^{th} order cumulants", Int. J. Sig. Proces., 4 (1), 158-168 (2008).

[5] C.Y. Chi and J.Y. Kung, "A new identification algorithm for allpass systems by higher-order statistics", Signal Processing 41 239- 256 (1995).

[6] J. Antari, A. El Khadimi, D. Mammas and A. Zeroual, "Developed Algorithm for Supervising Identification of Non Linear Systems using Higher Order Statistics: Modeling Internet Traffic", International Journal of Future Generation Communication and Networking, 5(4) (2012).

[7] J. Antari, A. Zeroual and S. Safi, "Stochastic analysis and parametric identification of moving average (MA) non Gaussian signal using cumulants", International Journal of Physical and Chemical News, 34 27-32 (2007).

[8] K. Abderrahim, R. B. Abdennour, G. favier, M. Ksouri and F. Msahli, "New results on FIR system identification using cumulants", 35 601-622 (2001).

[9] S. Safi, A. Zeroual and M. M. Hassani, "Prediction of global daily solar radiation using higher order statistics" Renewable Energy, 27 647666 (2002).

[10] S. Safi and A. Zeroual, "Blind identification in noisy environment of non-minimum phase Finite Impulse Response (FIR) using higher order statistics", Int. J. Sys. Anal. Modell. Simul., Taylor Francis, 43(5) 671681 (2003).

[11] J. Antari, R. Iqdour, A. Zeroual, "Forecasting the wind speed process using higher order statistics and fuzzy systems", Renewable Energy, 9 237 251 (2006).

[12] ETSI, "Broadband Radio Access Networks (BRAN), High Performance Radio Logical Area Network (HIPERLAN) Type 2; Requirements and architectures for wireless broadband access" (1999).

[13] ETSI, "Broadband Radio Access Networks (BRAN); HIPERLAN Type 2; Physical Layer" (2001).

[14] Vincent Le Nir, "Étude et optimisation des systèmes multi-antennes associés à des modulations multiporteuses", Thèse de doctorat, Institut National des Sciences Appliquées de Rennes, (2004).

Design and Implementation of 2-Input OR Gate based on XGM properties of Semiconductor Optical Amplifier

Chandra Kamal Borgohain[1], Chakresh Kumar[2] and Satyajit Bora[1]

Abstract — **In this paper we have implemented an all-optical OR-gate using simultaneous Four-Wave Mixing (FWM) and Cross-Gain Modulation (XGM) in a semiconductor optical amplifier (SOA). Which incorporates two semiconductor optical amplifiers (SOAs). The proposed OR logic is numerically simulated by solving nonlinear coupled equations that explain cross gain modulation (XGM) effect in individual SOAs.**

Keywords—**Semiconductor Optical Amplifier, Optical Logic Gates, Cross Gain Modulation, SOA, Four Wave Mixing.**

I. INTRODUCTION

At present, SOAs are the prime candidates for use in advanced optical communication functional components. The growth of large scale integration of SOA technology offers economical, high performance devices. SOAs exhibit non-linear properties due to carrier density changes induced by differences in power of the input signal. While these non-linear properties create problems for the use of SOAs as simple linear gain elements, they can be exploited to perform functions that are typically carried out by electronic signal processing circuits. In the case of all applications mentioned above, the data signal is processed in optical form, rather than first being converted to an electrical signal. SOA-based devices are compact, stable, integration-capable, and potentially independent of polarization and wavelength [4]. Also, it has the advantages of low switching energy and low latency [5]. A computation that might take more than eleven years by the conventional electronic takes only one single hour [6].The use of the optical fibers as nonlinear elements in switching devices gives so high speed operation since the nonlinear response of the fiber is extremely fast and the possibility of creating a rectangular switching by using a dispersive walk-off between the data and the control pulse but the nonlinear coefficient is usually very small in conventional fibers[8]. In this paper the full logic is developed in MATLAB platform.

[1]Department of Electronics and Communication Engineering, Tezpur (central) University, INDIA
[2]University School of Information & Communication Technology, Guru Gobind Singh Indraprastha University, Dwarka, New Delhi-110078, India
E-mail- borgohainchandrakamal176@gmail.com

II. SIMULATION METHOD

In this approach, we have taken the reference equations from Ref. [15] and different parameters which are taken into consideration are tabulated below in Table I. It is assumed that input pump, and probe pulses have the same temporal width as well as perfect pulse overlap, and in all of the cases, their powers are set to a ratio of 10:1. Numerical simulations have been undertaken to investigate the amplification of strong picoseconds optical pulses in semiconductor optical amplifiers (SOAs), taking into account carrier heating, spectral whole burning, carrier-carrier scattering (CCS) and carrier photon scattering (CPS). The result of interference of two co polarized pulses when propagating into SOA, one pump pulse at central frequency ω1 and the other probe pulse at central frequency ω0 ,induce a bit of carrier density pulsation at the frequency detuning Ω = ω1-ω0. This results a generation of a new frequency pulse at ω2 = ω0-Ω = 2ω0-ω1.The new pulse is phase conjugate replica of the probe pulses, and can be extracted from the input pulses using an optical filter. Here, A_j (Z, t), j = 0, 1, 2, correspond to the slowly varying envelopes of the pump, the probe, and the conjugate pulses, respectively, and Ω = ω1-ω0, is the frequency detuning.

The following Equation has been taken into consideration

$$A_0(L,t)=A_0(0,t)e^{\left(\frac{1}{2}\right)(1-i\alpha)h} \quad (1)$$

Where, $A_0\ (0,\ t)$, is the input pump pulse amplitude at any end of SOA,
$A_0\ (L,\ t)$, is the input pump pulse amplitude at any length L of SOA,

L is the length of SOA, t is time. The rest of parameters are already defined in Table I.

$$A_1(L,t)=A_0(0,t)\left[e^{\left(\frac{1}{2}\right)(1-i\alpha)h-\eta_{10}|A_0(0,t)|^2(e^h-1)}\right]cosh\left[\left(\frac{1}{2}\right)\sqrt{\eta_{02}\eta_{01}^*}|A_0(0,t)|^2(e^h-1)\right] \quad (2)$$

Where, $A_1(0, t)$, is the input probe pulse amplitude at any end of SOA.
$A_1(L, t)$, is the input probe pulse amplitude at any length L of SOA.
L= length of SOA. t is time. The rest of parameters are already defined in Table I.

$$A_2(L,t)=\frac{A_1^*(L,t)A_0(L,t)}{A_0^*(L,t)}\sqrt{\frac{\eta_{01}}{\eta_{02}^*}}x\ sinh\left[\left(\frac{1}{2}\right)\sqrt{\eta_{01}\eta_{02}^*}|A_0(L,t)|^2e^{-h}(e^h-1)\right] \quad (3)$$

Where
$A_2(0, t)$ is input conjugate pulse amplitude at any end of SOA.
$A_2(L, t)$ is input conjugate pulse amplitude at any length L of SOA. L= length of SOA, t is time. Rest parameters are already defined in Table I.

$$\eta_{01}=\eta_{01}^{CD}+\eta_{01}^{CH}+\eta_{01}^{SHB} \quad (4)$$

Where,

$$\eta_{01}^{CD}=\varepsilon_{cd}\frac{1-i\alpha}{((1+i\Omega\tau_1)+(1+i\Omega\tau_s))}$$

$$\eta_{01}^{CH}=\varepsilon_t\frac{1-i\alpha_T}{((1+i\Omega\tau_h)+(1+i\Omega\tau_1))}$$

$$\eta_{01}^{SHB}=\varepsilon_{shb}\frac{1-i\alpha_{shb}}{1+i\Omega\tau_1}$$

The amplification function h and coupling coefficient Ηij are defined in [15]. The effects of carrier depletion, carrier heating, spectral hole burning, two-photon absorption, and ultrafast nonlinear refraction are taken into account, leading to a successful description of wave mixing for optical pulses with strong pulse energy, and/or with pulse widths larger than several hundred femto seconds , as well as in active or passive optical waveguides. The parameters α, τ, and ε determine the strength and nature of the wave mixing process caused by each of the intraband mechanisms and their relative significance. The values of α, τand ε cannot be determined unanimously.

TABLE I
PARAMETERS USED IN SIMULATION WORK

Parameters	Symbols	Values	Unit
Length of the amplifier	L	450	μm
Small signal gain	G	$1.54*10^{-4}$	m^{-1}
Carrier lifetime	τ_s	300	ps
Nonlinear gain compression for carrier heating	ε_t	0.13	w^{-1}
Nonlinear gain compression for spectral hole burning	ε_{shb}	0.07	
Traditional line width enhancement factor	α	5.0	
Temperature l line width enhancement factor	α_T	3.0	
Line width enhancement factor for spectral hole burning	α_{shb}	0.1	
Time for carrier-carrier scattering	τ_1	50	fs
Time for carrier photon scattering	τ_h	700	fs
Carrier depletion coefficient	ε_{cd}	47	w^{-1}

III. RESULTS AND DISCUSSION

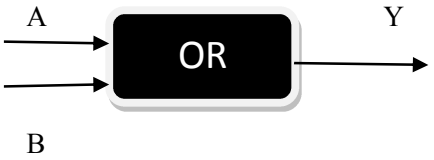

Fig. 1. OR Gate

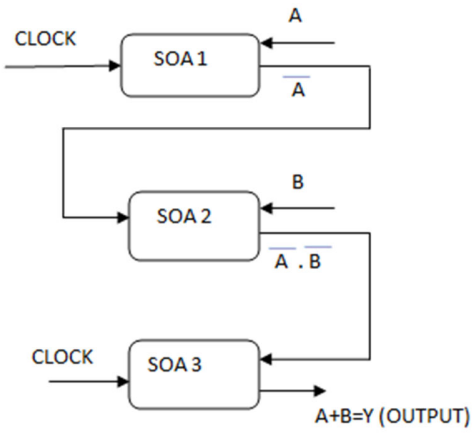

Fig. 2. OR using SOAs

TABLE II
TRUTH TABLE FOR OR LOGIC CAN BE GIVEN AS

A	B	A+B =Y
0	0	0
0	1	1
1	0	1
1	1	1

Fig. 2 shows the OR gate using SOAs. In SOA1 'A' acts as an input pump pulse and 'CLOCK' signal acts as an input probe pulse. In SOA 2 the output of SOA1 acts as input probe pulse and B acts as an input pump pulse. Similarly, in SOA 3 CLOCK signal acts as input probe pulse and the output of SOA2 acts as input pump pulse, which gives the required Boolean expression A+B.

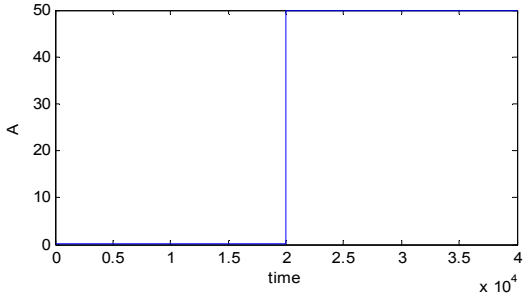

Fig. 3. Waveform of A = [0 0 1 1]

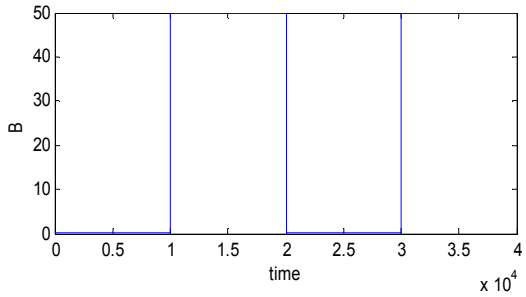

Fig. 4. Waveform of B = [0 1 0 1]

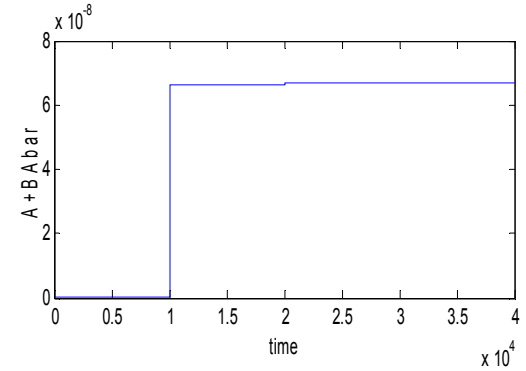

Fig. 5. Waveform of OR output = [0 1 1 1]

From Fig. 3, 4 and 5 we can observe that the simulation results clearly verify the truth table of OR gate.

IV. CONCLUSIONS

We have proposed and implemented a new all-optical OR gate using analytic solutions of nonlinear effects in semiconductor optical amplifier. This research has guided readers to design all-optical OR logic circuits so that anyone can construct any types of all-optical different logic circuits by utilizing the detailed process of designing the OR Gate. The simulated result verifies the truth table.

REFERENCES

[1] Jae Hun Kim, Young Il Kim, Young Tae Byun,* Young Min Jhon,Seok Lee, Sun Ho Kim and Deok HaWoo,Photonics Research Center, "All Optical Logic Gates Using Semiconductor Optical-Amplifier-Based Devices and Their Applications", Korea Institute of Science and Technology, Seoul 136 791

[2] T. Fjelde, D.Wolfson, A. Kloch, B. Dagens, A. Coquelin,I. Guillemot, F. Gaborit, F. Poingt and M. Renaud, Electron.Lett. 36, 1863 (2000).

[3] K. Vlachos, K. Zoiros, T. Houbavlis, A. Hatziefremidis and H. Avramopoulos, Proc. LEOS 768, 2 (1999).

[4] Alistair **J.** Poustie, K. J. Blow, A. E. Kelly and R. J. Manning, "All-optical parity checker". BT Laboratories, Martlesham Heath, Ipswich, IP5 3RE, U.K.,Tel: +44 1473 646442 Fax: +44 1473 646885

[5] C.K.Yow, Y.J.Chai, K.A.Williams, RV.Penty, 1.H.White. "Enhanced performance of an all-optical parity checker using a single Mach-Zehnder interferometer". Centre for Photonics Communications, Cambridge University Engineering Department, Trumpington Street, Cambridge CP2 1PZ United Kingdom Telephone*:* +44 01223 740103Fmc*:* 1-84 01223 740102E-mail cky21@cam ac uk

[6] Hossin Abdeldayem et al., " Recent Advances in Photonic Devices forOptical Computing", NASA Marshall Space Flight Center, Space Sciences laboratory, Huntsville, al 35812

[7] B. E. A. Saleh, and M. C. Teich, *Fundamentals of Photonics* (JohnWiley & Sons, New York, 1991),Chap. 19.

[8] Bengt- Erik Olsson, "All Optical Switching with the Nonlinear Optical Loop Mirror", School of electrical and computer engineering, Chalniers University of technology, Goteborg, Sweden, Technical Report No. 330,1998.

[9] Xia, T.J., Liang, Y., Ahn, K.H.: 'All-optical packet-drop demonstration using 100 Gb/s words by integrating fiber-based components', IEEE photonic technology letters, 1998, 10, (1), pp.153-155.

[10] Bogoni, A., Poti, L., Proietti, R., Meloni, G., Ponzini, F., Ghelfi, P.: 'Regenerative and reconfigurable all-optical logic gates for ultra-fast applications', Electronics Letters, 2005, 41, (7), pp.435-436.

[11] Stubkjaer, K.E.: 'Semiconductor optical amplifier-based all optical gates for high-speed optical processing', IEEE Journal on selected topics in quantum electronics, 2000, 6, (6), pp.1428-1435.IEEE photonic technology letters,2001, 13, (7), pp. 750–752.

[12] Martinez, J.M., Ramos, F., Marti, J.: 'All-optical packet headerprocessor based on cascaded SOA-MZIs', Electronics letters, 2004,40,(14), pp.894-895.

[13] Kim, J., Jhon, Y, Byun, Y., Lee, S., Woo, D., Kim, S.: 'All-optical XOR gate using semiconductor optical amplifiers without additional input beam', IEEE photonic technology letters, 2002, 14, (10), pp.1436-1438.

[14] Jae Hun Kim, Young Min Jhon, Young Tae Byun, Seok Lee, Deok HaWoo, and Sun Ho Kim "All-Optical XOR Gate

Using Semiconductor Optical Amplifiers Without Additional Input Beam ",IEEE PHOTONICSTECHNOLOGY LETTERS, VOL. 14, NO. 10, OCTOBER 2002

[15] S Junqlang et al., "Analytical solution of Four wave mixing between picosecond optical pulses in semiconductor optical amplifiers with cross gain modulation and probe depletion", Microwave and Optical technology Letters, Vol. 28, No. 1, pp 78 – 82, 2001.

[16] Vikrant k Srivastava, Devendra Chack, Vishnu Priye, "2-Input AND Gate For Fast Gating and Switching Based On XGM Properties of InGaAsP Semiconductor Optical Amplifier", International Journal of Advanced Computer Science and Applications, Vol. 1, No. 5, (2010).

[17] Vikrant k Srivastava, Devendra Chack, Vishnu Priye, Chakresh Kumar. "All-Optical XOR Gate Based on XGM Properties of SOA". International Conference on Computational Intelligence and Communication Network, IEEE computer society, 2010.

ISSN 1805-5443